

Propulsion Materials

FY 2016 Annual Report

May 2017

Vehicle Technologies Office
Materials Technology R&D

(This page intentionally left blank)

Propulsion Materials Research and Development Introduction

Enabling Material Technologies to Meet Vehicle Technologies Office Goals

The U.S. Department of Energy's Vehicle Technologies Office (VTO) is pleased to introduce the Fiscal Year 2016 annual progress report for the research and development (R&D) Propulsion (powertrain) Materials Program. With the U.S. Department of Energy's (DOE) national laboratories and in partnership with universities and private industry across the United States the Propulsion Materials Program continues to invest in R&D that provides enabling materials technologies to improve fuel efficiency of future commercial trucks and passenger vehicles.

This introduction summarizes the objectives and progress of the program during Fiscal Year 2016. Activity in the Propulsion Materials Program supports the energy security goals of VTO's Office of Energy Efficiency and Renewable Energy within the U.S. DOE. The Propulsion Materials Program works closely with other VTO teams to identify critical materials needs for next generation high-efficiency powertrains for both heavy and light-duty vehicles. The technical approaches used to improve vehicle efficiency through improved propulsion systems includes technologies that result in improved powertrain thermal efficiency, systems level efficiencies resulting from light weighting through increased power density, and petroleum displacement through fuel substitution strategies. The technical maturity of the projects for the propulsion materials portfolio ranges from basic science to subsystem prototype validation, with successful projects transitioning to teams with vehicle-level capabilities or to original engine manufacturers' commercialization pathways.

Enabling Advanced Technologies

Propulsion Materials Program activities focus on key technical deficiencies in materials performance that limit the expanded capabilities of advanced combustion engines, electric-drive systems, and fuels and lubricants. These activities provide materials R&D expertise and advanced materials testing and development that support the goals of combustion, hybrid, and power electronics development. The Propulsion Materials Program provides enabling materials support such as the following:

- Materials for intermediate high-efficiency (i.e., about 46% brake thermal efficiency) combustion strategies such as low-temperature (i.e., 150°C) combustion or homogenous-charge compression ignition
- Materials for near extremely high efficiency (i.e., 55 to 60% brake thermal efficiency), which operate at very high temperatures i.e., (180 to 210°C) and pressures (i.e., 300 BAR)
- Materials technologies for effective reduction of tailpipe emissions, including diesel particulate filters, low-temperature (i.e., 150°C) catalyst development, characterization and testing, and exhaust gas recirculation coolers
- Materials for alternate fuels, including engine and exhaust after treatment materials compatibility and corrosion in biofuels
- Support for the Materials Genome Initiative by evaluating existing computational tools and identifying gaps

necessary for seamless integration across multiple-length scales. Projects in the Materials Genome portfolio are validating the performance of existing tools, identifying gaps, and developing a suite of new materials with improved properties for engine applications.

The program supports these core technology areas by providing materials expertise, testing capabilities, computational expertise, and technical solutions for materials problems. The component development, materials processing, and characterization that the program provides are enablers of successful development of efficient, durable, and emissions-compliant engines.

Program Organization

The Propulsion Materials Program consists of the following R&D projects, which support VTO propulsion technologies. Each project consists of several R&D agreements.

- Materials for High-Efficiency Engines – Develop materials for next-generation, high-efficiency engines and address anticipated issues with engine cylinder block, head, crankshafts, pistons, valves and valve train, fuel injectors, turbochargers, and exhaust gas recirculation systems.
- Materials for Control of Exhaust Gases and Energy Recovery Systems – Develop materials for exhaust after treatment, exhaust gas recirculation systems, and waste heat recovery applications.
- Cast Alloys for Engines (Group of Competitively Awarded Industry-Led Projects) – Develop a suite of new, high-performance, low-cost cast alloys using an integrated computational materials engineering approach, targeting lightweight aluminum alloys for light-duty engines, high-strength cast ferrous alloys for heavy-duty engines, and high-performance cast steel alloys for high-performance crank shafts.
- Integrated Computational Materials Engineering (Application-Specific Materials Simulation, Characterization, and Synthesis) – Adopt computational materials design, including an atomic-scale characterization protocol to develop advanced materials for nitrogen oxides (NO_x) catalysts, cast engine components, and electric motors to provide a pathway to transition Basic Energy Science research to practical applications.

R&D projects are evaluated annually using strategic objectives. Activities are evaluated based on their relevance to VTO objectives, the supported team's (i.e., ACE, APEEM, and Fuels) assessment of the work, and the strength of industrial support for the activity. In order to meet future efficiency improvement targets, new projects and areas of research will be identified through assessments of VTO stretch objectives and resultant demands for increased material performance.

VTO competitively awards funding through funding opportunity announcement (FOA) selections, and projects are fully funded through the duration of the project in the year that the funding is awarded. The future direction for direct-funded work at the national laboratories is subject to change based on annual appropriations.

Felix Wu
Team Leader
Advanced Materials Technologies
Vehicle Technologies Office
Energy Efficiency and Renewable Energy

Jerry L. Gibbs
Technology Development Manager
Vehicle Technologies Office
Energy Efficiency and Renewable Energy

Acknowledgments

Authors

M. Berube

F. Wu

J. Gibbs

List of Acronyms

| | |
|-------|------------------------------------------------|
| Al | aluminum |
| AMOX | ammonia oxidation |
| APEEM | Advanced Power Electronics and Electric Motors |
| ASC | ammonia slip catalyst |
| ASTM | American Society for Testing and Materials |
| BTE | brake thermal efficiency |
| C | Celsius |
| CAD | computer-aided design |
| CFD | computational fluid dynamics |
| CGI | compacted graphite iron |
| CHA | Chabazite |
| CO | carbon monoxide |
| CRADA | cooperative research and development agreement |
| CTE | coefficient of thermal expansion |
| Cu | copper |
| DEF | diesel exhaust fluid |
| DFT | density functional theory |
| DOC | diesel oxidation catalyst |
| DOE | U.S. Department of Energy |
| DPF | diesel particulate filter |
| EDXS | energy disperse x-ray spectrometer |
| EERE | Energy Efficiency and Renewable Energy |
| EGR | exhaust gas recirculation |

| | |
|-----------------|------------------------------------------------|
| EPMA | electron probe microanalysis |
| FOA | Funding Opportunity Announcement |
| FSW | friction-stir welding |
| FTP | federal test procedure |
| FUL | full-useful-life |
| FY | fiscal year |
| g/s | grams per second |
| GM | General Motors |
| HC | hydrocarbon |
| HCF | highest common factor |
| HD | heavy-duty |
| ICME | integrated computational materials engineering |
| K | potassium |
| LEAP | local electrode atom probe |
| Mg | magnesium |
| mm | millimeter |
| μm | micrometer |
| MPa | megapascal |
| mpg | miles per gallon |
| Na | sodium |
| NO _x | nitrogen oxides |
| NREL | National Renewable Energy Laboratory |
| ORNL | Oak Ridge National Laboratory |
| p | phosphorus |

| | |
|-------|-----------------------------------------------------|
| PCP | peak cylinder pressure |
| Pd | palladium |
| PGM | platinum group metals |
| PNNL | Pacific Northwest National Laboratory |
| ppm | parts per million |
| Pt | platinum |
| R&D | research and development |
| Rh | rhodium |
| rpm | rotations per minute |
| RT | room temperature |
| SCR | selective catalytic reduction |
| Si | silicon |
| SLTNR | sustained low temperature NO _x reduction |
| STEM | scanning transmission electron microscope |
| TEM | transmission electron microscope |
| UTS | ultimate tensile strength |
| VTO | Vehicle Technologies Office |
| WPI | Worcester Polytechnic Institute |
| Zr | zirconium |

Table of Contents

| | |
|------------------------------------------------------------------------------------------------------------------------------------------------------------------------------------------------|----|
| Project-Materials for Hybrid and Electric Drive Systems..... | 1 |
| Agreement 23726 – Novel Manufacturing Technologies for High-Power Induction and Permanent Magnet Electric Motors (GM CRADA)..... | 1 |
| Project-Materials for High-Efficiency Engines..... | 7 |
| Agreement 9105 – Materials Issues Associated with EGR Systems..... | 7 |
| Agreement 9105 – Biofuel Impact on After-treatment Devices..... | 14 |
| Project-Integrated Computational Materials Engineering | 24 |
| Agreement 26391 – Applied Computational Methods for New Propulsion Materials – Future Engine Requirements | 24 |
| Project-Cast Alloys for Engines..... | 29 |
| Ford - ICME-Guided Development of Advanced Cast Aluminum Alloys for Automotive Engine Applications | 29 |
| Funding Opportunity Announcement (FOA) 648-3a – Computational Design and Development of a New, Lightweight Cast Alloy for Advanced Cylinder Heads in High-Efficiency, Light-Duty Engines | 37 |
| FOA 648-3a – High-Performance Cast Aluminum Alloys for Next Generation Passenger Vehicle Engines..... | 51 |
| Project-Materials for High Efficiency Engines..... | 57 |
| Agreement 13329 (Task 26190) – High-Temperature Materials for High-Efficiency Engines | 57 |
| Project-Materials for Control of Exhaust Gases and Energy Recovery Systems..... | 64 |
| PNNL – Innovative SCR Materials and Systems for Low-Temperature After-treatment (FCA US LLC CRADA)..... | 64 |
| Ford – Next Generation Three-Way Catalysts for Future, Highly Efficient Gasoline Engines | 69 |
| Cummins – Sustained Low-Temperature NOx Reduction..... | 73 |

List of Figures

| | |
|----------------------------------------------------------------------------------------------------------------------------------------------------------------------------------------------------------------------------------------|----|
| Figure 1. Initial rotor concepts fabricated with FSW..... | 3 |
| Figure 2. a) Rotor schematic, b) Cu end cap positioned on shorting bar ends prior to joining, and c) friction-stir tool and rotor in a fixture prior to welding..... | 4 |
| Figure 3. Schematic of end cap/shorting bar joined area..... | 4 |
| Figure 4. FSW full-size rotor end cap..... | 5 |
| Figure 5. Electrical resistance testing of the rotors at GM. Electrical clamps are connected, one on each end cap, across a bar..... | 5 |
| Figure 6. Test setup at GM for detection of interrupted bars..... | 5 |
| Figure 7. Tool temperature measurements and corresponding spindle speed as the weld progressed around the end cap..... | 6 |
| Figure 8. Larger inner hole on “reduced Cu” end cap design..... | 6 |
| Figure 9. Schematic of stationary shoulder design..... | 6 |
| Figure 10. Optical image of (a) a fouled fin surface and (b) after the deposit has been removed, the corresponding height map of (c) the fouled fin surface and (d) the cleaned fin surface. The flow direction was left to right..... | 10 |
| Figure 11. Surface height of maps from Figure 1(c) and 1(d) averaged across the fin width. The deposit thickness is also shown..... | 10 |
| Figure 12. Deposit thickness versus distance from the peak in the fin averaged from all 20 coolers. The blue lines show the location of the valleys in the sinusoidal wave..... | 10 |
| Figure 13. Ratio of deposit thickness on the upstream side of the peak to the downstream side versus smoke level. 11 | |
| Figure 14. Fouled spiral height, spiral location, and deposit thickness along the tube length. The x-axis covers 1-in. along the tube. These data are the average of four different tube sections. | 12 |
| Figure 15. Catalyst aging and emission testing configuration. | 16 |
| Figure 16. A five-cycle portion of the aging protocol. | 17 |
| Figure 17. NO _x emissions test results. The red line indicates the FUL NO _x limit of 0.33 g/bhp-hour and the green line is the FUL limit of 435,000 miles. | 17 |
| Figure 18. Pt particle size distribution in the DOC measured with STEM..... | 18 |
| Figure 19. Elemental map of Pt (red) and Na (blue) from the inlet of the fully aged DOC..... | 18 |
| Figure 20. Weibull distributions of the failure stress of 25 tiles from the new and aged DPFs. | 18 |
| Figure 21. CTE of the fresh (blue) and aged (red) DPFs versus temperature..... | 19 |
| Figure 22. PGM particle size distribution in the fresh and aged inlet DPF washcoat. | 19 |
| Figure 23. Elemental map of Pt (red) and Na (blue) from the inlet of the fully aged DPF..... | 19 |
| Figure 24. NO _x conversion efficiency versus temperature for the aged inlet SCR and after heat treatments..... | 20 |
| Figure 25. NH ₃ oxidation versus temperature for the aged inlet SCR and after heat treatments. | 20 |
| Figure 26. N ₂ O formation versus temperature for the aged inlet SCR and after heat treatments. | 20 |
| Figure 27. Measured thermal conductivity at a range of temperatures for CGI-450 compared with publicly available values for gray cast iron..... | 26 |
| Figure 28. Measured CTE at a range of temperatures for CGI-450 compared with publicly available values for gray cast iron and CGI-450..... | 26 |
| Figure 29. Short-term creep test result for CGI-450 at 500°C for three load conditions up to tensile failure..... | 27 |
| Figure 30. Temperature map (in K) of the head and valves at a low peak-cylinder pressure condition, showing spatial variations. Image produced by Jing Huang..... | 27 |
| Figure 31. (a) Scheil simulation of Heat 17 showing the solidification consequence; (b) back-scatter imaging of as- | |

| | |
|----------------------------------------------------------------------------------------------------------------------------------------------------------------------------------------------------------------------------------------------------------------------------------------------------------------------------------------------------------------------------------------------------------------------------------------------------|----|
| cast Heat 17 showing observed microstructure; (c) EDXS mapping of as-cast Heat 17 showing novel addition-contained primary phase, Al matrix, Al-Si eutectics, and partitioning of Cu and Mg into eutectic regions..... | 32 |
| Figure 32. Quantitative composition measurement of Al matrix by EPMA of as-cast Heat 15 and Heat 17, showing different cooling rates that arise to similar amount of X-additions and different content of Z-additions..... | 33 |
| Figure 33. (a) and (b) Back-scatter imaging and EDXS mapping of Heat 17 after first-stage treatment showing Cu has started to move into the Al matrix; (c) and (d) back-scatter imaging and EDXS mapping of Heat 17 after second-stage treatment showing most Cu has been dissolved into the Al matrix; (e) and (f) back-scatter imaging and EDXS mapping of Heat 17 after T7 treatment showing most Cu has been dissolved into the Al matrix..... | 33 |
| Figure 34. (a) Room temperature YS and UTS of Heat 16 and Heat 17 with different heat treatment, showing that all alloys can meet DOE requirements; (b) 300°C YS and UTS of Heat 16 and Heat 17 with a different heat treatment, showing only novel addition improved Heat 17 with an excess DOE target after 100 hours of pre-exposure..... | 34 |
| Figure 35. Room temperature and a 120°C endurance limit of Heat 16 and Heat 17 with different heat treatment, showing Heat 17-T ₇ has excellent 120°C fatigue strength..... | 34 |
| Figure 36. (a) Representative scanning electron microscope imaging of Heat 16 and Heat 17, showing the fraction surface of 120°C fatigue samples; (b) the average size of shrinkage pore for initiation sites, showing all Heat 17 samples have larger initiation shrinkage pore size than Heat 16..... | 35 |
| Figure 37. (a) TEM imaging of Heat 17 only, with first-stage treatment at T1 showing no precipitates observed; (b) TEM imaging of Heat 17 only, with first-stage treatment at T2 showing sparse novel addition-contained precipitates observed; (c) TEM imaging of Heat 17-T1 showing θ' and Q precipitates observed..... | 36 |
| Figure 38. QuesTek's iCMD and ICME technology..... | 39 |
| Figure 39. GM virtual cast component development modeling and simulation method for cast product property and life prediction..... | 40 |
| Figure 40. (Top panels) Atom probe measurements showing MgSi iso-surfaces, indicating Q-phase precipitate outlines (purple) and Si nano-precipitate outlines (green) for 1 and 72-hour aged samples at 200°C. (Bottom panels) TEM images showing the Q-phase rod-like precipitates and larger silicon particles..... | 41 |
| Figure 41. Atom probe measurements (left and top right) with iso-surfaces of: MgSi (purple) outlining Q phase, Cu (orange) outlining θ' , and Si (green) for 3 and 72-hour aged samples at 200°C..... | 42 |
| Figure 42. LEAP results showing Q-phase particles in Q-alloy with elemental addition samples aged for 24 hours at 200°C. WQ+Mn also shows the existence of alpha-Fe particles..... | 42 |
| Figure 43. Proxigrams across Q-phase precipitate boundary in Zn and Ni-containing Q-alloy samples hours at 200°C. WQ+Mn also shows the existence of alpha-Fe particles..... | 43 |
| Figure 44. Isothermal hardness profiles of alloy additions..... | 44 |
| Figure 45. LEAP and TEM validation of phase boundaries for the Q-phase..... | 45 |
| Figure 46. 200°C aging simulation versus micro-hardness measurements..... | 46 |
| Figure 47. 250°C aging simulations versus micro-hardness measurements..... | 47 |
| Figure 48. An image of the casting for evaluation of susceptibility to hot tearing..... | 53 |
| Figure 49. Model predictions and experimental hot tear resistance results for cast commercial baseline and new prototype high-temperature alloys..... | 54 |
| Figure 50. Images of hot tear castings that were performed at WPI..... | 54 |
| Figure 51. Hot cracking tendency for selected high-temperature cast Al alloy compositions..... | 54 |
| Figure 52. A full-scale cylinder head casting from a new alloy composition that was developed during the present CRADA project..... | 55 |
| Figure 53. Materials-by-design approach used for design of new valves alloys..... | 58 |
| Figure 54. Yield strength of some of the new ORNL alloys at 950°C exceed that of Alloy 520..... | 59 |
| Figure 55. Effect of temperature on the weight change measured in 1-hour cycles in air + 10% water vapor environment: (a) 900°C and (b) 950°C..... | 61 |
| Figure 56. Effect of reactive elements additions on oxidation behavior of an ORNL alloy in 1-hour cycles at 950°C in | |

| | |
|---------------------------------------------------------------------------------------------------------------------------------------------------------------------------------|----|
| air+ 10% water vapor. | 61 |
| Figure 57. Effect of alloy composition on the oxide scale after 500-hour exposure to air + 10% water vapor environment at 950°C: (a) Alloy 751 and (b) Alloy 161-12M. | 62 |
| Figure 58. Work plan focus areas for PNNL and FCA US LLC. | 65 |
| Figure 59. Standard NH ₃ -SCR light-off curves for the fresh Cu/SSZ-13 samples: addition of Na to 1%Cu/SSZ-13 (left), and addition of Na to 3%Cu/SSZ-13 (right)..... | 67 |
| Figure 60. Standard NH ₃ -SCR light-off curves for the Cu/SSZ-13 samples prepared in various batches..... | 67 |
| Figure 61. Light-off curves for CO, three HCs, and NO _x using a commercial three-way catalyst for gasoline vehicles. | 70 |
| Figure 62. Confirmation of catalyst structures using the Talos electron microscope at ORNL..... | 71 |

List of Tables

| | |
|-------------------------------------------------------------------------------------------------------------------------------------------------------------------------------------------------|----|
| Table 1. Target operating conditions for the EGR coolers. | 9 |
| Table 2. Prediction and measured Q-phase fraction at 200°C. | 47 |
| Table 3. A comparison of mechanical properties between DOE targets and Q-phase alloy. All high-temperature measurements made after 200 hours of conditioning at test temperature. | 48 |
| Table 4. A comparison of tensile properties measured in head castings compared to DOE targets and a 356 alloy cast into chill plates. Head properties made after 100 hours of conditioning..... | 49 |
| Table 5. Temperatures for 90% conversion of carbon monoxide, HCs, and nitrogen oxide..... | 72 |
| Table 6. Milestones for Budget Period 1 | 76 |
| Table 7. Milestones for Budget Period 2 | 78 |
| Table 8. Milestones for Budget Period 3 | 78 |
| Table 9. Milestone status in 2016..... | 79 |

(This page intentionally left blank)

Project-Materials for Hybrid and Electric Drive Systems

Agreement 23726 – Novel Manufacturing Technologies for High-Power Induction and Permanent Magnet Electric Motors (GM CRADA)

Glenn J. Grant
Principal Investigator
Materials Processing
Applied Materials and Performance
Pacific Northwest National Laboratory (PNNL)
902 Battelle Boulevard, K2-03
Richland, Washington 99356
Phone: (509) 375-6890; fax: (509) 375-4448
E-mail: glenn.grant@pnnl.gov

Blair E. Carlson
Manager, Lightweight Materials Processing
General Motors (GM) Research and Development
30500 Mound Road
Warren, Michigan 48090
E-mail: blair.carlson@gm.com

DOE Technology Manager: Jerry L. Gibbs
Phone: (202) 586-1182; fax: (202) 586-1600
E-mail: jerry.gibbs@ee.doe.gov

Field Technical Manager: Darrell Herling
Phone: (509) 375-6905; fax (509) 375-2186
E-mail: Darrell.herling@pnnl.gov

Contractor: PNNL
Prime Contract No.: DE-AC05-76RL01830

Objective

- To develop and deploy high-power induction and permanent magnet rotors and stators that are lighter weight, have better cooling, and are a lower cost to manufacture through application of novel solid-state joining and fabrication technologies.
- To apply solid-state processing techniques for improving performance of a low-cost, soft, magnetic material used in the rotors of high-power induction motors.

Approach

- Develop solid-state joining techniques and manufacturing processes that will increase the efficiency of electric motors through lightweighting; improvements in electric and magnetic properties; and improvements in assembly space efficiency, packaging, and cost.

- Develop the friction-stir welding (FSW) process parameters and evaluate proper tool materials and techniques to produce defect-free FSWs in copper (Cu) alloys specified by project partners.
- Develop a fundamental understanding of solid-state joints between Cu materials. This fundamental knowledge is expected to lead to strategies and techniques that will be used to produce a joining process with low thermal input and low distortion of adjacent parts and to produce joints with a high degree of structural integrity and with high thermal and electrical continuity.
- Using fundamental information gained, develop techniques to manufacture copper rotor and stator assemblies for high-power induction and permanent magnet motor systems. Joined or processed components will be evaluated and tested by industry collaborators to demonstrate efficiency benefits and commercial applications.
- Transfer performance data and manufacturing technology to industry through a cooperative research and development agreement (CRADA) with GM, ensuring a clear path to commercialization.

Milestones, Metrics, and Accomplishments

- **Milestone:** Apply software for producing a temperature-controlled weld in a full-size rotor end cap weld that can hold weld temperature to within $\pm 5^{\circ}\text{C}$ during the weld – completed.
- **Milestone:** Complete full-sized, weld defect and exit hole free rotor cage assemblies and submit to GM for electrical efficiency testing – completed.
- **Milestone:** Test the viability of modified end cap designs through experimental weld trials – completed.
- **Milestone:** Complete construction of a stationary shouldered tool assembly and demonstrate that defect-free welds can be made within 4 mm of the weld fixture wall, minimizing material wastage and part deformation – in process.
- **Future Milestone:** Optimize tool design features to increase welding speed and the processing parameter envelope – completed.
- **Future Milestone:** Complete weld trials of “reduced-copper” lightweight end cap designs and transfer all process data and results to GM – in process.

Introduction

The purpose of this project is to develop and deploy high-power induction and permanent magnet rotors and stators that are lighter weight, have better cooling, and are a lower cost to manufacture through the application of novel solid-state joining and fabrication technologies. Barriers to achieving these objectives that focus on the manufacturability of novel rotor designs have been identified. The project team will apply FSW to join copper subassemblies and to eventually produce prototype lightweight, high-efficiency rotor assemblies. Fundamental work tasks will first focus on Cu/Cu FSW joints. Later tasks will involve full rotor assembly and testing by GM. The project is a cost-shared CRADA between PNNL and GM.

Background

New manufacturing techniques can cause step changes in the overall cost of manufactured assemblies if the new technique creates a fundamental shift in the way a subsystem is constructed. For example, an electric motor has numerous components that are sensitive to high temperature. Fusion welding, which requires a very high

temperature to melt the materials being joined, cannot be accomplished directly adjacent to heat-sensitive parts (e.g., sensitive electronics, wiring, and insulation) or where coated laminates or substrates are located nearby. This restriction might require the part to be assembled through a much more complicated multi-step process. If another joining technology were available that did not heat the part, then the multi-step assembly could be avoided, thus saving cost.

One example of a joining technology that could satisfy the need for lower adjacent part temperatures is FSW. Previous work by PNNL and others has shown that FSW can be made in Cu alloys that have excellent mechanical, electrical, and thermo-mechanical performance. FSW has a particular advantage in welding Cu due to the wide range of weld-specific energy levels that can be applied by the process. Conventional fusion welding must deliver a high level of energy to melt the Cu on each side of the joint line. In many applications, the high part temperatures during fusion welding can lead to distortion or overheated adjacent parts. Often, Cu joining is required in assemblies where heat-sensitive electronics, wiring, or coated laminates or substrates are located nearby. FSW may provide a lower heat input joining technique in these special applications where adjacent parts in the assembly can be damaged.

Approach

The project will develop FSW process parameters and evaluate proper tool materials and techniques to produce defect-free FSWs in Cu alloys specified by project partners. In addition, the project team will develop statistical confidence around the manufacturing process used to fabricate high-power induction motor rotor assemblies by applying a set of mechanical test methods and procedures to evaluate process robustness.

This project primarily will focus on solid-state joining of Cu materials used in rotor assemblies of high-power induction motors.

The primary scope is to develop a weld process for joining the Cu end cap to the shorting bars that traverse the soft magnetic core of the rotor. These bars carry current up and down the rotor between the end caps to produce the magnetic moment that drives the rotor. The joint has several important characteristics. It needs strength because it will be subjected to high-tensional and cantilever loads when the rotor is moving at high rotations per minute (RPM); it also needs to have optimum electrical conductivity for high efficiency and, during the joining operation, it cannot get hot enough for the underlying electric steel laminates to damage their insulating coatings. Figure 2 shows a schematic of a rotor and a photo of a rotor end cap in place on the shorting bars just prior to joining.

Maximum electrical continuity is one of the key factors in rotor efficiency and lightweighting. The joint must be designed for the highest electrical cross-section at the minimum weight penalty. The thickness of the heavy Cu end cap is a key variable for optimization. Having the minimum end cap thickness

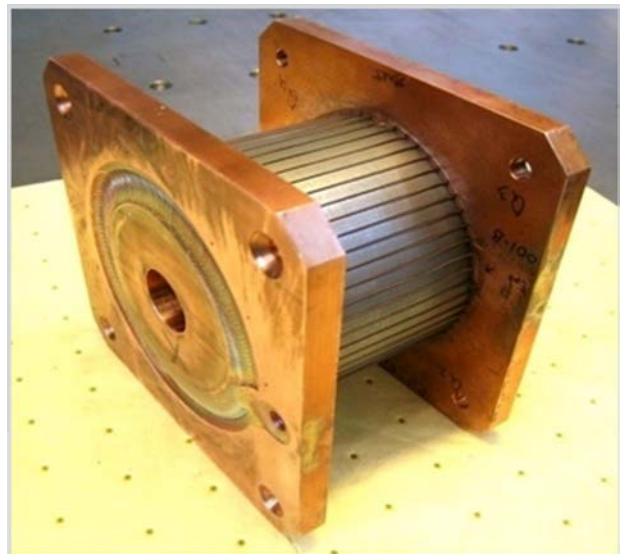


Figure 1. Initial rotor concepts fabricated with FSW.

for weight savings is desired, but so is the highest electrical cross-section for current flow. This requires the joined region to have the largest possible area between the end cap and the shorting bar. Figure 3 schematically shows the challenge. The joined area intersecting the end cap and shorting bar must have a maximum width and appropriate depth. The better the electrical continuity and current flow in this area, the thinner the end cap and the greater the weight savings. Much of the work during 2015/2016 was directed at creating a FSW joint that satisfies these demands. The joined area is a function of tool design, tool materials, process parameters, and boundary conditions during welding.

Results

The most significant milestone achieved during the 2015/2016 time period was manufacturing of the first, full-size, exit hole-free rotor cage assembly. This was the final step in a progressive development sequence from linear weld configuration, to circular end cap configuration in a rotary table, to finally welding of the full-size rotor end cap. The welding parameters developed in each step served as a starting point for the next one, because they had to be adapted each time to compensate for the different heat boundary conditions and geometric welding difficulties. After welding, the rotor was submitted to GM for electrical testing.

Resistance of the rotor was measured at GM using a Cropico microhmmeter. The resistance across the joined Cu shorting bars and at 180 degrees diagonally from end cap to end cap was equivalent to current rotor designs and better than braze designs due to the continuous Cu-joined region.

The weld quality was also evaluated by inductive measurement, meaning- the bars are moved through a magnetic field and current is induced in the rotor bars. The rotor was evaluated for full disconnection of the bars at the weld sections within the end rings. The results indicated that 100% of the bars are fully welded in the end ring.

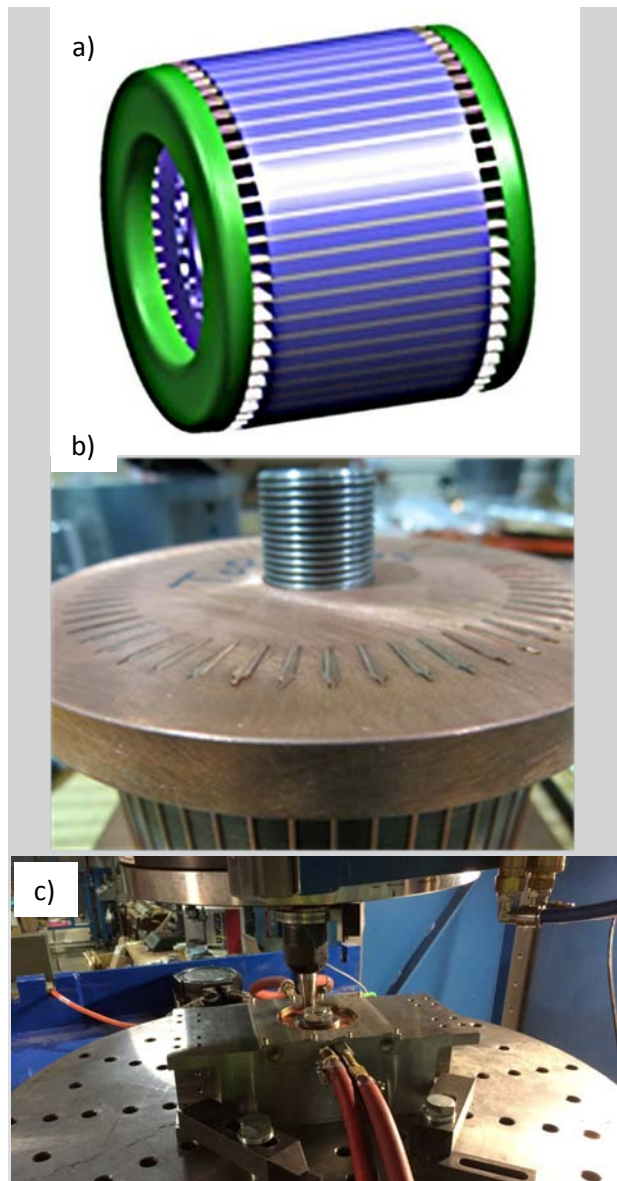


Figure 2. a) Rotor schematic, b) Cu end cap positioned on shorting bar ends prior to joining, and c) friction-stir tool and rotor in a fixture prior to welding.

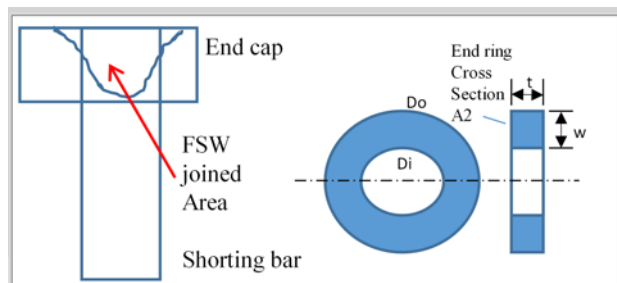


Figure 3. Schematic of end cap/shorting bar joined area.

The FSW rotor passed all electrical screening tests with excellent performance metrics.

Tool Temperature Management

In order to achieve the performance milestone, the weld development required application of an adaptive power control system for tool temperature management. Figure 7 shows temperature and spindle speed measurements during weld of the full-size rotor end cap. The control algorithm is robust enough to keep tool temperature during the weld within $\pm 5^{\circ}\text{C}$. It can be observed that to keep the temperature constant, spindle speed continually decreases to adapt to the variations in thermal conditions as the weld progresses. In order to increase the response time to variations in temperature, the thermocouple location within the tool was changed from behind the tool pin to the shoulder surface. Sensitivity of the tool temperature measurement can be observed in small temperature oscillations. They are not the result of signal noise, but they are real temperature values. The number of oscillations directly correlates with the



Figure 4. FSW full-size rotor end cap.



Figure 5. Electrical resistance testing of the rotors at GM. Electrical clamps are connected, one on each end cap, across a bar.



Figure 6. Test setup at GM for detection of interrupted bars.

number of shorting bars that form the cage.

“Reduced Copper” End Cap Designs

During 2016, additional welding trials were started on rotors that used end caps of different dimensions, specifically increased inner hole sizes. These end caps use 25% less Cu, which saves weight in the rotating assembly (and cost) without affecting the electrical properties. Figure 8 shows the results of weld trials on one of these new reduced Cu designs.

Work also progressed on stationary shoulder welding. This technique allows the tool pin to create a weld very close to the edge of the fixture, which saves on machining time and cost to turn the rotor down to final diameter.

Conclusions

During Fiscal Year (FY) 2016, the project delivered full-sized rotors to GM for testing. These assemblies were tested with excellent electrical and mechanical results. The project also developed the necessary temperature control algorithms required to keep the weld process in control. Upcoming work to complete the project will include welding rotors that have less Cu in the end cap to decrease weight and cost in the assembly. We will also develop a FSW technique (i.e., stationary shoulder welding) that has the potential for welding close to the fixture edge, eliminating more Cu, and decreasing final machining time and cost. At the conclusion of the project, process data and reports will be delivered to GM for commercialization decisions.

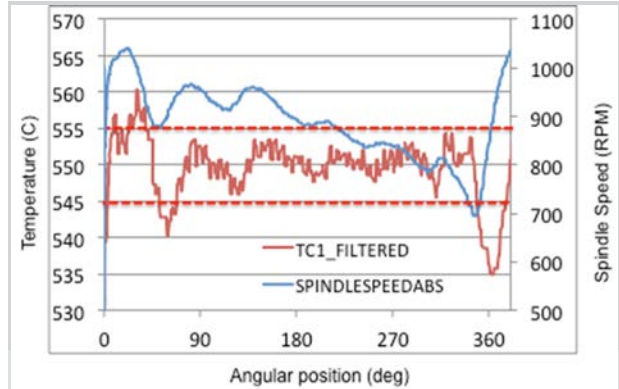


Figure 7. Tool temperature measurements and corresponding spindle speed as the weld progressed around the end cap.

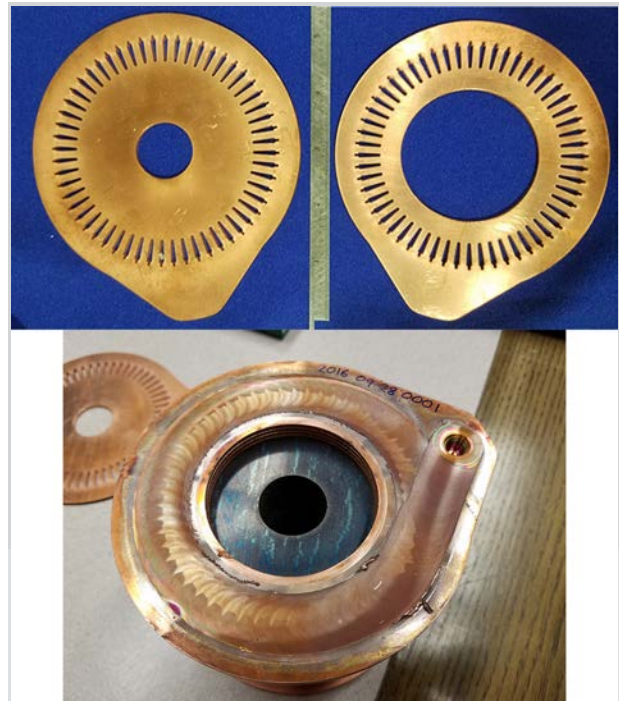


Figure 8. Larger inner hole on “reduced Cu” end cap design.

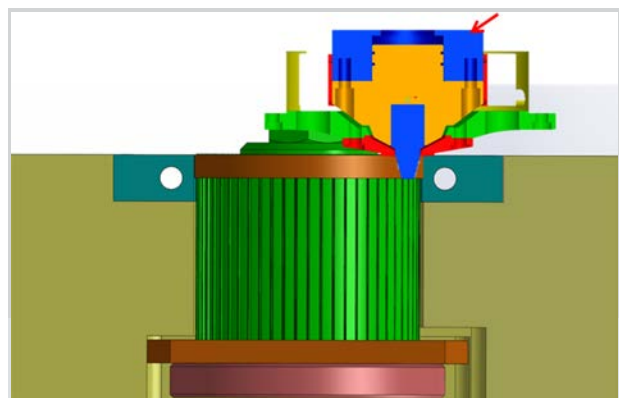


Figure 9. Schematic of stationary shoulder design.

Project-Materials for High-Efficiency Engines

Agreement 9105 – Materials Issues Associated with Exhaust Gas Recirculation (EGR) Systems

M. J. Lance
Ceramic Science and Technology Group
Oak Ridge National Laboratory (ORNL)
P.O. Box 2008, MS 6068, Building 4515
Oak Ridge, Tennessee 37831-6068
Phone: (865) 241-4536; fax: (865) 574-6098
E-mail: lancem@ornl.gov

DOE Technology Manager: Jerry L. Gibbs
Phone: (202) 586-1182; fax: (202) 586-1600
E-mail: Jerry.gibbs@ee.doe.gov

ORNL Technical Advisor: J. Allen Haynes
Phone: (865) 576-2894; fax: (865) 574-4913
E-mail: haynesa@ornl.gov

Contractor: ORNL, Oak Ridge, Tennessee
Prime Contract No.: DE-AC05-00OR22725

Objectives

- Provide information to industry about fouling deposit properties to enable improved models and potential design improvements for reducing fouling and its impact on the performance of exhaust gas recirculation (EGR) coolers.
- Develop a protocol for refreshing the EGR cooler during use or during service.

Approach

- Assemble EGR engineers from member companies of the diesel crosscut team to serve as an advisory board for this project.
- Determine novel cooler geometries that will promote deposit removal.

Accomplishments

- Used structured light optical profilometry to explore the effect of cooler geometry on deposit thickness on industry provided coolers.
- Deposit thickness was thinner on the upstream side of the peak in sinusoidal coolers. Preliminary measurements revealed that it also was thinner near turbulence structures on stamped winglet and spiral EGR tubes; this shows the importance of turbulence for controlling the deposit removal mechanism.

Future Directions

- Recommendations for improved EGR cooler design will be made by incorporating deposit removal into computational fluid dynamics models using our measurements as inputs.
- Coolers donated by industry will be revisited and deposit thickness measured. These coolers have a variety of designs, including segmented fins, spiral tubes, and stamped winglet designs that will provide a broad range of cooler geometries to compare to the sinusoidal fin studied here.

Introduction

One method used to control NO_x emissions is EGR, where a fraction of the exhaust is routed back to the engine combustion chambers via the engine intake and it acts to reduce combustion temperatures. The exhaust gas is normally cooled in a heat exchanger, or cooler, in order to enhance the EGR effect. Some particulate matter and hydrocarbon (HC) present in the exhaust gas will form a deposit inside the EGR cooler through thermophoresis and condensation, respectively. The deposit is an excellent thermal insulator [1] and will significantly decrease the effectiveness of the EGR cooler. In addition, as the deposit thickens, it will impede the flow of exhaust through the cooler leading to a loss in engine efficiency [2].

Previous studies have focused on deposit formation and removal on flat tubes [3-6]; however, less work has been reported on substrates with turbulated structures that are frequently used in production EGR coolers. Field-returned coolers have been observed to have microstructural features on the deposit surface, which suggest that deposit removal is occurring on the upstream side of the fin during operation where shear stresses are high [7]. Previous attempts to image EGR deposits nondestructively and thereby characterize how the turbulence structures impact deposition and removal using neutron tomography was successful for high-HC plugging deposits; however, it produced mixed results for low-density deposit layers that are far more common in the field [8].

At the start of this project, an advisory team consisting of engineers responsible for EGR systems was assembled from nine diesel engine manufacturers: Caterpillar, Cummins, Detroit Diesel, Ford, GM, John Deere, Navistar, DAF Trucks, and Volvo/Mack and one heat exchanger supplier, Modine. They were asked what the biggest problem facing EGR cooling systems is and the clear winner was fouling. Over the course of this project, the EGR team has been notified of the generated results and have contributed coolers for forensic analysis of fouling deposits.

This progress report describes experimental approaches that allowed for direct measurement of deposit location and thickness on full production EGR coolers fouled under various engine operating conditions. The deposit thickness was found to be highly non-uniform and varied with the underlying substrate temperature, the location along the sinusoidal fin, and engine operating conditions. These measurements suggest that EGR cooler geometry could be altered to mitigate fouling, either by retarding deposition or by promoting deposit removal.

Methods

A 9-L, heavy-duty engine and ultra-low sulfur diesel fuel was used to foul 20 EGR tube-in-shell coolers by varying five factors: (1) EGR flow rate, (2) EGR inlet gas temperature, (3) soot level, (4) HC concentration, and (5) coolant temperature. Table 1 shows the target operating conditions. A five factor, two-level design-of-experiments required 16 coolers to test all combinations; however, an additional four coolers were operated

using midpoints for some or all the factors for a total of 20 coolers. Coolers were run until the effectiveness stabilized (typically 40 to 70 hours), were cooled down to room temperature, and then run for an additional few hours in order to measure the change in effectiveness due to shut down. High HC could not be achieved with a high EGR inlet gas temperature due to burning the HC prior to entering the cooler. All testing was performed by John Deere, who is a member of the EGR advisory team.

Table 1. Target operating conditions for the EGR coolers.

| Factor | Low | Midpoint | High |
|-----------------------------------|------|----------|-------|
| EGR Rate (g/s) | 83.3 | 118.1 | 152.8 |
| EGR Inlet Gas Temperature (°C) | 350 | 450 | 550 |
| Smoke Level (Filter Smoke Number) | 0.5 | 1.25 | 2.0 |
| HC Concentration (ppm) | 25 | 50 | 75 |
| Coolant Temperature (°C) | 85 | 92.5 | 100 |

Each cooler had 12 oblong tubes bundled in a 6 x 2 pattern inside a shell that contained the coolant. Each tube was 480-mm long, 44-mm tall, and 7.6-mm wide. There were 20 fins inside each tube spaced about 2 mm apart from one another. Along the flow direction, the fins formed a sinusoidal wave with a wavelength of 10 mm and an amplitude of about 0.65 mm. All fins were in phase with one another, which resulted in a constant fin spacing down the cooler length.

Following testing, a single tube from the center of each cooler was extracted and sectioned into 25 19-mm long segments. A 19-mm long section from half-way down the length of each tube was opened by milling two lines running parallel to the exhaust flow on either side of the section to a depth of about 25 μm . The samples were carefully peeled open along these two lines, exposing the undisturbed deposit surface. At least one complete wavelength (i.e., 10 mm) of the sinusoidal wave of the fin was revealed in this manner. The surface profile was then determined using a Keyence VR-3100 optical profilometer, which measures height by illuminating bands of light on the surface. When the reflected light was collected from another angle, height differences on the surface appeared as distortions of the shapes of the incident light bands. Triangulation calculations were then performed to measure the surface height at each point to a resolution of about 1 μm across a field-of-view 17 x 24 mm, thereby allowing the entire three-dimensional surface profile of the sample to be acquired in less than 1 minute. Determination of deposit thickness using this profilometer will be described in more detail in the results section.

Results

Mounting the cooler sections in epoxy tended to collapse the deposit structure thereby preventing the direct measurement of thickness on these samples. To measure true deposit thickness and how it varied across a sinusoidal fin, height maps of the surface before and after removing the deposit were collected. Figure 10a shows the surface of a single fin coated with deposit and Figure 10b shows the same region after the deposit was cleaned off with a lint-free swab and vacuum. The sample was held in place with a vice that was affixed to the microscope stage to ensure the sample did not move during cleaning. The height maps before and after cleaning are shown in Figure 10(c) and 10(d), respectively. All height maps captured at least one complete wavelength of the sinusoidal fin (10 mm) and the entire fin width (7.6 mm).

Each pair of height maps were further processed by averaging height across the fin width (i.e., the vertical direction in Figures 10(c) and 10(d)) (Figure 11). The average height profiles were also corrected for any sample tilt and were re-zeroed. Figure 11 also shows deposit thickness along the length of the fin, which is generated by subtracting the height profile without the deposit from the profile with the deposit.

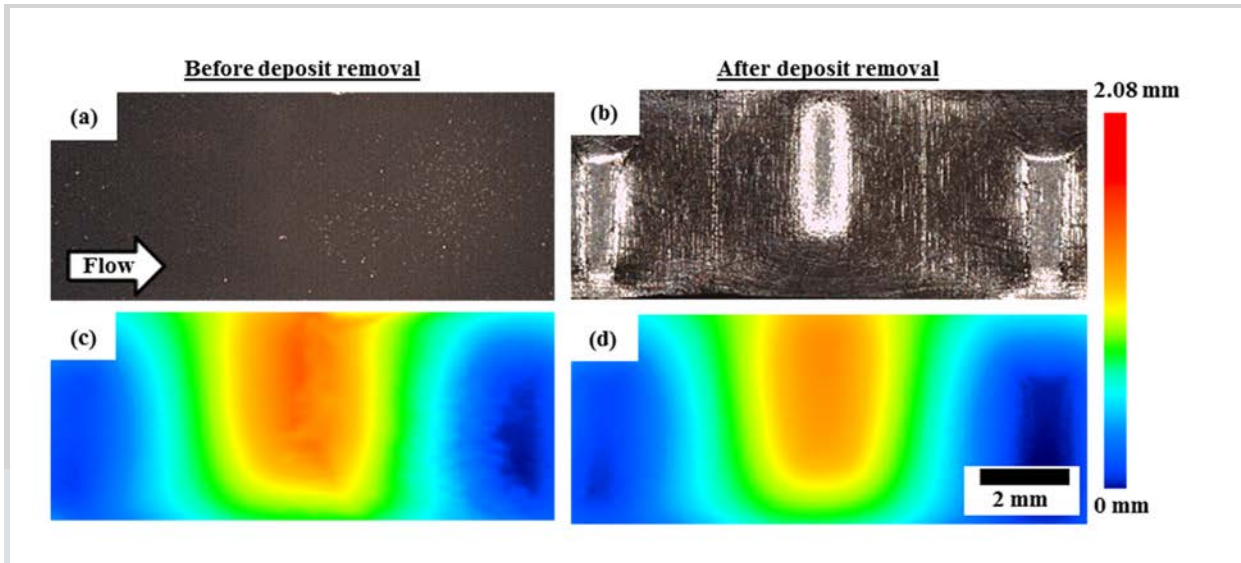


Figure 10. Optical image of (a) a fouled fin surface and (b) after the deposit has been removed, the corresponding height map of (c) the fouled fin surface and (d) the cleaned fin surface. The flow direction was left to right.

Figure 12 shows the deposit thickness measured using the above method averaged from all 20 coolers. The peak in the sinusoidal wave of the fin was set at 0 mm. Moving from left to right along the flow direction, the deposit thickness decreases after the valley in the fin sinusoidal wave (i.e., first blue line in Figure 12) and reaches a constant thickness of about 60 μm . Within 1 mm of the peak of the sinusoidal wave, the deposit thickness

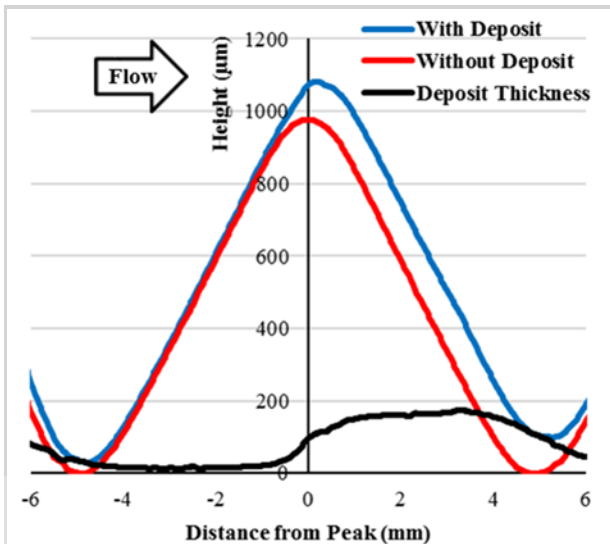


Figure 11. Surface height of maps from Figure 1(c) and 1(d) averaged across the fin width. The deposit thickness is also shown.

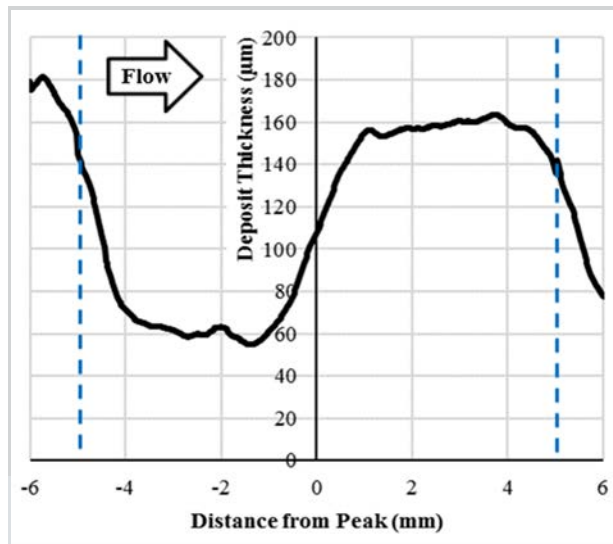


Figure 12. Deposit thickness versus distance from the peak in the fin averaged from all 20 coolers. The blue lines show the location of the valleys in the sinusoidal wave.

increases and reaches a thickness of about 160 μm approximately 1 mm downstream from the peak. The thickness remains constant until it decreases as it nears the next valley in the sinusoidal wave. The ratio of the deposit thickness from the upstream side of the peak (-5 to 0 mm) to the downstream side (0 to 5mm) was 2:1. Computational fluid dynamics modeling by Nagendra et al. [9] predicted a thinner deposit on the downstream side; this was the opposite of the results in Figure 12. Their model predicted that the impact of the exhaust gas against the upstream side of the fin would lead to a thinner boundary layer that increases the temperature gradient and thermophoretic deposition of particulate matter. However, the exhaust gas will also create shear forces on the upstream side of the fin, which may lead to lower deposition rates and deposit removal that were not included in the model. Indeed, microstructural evidence of deposit removal has been observed on field-returned coolers [7], suggesting that shear removal must be considered when modeling fouling in EGR coolers.

Based on Figure 12, a useful parameter for determining the effect the five factors in Table 1 had on deposit location is to divide the total deposit thickness on the upstream side by the downstream side. The only factor that significantly affected this parameter was the smoke level (Figure 13). Higher smoke levels made the deposit thickness more uniform along the sinusoidal wave, reducing the effect of the cooler geometry. The lowest smoke level had almost no deposit on the upstream side of the fin, showing that fouling had hardly occurred there. This cooler also had the lowest pressure drop and highest heat transfer. Conversely, the deposit that formed using the highest smoke level was uninfluenced by the sinusoidal wave of the fin; this shows that with enough particulate matter in the exhaust, the deposition rate exceeds the removal rate and fouling will proceed in an uncontrolled manner. This cooler also had the highest pressure drop and lowest heat transfer.

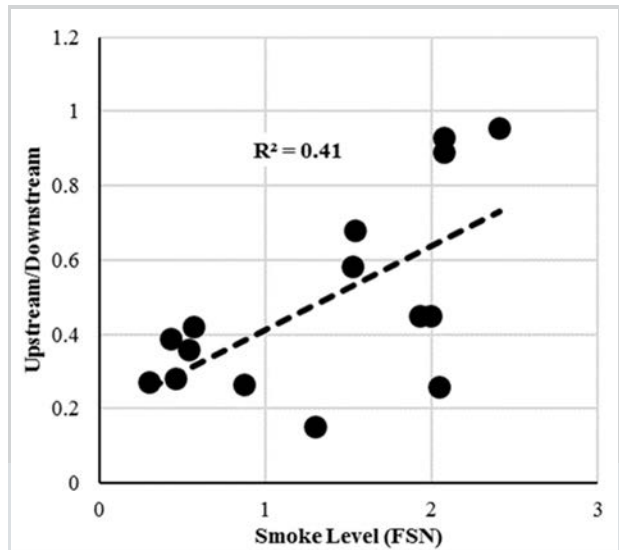


Figure 13. Ratio of deposit thickness on the upstream side of the peak to the downstream side versus smoke level.

Industry-provided coolers that had a spiral geometry were also measured using structured light profilometry. Figure 14 shows deposit thickness and the metal substrate height measured along the exhaust flow direction in this tube. The results show that the spiral bumps coincide with a thinner deposit. This compares well to observations made on deposits formed on sinusoidal-wave geometries, which also appear thinner adjacent to the peak in the sine wave. It is speculated that turbulence structures produce thinner deposits by promoting shear removal of the deposit by exhaust gas during operation. Observing these phenomena on EGR cooler designs that are not the standard sinusoidal-wave geometry broadens our understanding of the role of turbulence structures and will be used in future modelling efforts of EGR cooler fouling.

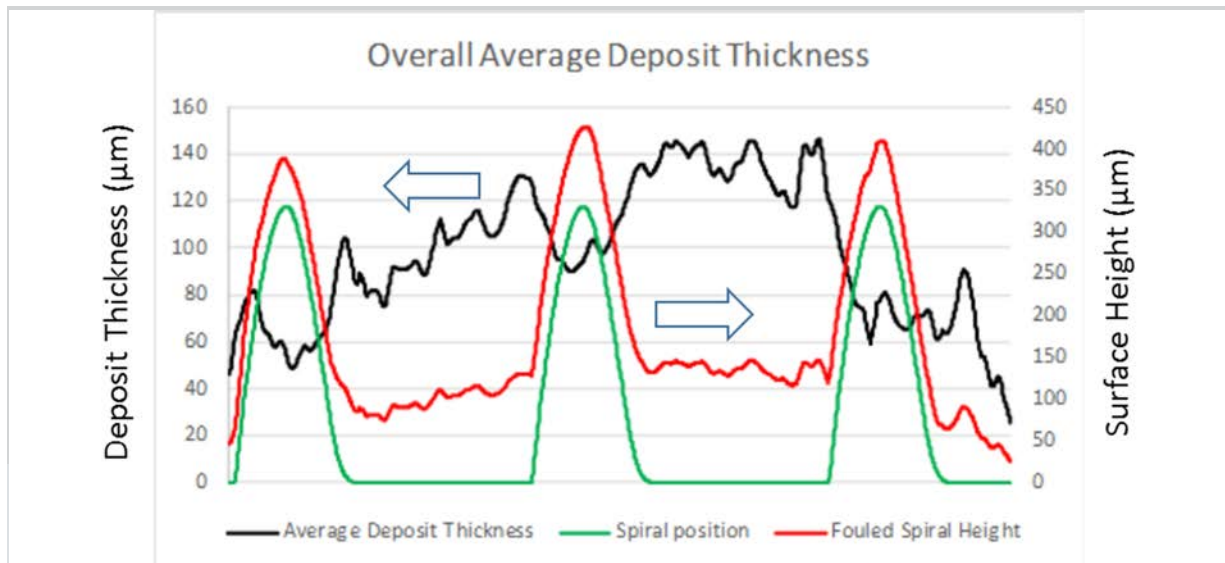


Figure 14. Fouled spiral height, spiral location, and deposit thickness along the tube length. The x-axis covers 1-in. along the tube. These data are the average of four different tube sections.

Summary/Conclusions

EGR coolers were fouled by varying five engine operating conditions using a 9-L, heavy-duty engine. Top-down measurement of deposit thickness on sinusoidal fin surfaces was used to measure the deposit location in fouled EGR coolers. Deposit thickness measurements along the sinusoidal fin surface showed twice as much deposit on the downstream side of the peak in the fin than the upstream side; this contradicted some computational fluid dynamics (CFD) modeling and illustrated the importance of shear forces and cooler geometry in fouling. Operating conditions that generate high levels of particulate matter overwhelmed the beneficial effects cooler geometry has on deposit removal.

References

- Abarham, M., P. Zamankhan, J. W. Hoard, D. Styles et al., 2013, "CFD analysis of particle transport in axisymmetric tube flows under the influence of thermophoretic force," *International Journal of Heat and Mass Transfer* 61: 94-105, doi:10.1016/j.ijheatmasstransfer.2013.01.071.
- Abd-Elhady, M. S. and M. R. Malayeri, 2013, "Asymptotic characteristics of particulate deposit formation in exhaust gas recirculation (EGR) coolers," *Applied Thermal Engineering* 60(1-2): 96-104, doi:10.1016/j.applthermaleng.2013.06.038.
- Han, T., H. Sul, J. Hoard, C.-K. Kuan et al., 2016, "The Effects of Temperature, Shear Stress, and Deposit Thickness on EGR Cooler Fouling Removal Mechanism - Part 1," *SAE International Journal of Materials Manufacturing* 9(2): 236-244, doi:10.4271/2016-01-0183.
- Hoard, J., M. Abarham, D. Styles, J. M. Giuliano et al., 2008, "Diesel EGR Cooler Fouling," *SAE International Journal of Engines* 1(1): 1234-1250, doi:10.4271/2008-01-2475.
- Lance, M. J., C. S. Sluder, H. Wang, and J. M. E. Storey, 2009, "Direct Measurement of EGR Cooler Deposit Thermal Properties for Improved Understanding of Cooler Fouling," SAE Technical Paper 2009-01-1461, doi:10.4271/2009-01-1461.

- Lance, M. J., C. S. Sluder, S. Lewis, and J. Storey, 2010, "Characterization of Field-Aged EGR Cooler Deposits," *SAE International Journal of Engines* 3(2): 126-136, doi:10.4271/2010-01-2091.
- Lance, M. J., H. Bilheux, J.-C. Bilheux, S. Voisin et al., 2014, "Neutron Tomography of Exhaust Gas Recirculation Cooler Deposits," SAE Technical Paper 2014-01-0628, doi:10.4271/2014-01-0628.
- Nagendra, K., D. K. Tafti, and A. K. Viswanathan, 2011, "Modeling of soot deposition in wavy-fin exhaust gas recirculator coolers," *International Journal of Heat and Mass Transfer* 54(7-8): 1671-1681, doi:10.1016/j.ijheatmasstransfer.2010.10.033.
- Sluder, C. S., J. M. E. Storey, and M. J. Lance, 2014, "Effectiveness Stabilization and Plugging in EGR Cooler Fouling," SAE Technical Paper 2014-01-0640, doi:10.4271/2014-01-0640.

Publications and Presentations

- Lance, Michael J., 2016, "Materials Issues Associated with EGR Systems," *U.S. DOE Vehicle Technologies Office 2016 Annual Merit Review and Peer Evaluation Meeting*, Washington D.C., June 9, 2016.

Project-Materials for High-Efficiency Engines

Agreement 9105 – Biofuel Impact on After-treatment Devices

M. J. Lance and T. J. Toops*
Ceramic Science and Technology Group
ORNL
P.O. Box 2008, MS 6068, Bldg. 4515
Oak Ridge, Tennessee 37831-6068
Phone: (865) 241-4536; fax: (865) 574-6098
E-mail: lancem@ornl.gov
*Fuels, Engines, and Emissions Research Center, ORNL

DOE Technology Manager: Jerry L. Gibbs
Phone: (202) 586-1182; fax: (202) 586-1600
E-mail: jerry.gibbs@ee.doe.gov

ORNL Technical Advisor: J. Allen Haynes
Phone: (865) 576-2894; fax: (865) 574-4913
E-mail: haynesa@ornl.gov

Contractor: ORNL, Oak Ridge, Tennessee
Prime Contract No.: DE-AC05-00OR22725

Objectives

- To characterize, diesel oxidation catalyst (DOC), diesel particulate filter (DPF), and selective catalytic reduction (SCR) devices following exposure to elevated levels of metal contaminants present in biodiesel in order to identify the deactivation and degradation mechanisms that may occur in emissions control devices operated with biodiesel fuel.

Approach

- Use state-of-the-art characterization tools within the High-Temperature Materials Laboratory to analyze the degradation mechanisms occurring in emissions control devices that underwent accelerated aging in biodiesel received from our collaboration with Cummins, the National Renewable Energy Laboratory (NREL), the Manufacturers of Emission Controls Association, and the National Biodiesel Board.

Accomplishments

- DOC: Laboratory diagnostics suggested that sodium (Na) contamination is not a key factor in the degradation of NO oxidation. Degradation was likely caused by phosphorus (P) contamination and hydrothermal aging.
- DPF: The increase in ash content from biodiesel was shown to shorten the DPF maintenance interval to an unacceptable level. The decline of catalytic function during aging was due to increased ash accumulation, P inhibition, or observed platinum group metals (PGM) sintering.
- SCR: When SCR is downstream of DPF, there is little Na contamination of SCR. The observed SCR activity loss is consistent with low levels of platinum (Pt) contamination possibly caused by an atypical thermal event.

Future Directions

- Fresh versions of the same after-treatment devices will be tested using a stationary genset for much lower cost, which allows us to test with and without fuel dopant to isolate the effect of Na.
- A used catalyst system from a truck that uses mainly B20 will be acquired and compared to our accelerated-aging samples.

Introduction

Alkali and alkaline earth metals can potentially enter diesel fuel from refinery salt driers, tank water bottoms, pipeline corrosion inhibitors, or seawater used as tanker ballast. Biodiesel (i.e., fatty acid methyl esters) is another potential source because Na or potassium (K) methoxide catalyzes the reaction of vegetable oils with methanol to form methyl esters. Residual amounts of Na or K can remain in the biodiesel, and small amounts of calcium or magnesium (Mg) can also contaminate biodiesel from the purification process [1, 2]. Both Na + K and calcium + Mg are limited to no more than 5 ppm in American Society of Testing and Materials D6751, “Standard Specification for Biodiesel Fuel Blend Stock (B100) for Middle Distillate Fuels” [3]. These metal contaminants can form an inorganic ash consisting of oxides, sulfates, hydroxides, or carbonates in the combustion process, which is then deposited onto exhaust emission control devices. Alkali metals are well known for poisoning certain catalysts and impacting the mechanical properties of ceramic substrates [4, 5]. Furthermore, alkali metal hydroxides are volatile in the presence of steam and can penetrate the catalyst washcoat or substrate or potentially move from one emission control system component to another.

Research has examined the long-term durability impacts of biodiesel on emission control systems. Engine dynamometer testing that simulated 120,000 miles of use in a light-duty car showed no negative impacts on DPF or oxides of nitrogen (NO_x) adsorber catalyst durability for a commercial biodiesel (B20 blend) [6]. Similar testing of a urea SCR catalyst demonstrated no catalyst activity loss in comparison to conventional diesel, although both the diesel and B20-exposed systems experienced a relatively high degree of catalyst deactivation that the vehicle would not have been able to meet the Tier 2 Bin 5 emission standards at the end of the test [7]. Subsequent studies examined the impact of residual metals (i.e., Na, K, Mg, and calcium) that can be present in biodiesel and how these metals might impact catalyst durability. In a follow-up study, the emission control system on a Ford F250 truck was exposed to the equivalent of 150,000 miles of a biodiesel (B20) exhaust containing Na, K, or calcium [8]. The system included a DOC, a urea SCR catalyst, and a DPF mounted on the engine in that order.

Over the course of the catalyst aging, no activity loss or increase in emissions from the truck was observed. However, detailed investigation of the fate of the metals on the catalysts and the activity at different locations in the catalyst parts showed significant impact. Bench flow reactor experiments conducted on samples taken from aged SCR catalysts showed that parts exposed to Na and K (the first few centimeters of the catalyst monolith) had reduced activity. Bench flow reactor and electron probe microanalysis (EPMA) of the DOCs also showed signs of deactivation for parts exposed to Na and K. These results imply that heavy-duty truck systems with longer lifetimes and exposure to a larger volume of exhaust may prove more sensitive to these contaminants. The metals aging study accelerated catalyst exposure by doping the fuel with high levels of metal. A related study investigated the possibility that this approach to accelerated aging created deactivation modes that would not be observed at normal fuel metal levels [9]. Results showed that beyond a certain threshold, the acceleration rate creates an artificial mechanism for catalyst deactivation.

Research has also examined the impact of biodiesel metals on heavy-duty catalyst system deactivation. Fuel doped with high levels of biodiesel metals was burned in an engine and used to expose heavy-duty catalyst parts to the equivalent of 435,000 miles of metals [10]. The system consisted of a DOC, DPF, and urea SCR mounted on the engine in that order. No evidence of SCR catalyst deactivation was observed, but some degradation of DOC activity and of DPF thermal shock resistance was observed. However, at the time this study was conducted, heavy-duty emission control systems were in development and not yet commercially available. Engine and catalyst manufacturers anticipated that occasional temperature excursions to 850°C could occur and a fraction of catalyst aging time was spent at this very high temperature. After introduction of these systems into the market in 2010, manufacturers determined that temperatures above 650°C were rare if ever encountered. Thus, the catalyst and filter degradation observed in this study may have been an artifact of the very high temperatures utilized.

The Fiscal Year (FY) 2016 research described here used accelerated catalyst deactivation to determine the impact of Na on a commercial 2010 emissions-compliant emission control system operated to full-useful-life (FUL)-equivalent fuel exposure. Results indicate that the only adverse impact of Na was on total ash loading in DPF.

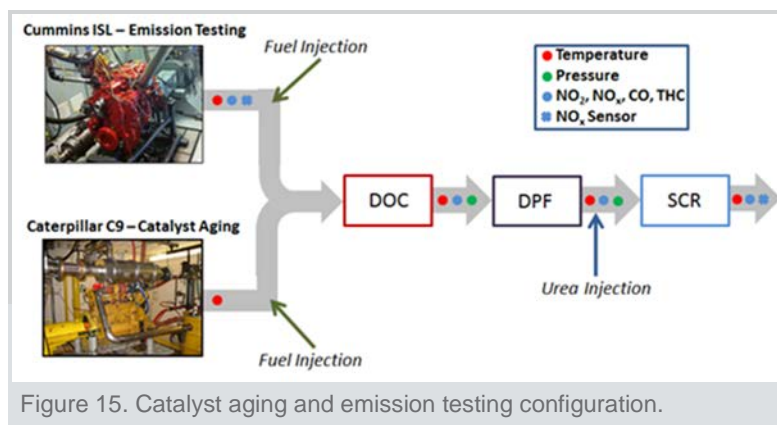
Methods

A full production exhaust system from a 2010 Cummins ISL engine was subjected to accelerated aging. The after-treatment devices from front to back were DOC, DPF, SCR, and an ammonia slip catalyst (ASC). Two identical exhaust systems were acquired: one to serve as a baseline and the second for accelerated aging. These parts were de-greened on the 2010 Cummins ISL engine using a 4-hour proprietary break-in cycle followed by five hot-start federal test procedure (FTP) cycles and six software-forced DPF regenerations.

Catalyst aging was conducted using a Caterpillar C9 ACERT engine in a dynamometer test cell at the SGS-Environmental Testing Center in Denver, Colorado. The FTP emissions evaluation was performed on the 2010 Cummins ISL at NREL’s Renewable Fuels and Lubricants Laboratory in a dynamometer test. Engine intake air temperature, pressure, and humidity were controlled. NO_x emissions were measured by chemiluminescence, carbon monoxide (CO), and carbon dioxide by nondispersive infrared and unburned HC by continuous flame ionization detector.

The engine and emission control system configuration is shown in Figure 15. Note the Cummins engine was never operated on B20 or Na-doped fuel during this test program. Temperature and pressure were monitored at the outlet of each after-treatment device.

The aging fuel was B20 doped with 14 ppm Na in the form of dioctyl sulfosuccinate Na salt, which resulted in 14 times the effective American Society of Testing and Materials (ASTM) limit (based on a B100 limit of 5 ppm Na). To reach FUL of 435,000 miles (i.e., a line haul truck with a fuel



economy of 6 mpg requires 72,500 gallons of B20 [435,000 miles/6.0 mpg]). Dividing this volume by 14 gives 5,179 gallons of B20 doped with 14 ppm Na to reach the FUL-equivalent Na exposure. The actual amount of fuel burned was 5,381 gallons, which is within 4% of the target amount. The lubricant (i.e., Chevron Delo LE SAE 15W-40) was changed at 250-hour intervals and oil consumption was quantified by weighing the oil before and after each oil drain interval.

FUL was simulated in 1,001 hours following the three-mode, 65-minute aging cycle shown in Figure 16. Each cycle included a 25-minute hold at a DOC outlet temperature of 260°C and DOC space velocity of 63K h⁻¹, a 25-minute hold at 380°C and a DOC space velocity of 133K h⁻¹, and a 15-minute ramp and hold at 550°C and a DOC space velocity of 89K h⁻¹. Once every five cycles, a high-temperature spike to 600°C for 200 seconds was included to simulate a temperature excursion during DPF regeneration. This aging cycle does not allow buildup of a normal soot cake, but simulates exposure to high temperatures for times that equate to FUL. This protocol was repeated for 923 cycles, resulting in 179 hours spent above 550°C. Urea was injected during the entire aging process with a target ammonia-NO_x ratio of 1.0.

Results

Engine Emissions Testing

The NO_x emissions measured using the FTP composite test on the Cummins ISL engine are shown in Figure 17. The FUL NO_x limit of 0.33 g/bhp-hour for this engine was reached before the 435,000-mile-equivalent aging was completed. This limit was exceeded about halfway into the test. This result was unexpected because Na-containing compounds should theoretically be in the form of particles that are trapped by the DPF prior to reaching the SCR. After aging was completed, hot-start FTP testing was conducted to assess the contributions of the DOC, DPF, and SCR to changes in the after-treatment system performance by systematically swapping aged for de-greened components. The results of this testing showed that all component after-treatment devices were impacted by the aging, but it was not clear from this systems-level test whether or not the degradation is due to Na or what the degradation mechanisms are for each individual component. Further analysis using bench reactor testing and materials characterization on the individual after-treatment components were carried out and are discussed in the next sections. Some of these results were discussed in last year's annual report and only more recent results will be shown here.

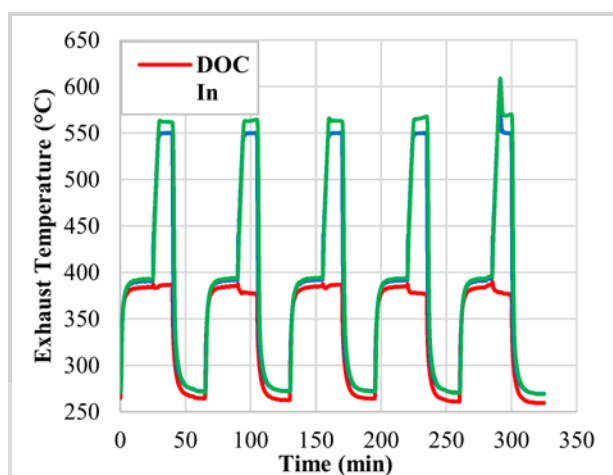


Figure 16. A five-cycle portion of the aging protocol.

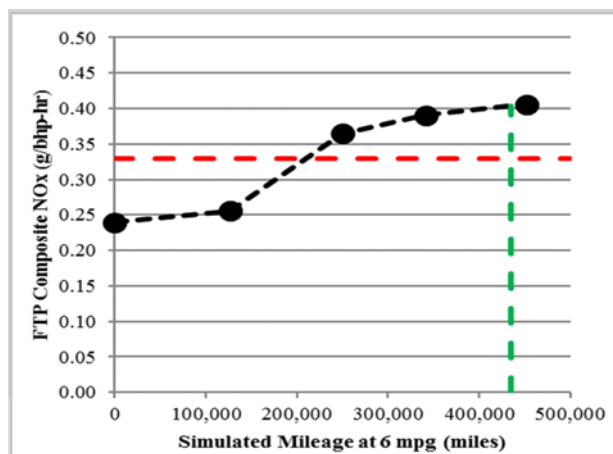


Figure 17. NO_x emissions test results. The red line indicates the FUL NO_x limit of 0.33 g/bhp-hour and the green line is the FUL limit of 435,000 miles.

Diesel Oxidation Catalyst Postmortem Analysis

During FY 2015, elemental analysis of aged micro-cores that had been cleaned using protocols developed at Cummins to remove Na, sulfur, and P one at a time revealed that P was the origin of DOC degradation. During the current fiscal year, additional analyses were performed using scanning transmission electron microscopy (STEM) to measure hydro-thermal aging and Na catalyst poisoning of the DOC samples.

Particle size analysis of STEM images was used to measure the Pt particle size (results shown in Figure 18). The aged inlet DOC sample had a slightly higher average Pt particle size of 4.9 ± 3.2 nm compared to 3.2 ± 1.7 nm for a fresh DOC and the distribution shifted to larger particle sizes. However, the Pt particle size near the outlet of the DOC was substantially larger at 19.0 ± 8.5 nm with some particles larger than 40 nm in diameter. This result shows that hydrothermal aging (i.e., Pt sintering) occurred predominantly at the DOC outlet. This is consistent with expectations, because HC oxidation over DOC during regeneration events results in higher temperatures toward the DOC outlet. This higher level of hydrothermal aging is also consistent with irreversible loss in the outlet DOC catalytic activity.

STEM combined with energy-dispersive x-ray spectroscopy elemental mapping was also used to assess the location of Na in relation to Pt in the washcoat. Figure 19 shows a map of Na and Pt where Na appears evenly distributed throughout the Al_2O_3 wash coat and has not segregated to the Pt surface. This assessment provides further evidence that Na is not poisoning the DOC catalyst. It should be noted that due to the overlap in the x-ray spectral lines of P and Pt, no imaging of the location of P in the washcoat could be performed.

Diesel Particulate Filter Postmortem Analysis

The fracture strength of DPF before and after aging is

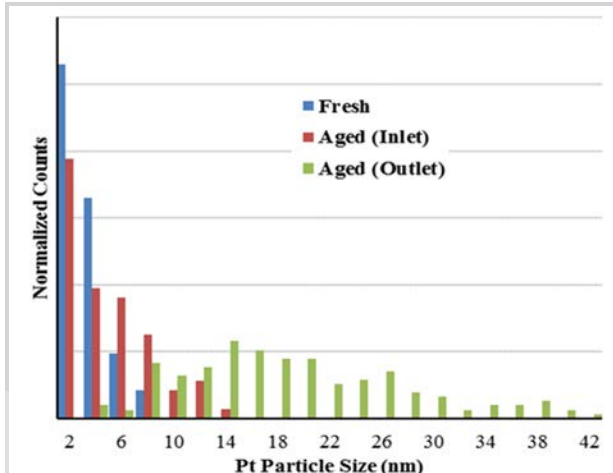


Figure 18. Pt particle size distribution in the DOC measured with STEM.

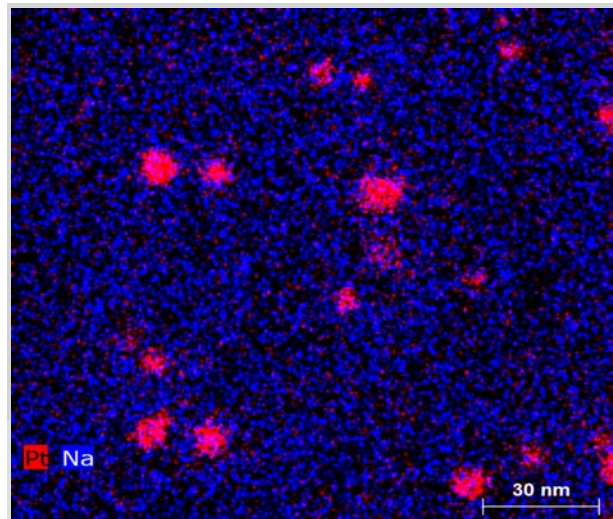


Figure 19. Elemental map of Pt (red) and Na (blue) from the inlet of the fully aged DOC.

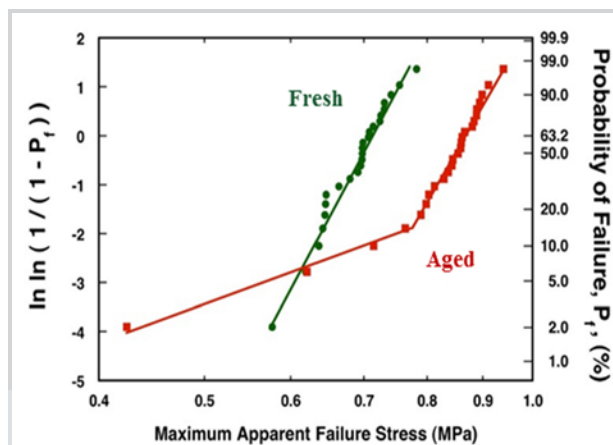


Figure 20. Weibull distributions of the failure stress of 25 tiles from the new and aged DPFs.

shown in the form of a statistical Weibull distribution plot in Figure 20, which represents data as probabilities to failure. The average apparent equibiaxial strengths of the fresh and aged DPF were 0.69 ± 0.05 MPa and 0.82 ± 0.11 MPa, respectively. This increase in average failure stress is due to a change in equilibrium state and may be due to ash imparting some strength to the cordierite structure. Of some concern are the two Weibull slopes for the aged DPF data in Figure 20, which may indicate that a second failure mechanism has been activated following aging. If the cause of the low-strength outliers was understood and consequently avoided, then the observed aging-induced strengthening would be beneficial to the thermal shock resistance of the cordierite.

The coefficient of thermal expansion (CTE) was measured before and after aging and is shown in Figure 21. All samples exhibited a decline in CTE at low temperatures, reaching negative values around 200°C and increasing at temperatures above that. A total of six samples were measured for each condition. However, owing to the difficulty of correctly seating the push rod onto the samples, only two runs from the aged and four from the fresh resulted in usable data. Of these, the two aged samples seemed to have higher CTEs between 200 and 400°C, but reached the same plateau as the fresh samples of about 2 ppm/°C at 600°C. This small difference is not likely to impact the thermal shock resistance, particularly when compared to the previous work, which showed a greater than 200% increase in CTE following FUL aging [10].

Figure 22 shows the PGM particle size distribution in the fresh and aged DPF washcoat measured by analyzing STEM images collected from samples generated by focused-ion beam. The PGM particle size increased from 4.0 ± 1.5 to 15.2 ± 3.5 nm following aging. These results show that some of the degradation of DPF NO oxidation performance is due to hydrothermal aging, which will coarsen the PGM particles, leading to a lower surface area available for catalysis.

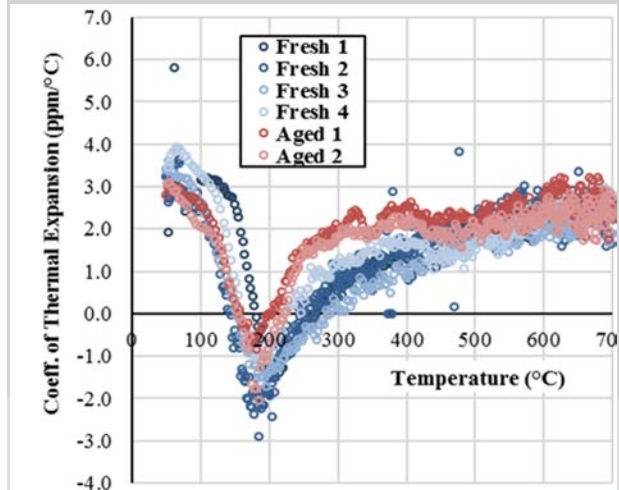


Figure 21. CTE of the fresh (blue) and aged (red) DPFs versus temperature.

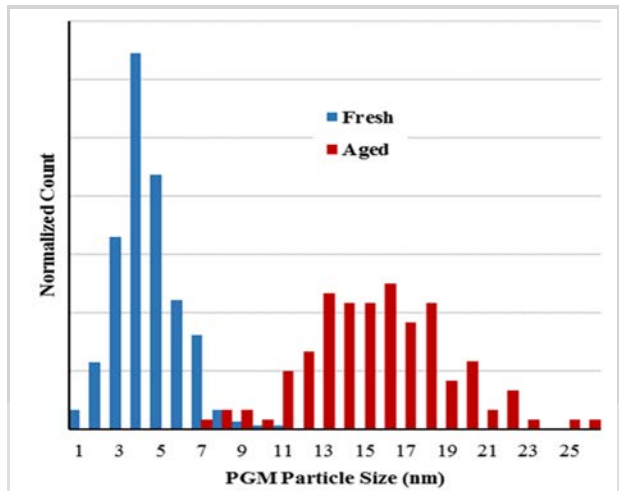


Figure 22. PGM particle size distribution in the fresh and aged inlet DPF washcoat.

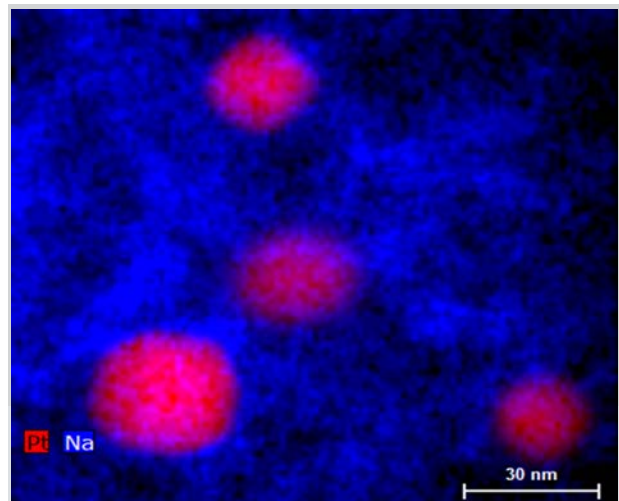


Figure 23. Elemental map of Pt (red) and Na (blue) from the inlet of the fully aged DPF.

Similar to the DOC map in Figure 19, an elemental map of the PGM particles in DPF was collected (Figure 23). Just as with DOC, Na did not appear to preferentially segregate to the PGM surface, which shows that Na is not directly poisoning the DPF catalyst.

Selective Catalytic Reduction Postmortem Analysis

Micro-cores taken from the 1,001-hour aged SCR were characterized on a bench reactor. The aged sample results are compared to a laboratory reference sample (de-greened 2 hours at 600°C) in Figures 24, 25, and 26, where NO_x conversion, ammonia (NH₃) oxidation, and N₂O formation are shown, respectively. The plot in Figure 24 shows that the NO_x conversion of the “as received” aged SCR sample is significantly lower than the laboratory reference over the entire temperature range. In addition, NH₃ oxidation and N₂O formation on the “as received” SCR catalyst is much higher than the laboratory-aged reference sample (Figures 25 and 26).

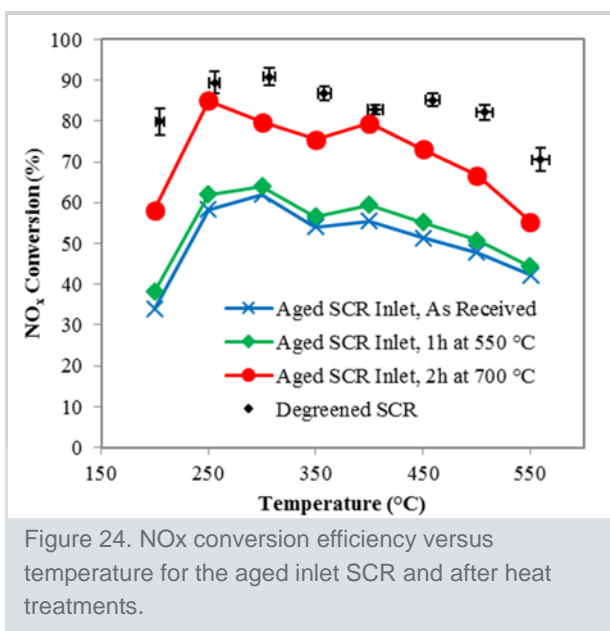


Figure 24. NO_x conversion efficiency versus temperature for the aged inlet SCR and after heat treatments.

Previous work [11] shows that S poisoning tends to cause NO_x performance degradation at temperatures below 350°C and reduced NH₃ oxidation activity at higher temperatures. The “as received” sample NO_x and NH₃ performance changes do not show these signatures and strongly suggest that S poisoning is not the key aging mechanism.

Previous work indicates that if the degraded performance was caused by HC deposits or coking effects, the performance would recover after exposure to 500°C for 1 hour [12]. Because the NO_x, NH₃, and N₂O performance did not change with treatment at 500°C for 1 hour, HC deposits or coking are not the root cause of the degraded performance.

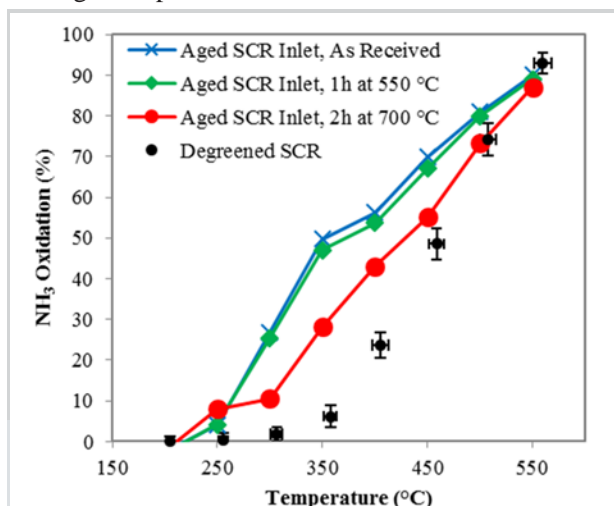


Figure 25. NH₃ oxidation versus temperature for the aged inlet SCR and after heat treatments.

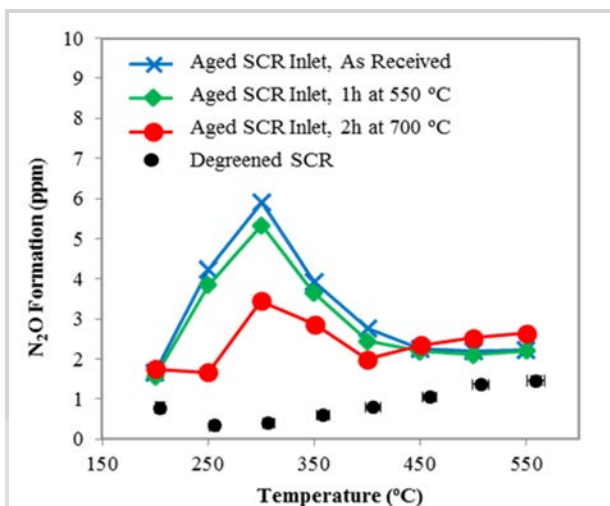


Figure 26. N₂O formation versus temperature for the aged inlet SCR and after heat treatments.

The NO_x , NH_3 , and N_2O performance all recover substantially toward the laboratory reference after exposure to 700°C for 2 hours. This recovery with high-temperature exposure indicates that the degraded “as received” performance is not caused by non-reversible hydrothermal aging. Instead, the combination of low NO_x performance, high NH_3 oxidation, and N_2O formation are consistent with the symptoms of Pt contamination on SCR catalyst (Chen et al.’s study [13]). In that study, the Pt poisoning on SCR catalysts could be unambiguously diagnosed if higher N_2O selectivity and poor NO_x conversion are seen at temperatures above 300°C because Pt acts to increase the redox activity of the catalyst. In addition, Chen et al.’s study shows that this redox activity is reduced upon exposure to high temperatures. It is speculated that the loosely deposited Pt sinters, leading to lower Pt activity. The SCR samples in this study, upon exposure to 700°C for 2 hours, show that the redox activity is reduced, entirely consistent with all symptoms of Pt contamination.

The quantitative elemental analysis using inductively coupled plasma-mass spectrometry on SCR also showed slightly higher amounts of precious metal compared with the baseline reference sample. Typically, Pt contamination is not observed unless there is a significant over-temperature event across the DOC/DPF. The trace amounts of precious metal deposited at the SCR inlet would oxidize NH_3 , thereby reducing the amount of NH_3 available to convert NO_x . This would lead to lower NO_x conversion, particularly at high temperatures, and could partly explain the higher than expected rise in tailpipe NO_x emissions over the aging cycle.

Summary/Conclusions

During this exhaustive study that examined the potential impact of biodiesel-based Na at the uppermost specification value over simulated FUL on a DOC/DPF/SCR heavy-duty emissions control system, it was determined that the only effect that can be directly attributed to Na is increased ash deposition in DPF. For the system used in this study, the increased ash content is up to 50% higher than would be expected for ultra-low sulfur diesel operation. The increased ash content is relevant because it may have a detrimental effect on the DPF ash cleaning interval. Several other deactivation mechanisms were observed in each device studied; however, they could not be directly correlated to increased Na exposure. For instance, both lube-oil-based P and fuel-borne Na were observed in DOC and, only upon removal of P, did DOC regain its activity to NO to NO_2 oxidation. In addition to increased ash accumulation, thermal aging of DPF resulted in sintered PGM in the washcoat. This sintering is known to also impact reactivity and would result in decreased NO to NO_2 oxidation across DPF. Additionally, the overall NO_x reduction functionality of the SCR catalyst was degraded even though no Na was observed in SCR. After a thorough investigation, it was determined that the likely reason for deactivation was PGM from the upstream DOC or DPF had deposited on the SCR catalyst. This deposition resulted in increased NH_3 oxidation and limited overall NO_x reduction. In the end, for emission control systems with DOC/DPF upstream of SCR, the concerns associated with Na in the fuel should focus on increased ash accumulation. Therefore, debate on whether the metal contamination specification for biodiesel should be lowered from its current limit should target DPF cleaning strategies and required frequency.

References

- Alleman, T. L. and R. L. McCormick, 2008, "Results of the 2007 B100 Quality Survey," NREL/TP-540-42787, National Renewable Energy Laboratory.
- Alleman, T. L., L. Fouts, and G. Chupka, 2013, "Quality Parameters and Chemical Analysis for Biodiesel Produced in the United States in 2011," NREL/TP-5400-57662, National Renewable Energy Laboratory.
- ASTM, 2012, "Standard Specification for Biodiesel Fuel Blend Stock (B100) for Middle Distillate Fuels," ASTM D6751, American Society for Testing and Materials International.
- Chen, X. et al., 2013, "Mitigation of Platinum Poisoning of Cu-Zeolite SCR Catalysts," *SAE International Journal of Engines* 6(2): 856-861.
- Cavataio, G. et al., 2009, "Laboratory Study to Determine Impact of Na and K Exposure on the Durability of DOC and SCR Catalyst Formulations," SAE International.
- Dou, D. and J. Balland, 2002, "Impact of Alkali Metals on the Performance and Mechanical Properties of NOx Adsorber Catalysts," SAE International.
- Kumar, A., K. Kamasamudram, and A. Yezerets, 2013, "Hydrocarbon Storage on Small-Pore Cu-Zeolite SCR Catalyst," *SAE International Journal of Engines* 6(2): 680-687.
- Kumar, A. et al., 2016, "Chemical deSOx: An effective way to recover Cu-zeolite SCR catalysts from sulfur poisoning," *Catalysis Today* 267: 10-16.
- Tatur, M. et al., 2008, "Effects of Biodiesel Operation on Light-Duty Tier 2 Engine and Emission Control Systems," *SAE International Journal of Fuels and Lubricants* 1(1): 119-131.
- Tatur, M. et al., 2009, "Biodiesel Effects on U.S. Light-Duty Tier 2 Engine and Emission Control Systems - Part 2," *SAE International Journal of Fuels and Lubricants* 2(1): 88-103.
- Williams, A. et al., 2011, "Impact of Biodiesel Impurities on the Performance and Durability of DOC, DPF and SCR Technologies," *SAE International Journal of Fuels and Lubricants* 4(1): 110-124.
- Williams, A. et al., 2013, "Impact of Fuel Metal Impurities on the Durability of a Light-Duty Diesel Aftertreatment System," SAE International.
- Williams, A. et al., 2014, "Effect of Accelerated Aging Rate on the Capture of Fuel-Borne Metal Impurities by Emissions Control Devices," *SAE International Journal of Fuels and Lubricants* 7(2).

Publications

- Lance, M., A. Wereszczak, T. J. Toops, R. Ancimer et al., 2016, "Evaluation of Fuel-Borne Sodium Effects on a DOC-DPF-SCR Heavy-Duty Engine Emission Control System: Simulation of Full-Useful Life," *SAE International Journal of Fuels and Lubricants* 9(3), doi:10.4271/2016-01-2322.

Presentations

- Lance, Michael J., Todd J. Toops, Andrew A. Wereszczak, Robert McCormick, Adam Ragatz, Richard Ancimer, Hongmei An, and Leigh Rogoski, 2015, "Impact of Metal Impurities in Biodiesel on Catalyst Durability," *Consortium to Optimize Lubricant and Diesel Engines for Robust Emission Aftertreatment Systems*, Massachusetts Institute of Technology, Cambridge, Massachusetts, September 29, 2015.
- Lance, Michael J., Todd J. Toops, Andrew A. Wereszczak, Robert McCormick, Adam Ragatz, Richard Ancimer, Hongmei An, and Leigh Rogoski, 2015, "Impact of Metal Impurities in Biodiesel on Catalyst Durability," *Biodiesel Technical Workshop*, October 21, 2015.

Lance, Michael J., Todd J. Toops, Andrew A. Wereszczak, Robert McCormick, Adam Ragatz, Richard Ancimer, Hongmei An, and Leigh Rogoski, 2015, "Impact of Metal Impurities in Biodiesel on Catalyst Durability," *Tenth International Congress on Catalysis and Automotive Pollution Control*, Brussels, Belgium, October 29, 2015.

Lance, Michael J., Todd J. Toops, Andrew A. Wereszczak, Robert McCormick, Adam Ragatz, Richard Ancimer, Hongmei An, and Leigh Rogoski, 2016, "Impact of Metal Impurities in Biodiesel on Catalyst Durability," *Advanced Engine Cross-cut Team Meeting*, January 14, 2016.

Lance, Michael J. and Todd J. Toops, 2016, "Biofuel Impacts on Aftertreatment Devices," *U.S. DOE Vehicle Technologies Office 2016 Annual Merit Review and Peer Evaluation Meeting*, Washington D.C., June 9, 2016.

Project-Integrated Computational Materials Engineering

Agreement 26391 – Applied Computational Methods for New Propulsion Materials – Future Engine Requirements

Charles E.A. Finney
Fuels, Engines, and Emissions Research Center
Energy and Transportation Science Division
2360 Cherahala Boulevard
Knoxville, Tennessee 37932
Phone: (865) 946-1243; fax: (865) 946-1398
E-mail: finneyc@ornl.gov

DOE Technology Manager: Jerry L. Gibbs
Phone: (202) 586-1182; fax: (202) 586-1600
E-mail: jerry.gibbs@ee.doe.gov

ORNL Technical Advisor: J. Allen Haynes
Phone: (865) 576-2894; fax: (865) 574-4913
E-mail: haynesa@ornl.gov

Contractor: ORNL, Oak Ridge, Tennessee
Prime Contract No.: DE-AC05-00OR22725

Objectives

- Study the effects of operating heavy-duty internal combustion engines at higher peak cylinder pressure (PCP) to increase engine thermodynamic efficiency.
- Evaluate performance of currently available materials at current and projected future PCP conditions.
- Identify properties requirements of materials suitable for withstanding a lifetime of operation at the elevated temperatures and pressures in future higher-efficiency, heavy-duty engines.

Approach

- Use computational simulations to estimate combustion intensity and heat transfer using computational fluid dynamics software and evaluate the thermo-mechanical effects on materials using finite element modeling software.
- Focus on three conditions: 192 bar [1 bar = 10^5 Pa] (current baseline), 250 bar (current stretch), and 300 bar (projected future) PCP.
- Measure relevant properties at a range of temperatures for an intermediate-grade material (i.e., CGI-450) for use in models.
- Evaluate materials stresses and design safety factors with current materials and engine design, with a focus on the cylinder head, valve faces, liner, and piston.

- Use steady-state conditions cycling between pressure extrema to estimate fatigue life.

Accomplishments

- Tuned engine combustion model to match loads, using constant boundary temperatures.
- Began tuning engine combustion model for variable energy-transfer mechanisms and boundary temperatures.
- Measured relevant materials properties at a range of temperatures for CGI-450 samples.

Future Directions

- Evaluate and complete engine combustion simulations with high-fidelity temperature and heat flux treatment.
- Evaluate thermal and mechanical stresses in selected engine components at the three PCP conditions using finite-element analysis.
- Identify properties needed for prospective materials to be suitable for future production environments.
- Develop a constitutive model for CGI-450 to assist in engine analysis and design.
- Extend this methodology to light-duty engine applications.

Introduction

Heavy-duty internal combustion engines for the transportation sector are operating at increasingly high PCP to increase brake thermal efficiency. Current operating ranges are 75 to 190 bar PCP and the next decade could see over 300 bar PCP. The current generation of materials (such as gray cast iron) is not adequate for the projected higher pressures and temperatures of future higher-efficiency engines. Although candidate replacement materials (such as compacted graphite iron [CGI]) are being developed and evaluated for use in intermediate applications, a robust understanding of near-cylinder stresses and the materials properties necessary to enable desired engine efficiency and power densities of future heavy-duty engines is lacking.

Numerical simulations offer insight into the cylinder environment at such elevated pressures and temperatures and can help identify design needs and changes more rapidly than those identified experimentally. The current practice of simulation can achieve low or high-dimensional modeling of the combustion environment or the cylinder/engine structure, but a fully coupled, high-dimensional CFD-finite element analysis simulation of combustion, heat transfer, and consequential material temperatures and stresses is a fundamental development need.

Part of this limitation is the time and level of detail required to set up simulations. For finite element analysis particularly, a proper meshing of complex geometries for high-fidelity calculation of materials stresses with conjugate heat-transfer can be extremely labor-intensive. However, with simplifications, a sufficient first-order estimate of future required materials properties can be gauged with simulations. This project employs an incremental process for this problem, starting with use of CFD results as inputs to finite element analysis simulations.

Results

Activity this year focused on two efforts: (1) experimental measurement of relevant mechanical properties of an advanced, engine-grade material and (2) numerical simulation of combustion in a production engine cylinder at different operating conditions. The materials properties will be used for numerical simulations of thermal and mechanical stresses in the engine at three peak cylinder pressure conditions. The combustion simulations will be used to provide boundary conditions for finite element modeling of the engine to evaluate suitability of materials for a lifetime of commercial operation under cylinder conditions of varying pressure and temperature.

This year, a quantity of CGI-450 was acquired from a commercial original equipment manufacturer, which is developing CGI materials for use in heavy-duty engines. Test samples were prepared for various measurements of selected thermal and mechanical properties and obtained in ambient conditions at various increments from room temperature up to 650 or 800°C. Properties measured this year included the following:

- Tensile strength
- Thermal diffusivity
- CTE
- Critical temperatures
- Specific heats
- Short-term creep

Certain values are compared with publicly available data, where available. For example, Figure 27 displays thermal conductivity of CGI-450 measured at ORNL with publicly available data for a gray cast iron that is typical of that used in heavy-duty engines. Figure 28 shows a similar comparison for CTE, with the addition of limited, publicly available values for CGI-450. These data range in temperatures not previously reported for CGI-450.

A test matrix of ambient temperature and loads was explored in a series of short term creep experiments. At each ambient temperature, a test sample was subjected to a step tensile load, which was maintained while sample strain was measured over time before the next step load was applied. Figure 29 shows one short-term creep test for the CGI-450 sample at 500°C, where the sample failed after a limited period at the third applied load.

Results for all materials property measurements are

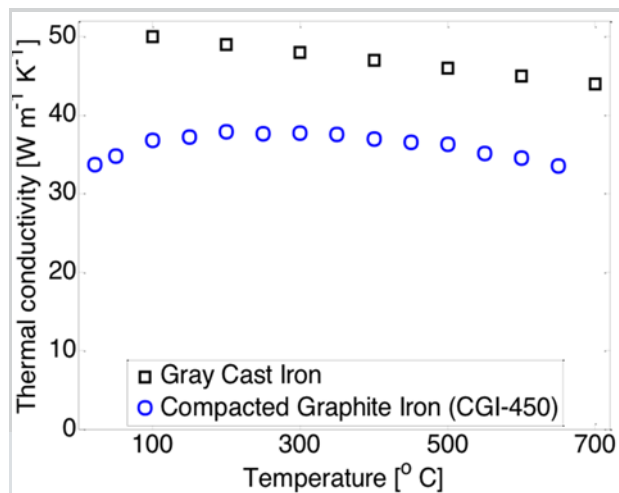


Figure 27. Measured thermal conductivity at a range of temperatures for CGI-450 compared with publicly available values for gray cast iron.

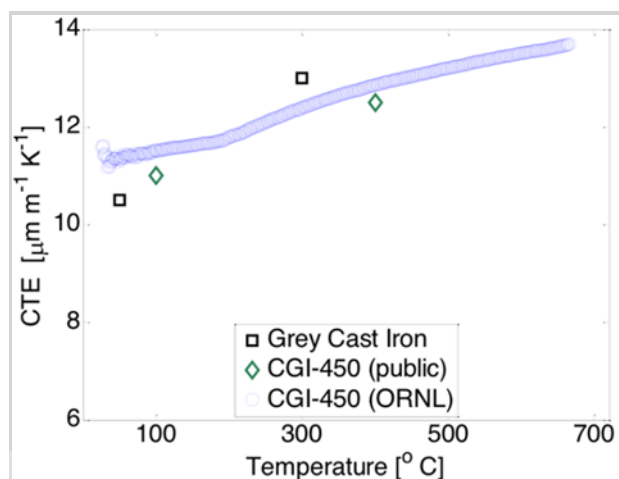


Figure 28. Measured CTE at a range of temperatures for CGI-450 compared with publicly available values for gray cast iron and CGI-450.

being prepared (and reviewed by industry contributors) for reporting and for input into the computational models. Additional plans include concluding experiments sufficient to create a constitutive model for CGI-450 suitable for analysis needs of future engine performance.

In the computational fluid dynamics simulations of engine combustion, progress this year included completion of parametric sensitivity studies using fixed cylinder wall temperatures and initiation of conjugate heat transfer simulations to calculate wall temperatures and heat fluxes iteratively. Previous simulations in Year 1 used static temperatures for the head, liner, valve-face, and piston crown; however, these temperatures presently are undetermined at the operating conditions in this study. Advanced conjugate heat transfer simulations were begun to tune combustion to achieve target engine performance at the three peak cylinder pressures of interest. The resulting temperature distributions (Figure 30) and heat flux maps through the cylinder walls will give the most accurate estimates of temperatures and thermal stresses available and provide high-fidelity inputs for the stress and fatigue models.

Conclusions

The integrated approach of this project is permitting definition of materials properties in an accelerated fashion and without significant experimental development. A comprehensive measurement study of CGI-450 has provided thermal and mechanical properties for a highly relevant intermediate engine material. The measured property values compare well with the limited data for CGI-450 that is available publicly; however, the present study extends properties knowledge into temperatures relevant in future engine operation. The conjugate heat transfer methodology being employed in the CFD combustion simulations is providing temperature and heat flux spatial data not otherwise available and will serve as a template for future studies in other engine applications.

Future Directions

Using the methodology developed during this project, the next step is materials optimization of light-duty engines, which in some sense have more stringent needs than heavy-duty engines. An integrated thermal-mechanical simulation approach, guided by targeted experimental studies, can reduce development cycle time. Continuous improvement in computational resources will allow truly coupled CFD and finite

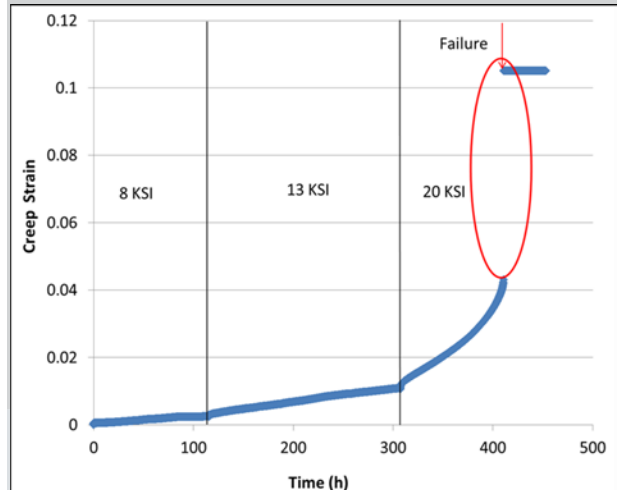


Figure 29. Short-term creep test result for CGI-450 at 500°C for three load conditions up to tensile failure.

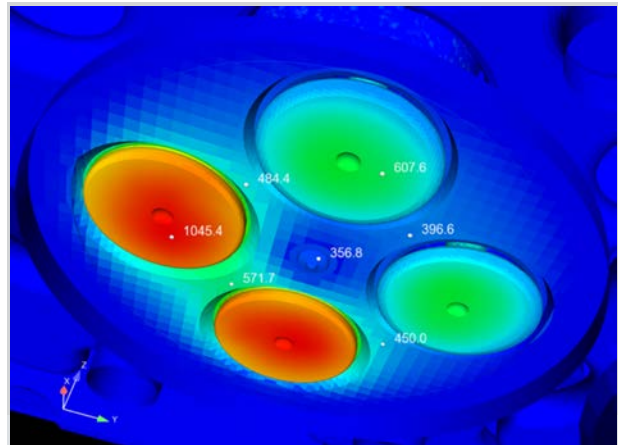


Figure 30. Temperature map (in K) of the head and valves at a low peak-cylinder pressure condition, showing spatial variations. Image produced by Jing Huang.

element method simulations and can allow expanded domains such as simulations with very high spatial resolution, high-fidelity physics, or whole-engine domains with all cylinders and auxiliary systems included.

Presentations

Finney, Charles, 2016, “Applied Computational Methods for New Propulsion Materials – Future Engine Requirements,” *U.S. DOE Vehicle Technologies Office 2016 Annual Merit Review and Peer Evaluation Meeting*, Washington D.C., June 9, 2016.

Project-Cast Alloys for Engines

Ford - ICME-Guided Development of Advanced Cast Aluminum Alloys for Automotive Engine Applications

Ford Contracts Manager: Melissa Hendra
Ford Research and Advanced Engineering Laboratory
Dearborn, Michigan 48124
Phone (313) 594-4714; fax: (313) 322-7162; e-mail: mhendra@ford.com

DOE Technology Manager: Jerry L. Gibbs
Phone: (202) 586-1182; fax: (202) 586-1600
E-mail: jerry.gibbs@ee.doe.gov

Ford Technical Advisor: Mei Li
Phone: (313)-206-4219
E-mail: mli9@ford.com

Contractor: Ford Research and Advanced Engineering Laboratory, Dearborn, Michigan
Prime Contract No.: DE-EE0006020

Objectives

- To develop a new class of advanced, cost-competitive Al casting alloys, providing a 25% improvement in component strength relative to components made with A319 or A356 alloys using sand and semi-permanent casting processes for high-performance engine applications.
- To demonstrate the power of integrated computational materials engineering (ICME) tools for accelerating development of new materials and processing techniques, as well as identifying the gaps in ICME capabilities.
- To develop comprehensive cost models to ensure components manufactured with these new alloys do not exceed 110% of the cost using incumbent alloys A319 or A356.
- To develop a technology transfer and commercialization plan for deployment of these new alloys in automotive engine applications.

Approach

- Start the alloy design process with a baseline alloy in line with 356/319 alloys with well quantified properties.
- Evaluate the heat treatment response and strengthening effect of some heat resistance elements of interest in simple model alloys, particularly at high temperature (300°C).
- With the aid of ICME tools, design and optimize the chemical composition and heat treatment process of the baseline alloys, with novel alloying additions proving to be effective for improving elevated temperature properties in simple model alloys.
- Demonstrate new alloys' performance at both room and elevated temperature through a series of mechanical tests, including yield strength, ultimate tensile strength, endurance, and so on.

- With the aid of ICME tools, develop a commercialization prototyping plan and investigate the performance of new alloys as automotive engine components through this prototyping plan.

Accomplishments

- Identified several novel elements that could potentially address the challenge of high temperature (300°C) mechanical property degradation experienced by existing cast Al alloys.
- Successfully developed a promising Heat 17 alloy with balanced baseline composition and novel alloying additions that is capable of reaching DOE's Target on yield strength (YS) and ultimate tensile strength (UTS) at 300°C, but shows 30% incensement of the 120°C endurance limit when compared with the baseline alloys.
- Took into account the cost of alloy composition, the casting conditions, and the heat treatment procedures throughout the ally design process so the properties of Heat 17 alloy are directly applicable to production.

Future Directions

- Understanding the mechanism that gives rise to the excellent elevated temperature endurance limit of Heat 17.
- Identify the gap between ICME and experiments.
- Investigate the performance of Heat 17 as automotive engine components with a prototyping plan, including cylinder block and head.

Introduction

Recently legislated fuel economy standards require new U.S. passenger vehicles to achieve at least 34.1 mpg on average by model year 2016 and 58 mpg by 2030, which is up from 28.8 mpg today. Two major methods of achieving improved fuel economy in passenger vehicles are reducing the weight of the vehicle and developing high-performance engines. However, to increase engine efficiency, the maximum operation temperature of these components increased from approximately 170°C in earlier engines to peak temperatures well above 200°C in recent engines. The increase in the operational temperatures requires a material with optimized properties in terms of tensile, creep, and fatigue strength. This program focuses on developing advanced cast Al alloys for automotive engine applications to meet these challenging requirements.

Several alloys compositions have been proposed in past 3 years. Among them, Heat 15 (i.e., 319-based with alloying of novel additions) shows higher 300°C YS and UTS than DOE targets, even after a 100-hour pre-exposure at testing temperature. However, the cooling rates for preparation of Heat 15 are high, thus generating a second dendrite arm spacing of about 15 μm . This is much finer than observed in an industrial engine (i.e., about 25 μm). To assure the alloys' properties achieved in our laboratory can be reproduced in industrial production, the casting process has been modified by coating the iron molds. Heat 17, the latest developed alloy, is prepared from a modified casting process, which has the same composition as Heat 15 but has a second dendrite arm spacing of 25 μm . In addition, in order to take advantage of novel alloying additions, a three-stage heat treatment has been designed and compared with traditional two-stage heat treatment. Thus, the focus this year has been placed on demonstration of Heat 17 via two-stage aging treatment that can meet all requirements proposed by DOE.

Results

Alloys' Chemical Composition and Heat Treatment Condition

Heat 16 and Heat 17 (i.e. the latest alloys developed by coated iron molds) are 319-based alloy and 319-based alloy with novel additions, respectively. The second dendrite arm spacing of these two alloys is around 25 μm and close to the value observed in the industrial engine.

The aim of alloying novel additions in Heat 17 is to provide solution strengthening or/and precipitation strengthening at elevated temperature through heat treatment. However, the traditional heat treatment process (e.g., T6 or T7) cannot help these additions achieve this goal. First, experimental results prove that the content of these additions in the Al matrix after casting is higher than their solubility at solution treatment temperature. Thus, these additions will coarsen rapidly to form equilibrium phases that provide no solution or precipitation strengthening at all during high-temperature and long-duration solution treatment. Second, the aging temperature of traditional heat treatment is still too low for these additions to form precipitates if Heat 17 anticipates obtaining precipitation strengthening from them. To take advantage of a novel alloying addition, a three-stage heat treatment is proposed.

Two different temperatures are used for first-stage treatment: a low temperature T_1 is used to maintain novel additions in the Al matrix, while a high temperature T_2 is used to form addition-contained precipitates. Cu and Mg also dissolve into the Al matrix during first-stage treatment. Rather than a long-duration solution treatment, a short-time, high-temperature solution treatment is used as second-stage treatment to avoid coarsening of the addition-contained phases. Combined with first-stage treatment, this short-time solution treatment is also able to dissolve enough Cu and Mg into the Al matrix and form semi-coherent theta'-AlCu and Q-AlSiMgCu precipitates during the third-stage treatment to improve the alloys' mechanical properties. Four combinations of alloys and heat treatment are investigated in this report: Heat 16-T7, Heat 17-T7, Heat 17- T_1 , and Heat 17- T_2 .

Microstructures and Composition Analysis of As-Cast and As-Heat Heat 17

The Scheil solidification simulation shown in Figure 31(a) using the PanAl2016 thermodynamic database indicates that novel addition-related phases form first from liquid at 710°C, followed by formation of the Al matrix between 605 and 565°C. After that, the solidification pathway follows the consequence of Al-Si eutectics, beta-AlFeSi phases, theta-AlCu phases, and Q-AlSiMgCu phases. The simulation results are well in agreement with experimental observation by back-scatter imaging and energy disperse x-ray spectrometer (EDXS) in Figure 31(b) and (c), respectively.

Because novel addition-related phases are observed as primary precipitates, the amount of them in the Al matrix should be much less than the nominal composition. In addition, the amount of novel additions is determined by solute trapping that is occurring during non-equilibrium solidification, rather than post-solidification solution treatment due to their extremely slow diffusivities and low solubility in the Al matrix. In fact, to achieve a considerable amount of these additions in the Al matrix, rapid solidification techniques (e.g., melt-spinning and chilling mold casting) are always used to prepare samples in literatures. However, Heat 17 is cast with slow cooling rates. Thus, a crucial problem concerns how much additions can be dissolved in the Al matrix, especially compared with Heat 15, which is prepared with a faster cooling rate.

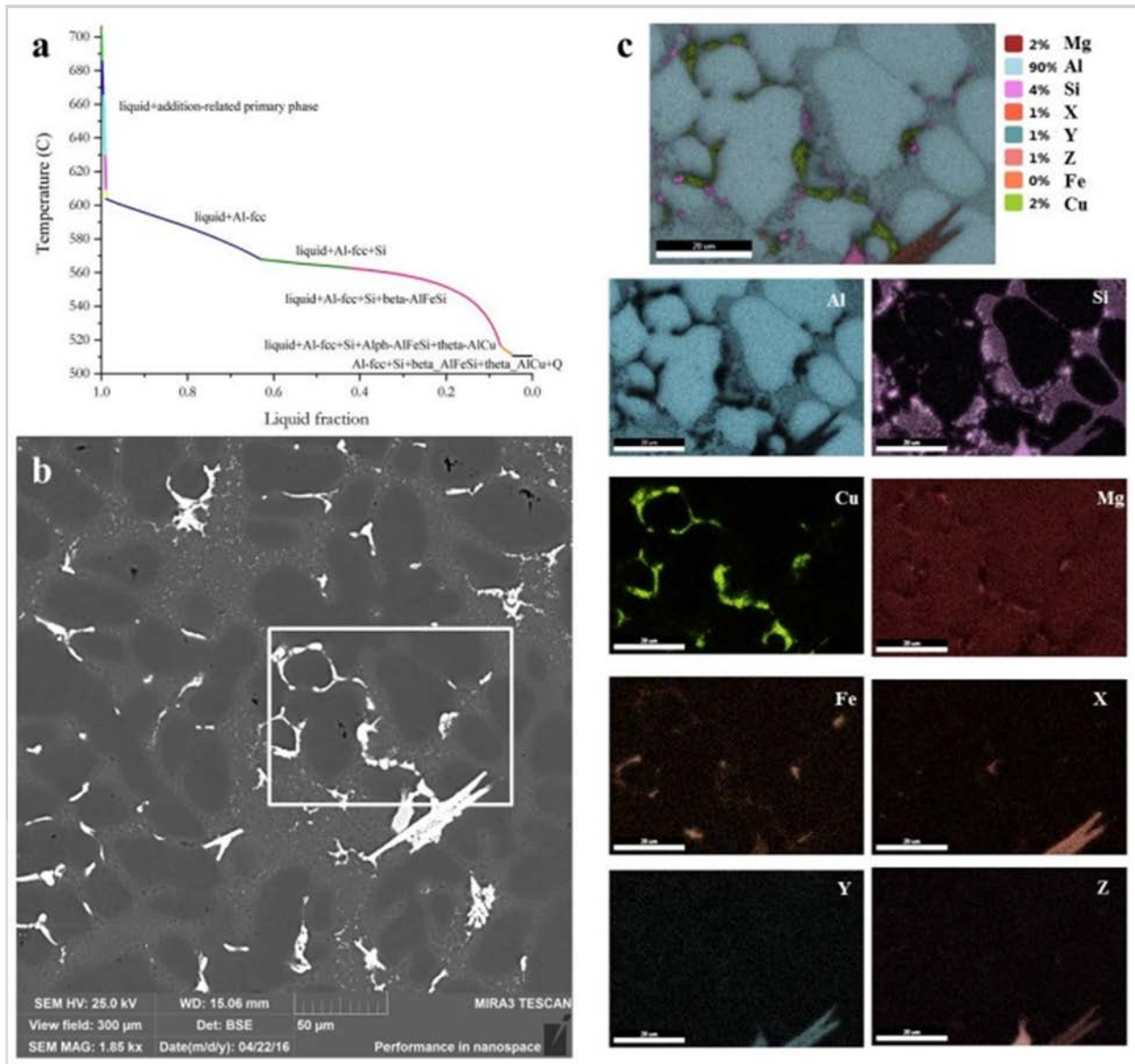


Figure 31. (a) Scheil simulation of Heat 17 showing the solidification consequence; (b) back-scatter imaging of as-cast Heat 17 showing observed microstructure; (c) EDXS mapping of as-cast Heat 17 showing novel addition-contained primary phase, Al matrix, Al-Si eutectics, and partitioning of Cu and Mg into eutectic regions.

A quantitative composition measurement of the Al matrix is investigated by EPMA. Two different methods are employed: (1) point and (2) grid measurement. For point measurement, 100 points are selected for each sample at the core of the Al dendrites. On the other hand, the grid measurement developed by Ganesan et al. is a powerful technique for determining macro-segregation during solidification. According to the results shown in Figure 32, both the point and grid measurements reveal similar results: Heat 17 has a comparable amount of X additions and a lower content of Z additions in the Al matrix when compared with Heat 15. It should be noted that the measured amount of novel additions is larger than solubility at the solution treatment temperature in the traditional heat treatment predicted by thermodynamic calculation. Thus, most novel additions will lose their strengthening due to transformation to their equilibrium phases if traditional heat treatment is used.

The microstructure change of Heat 17 at different heat treatment stages is also examined by back-scatter imaging (Figure 33). First, for all heat treatment conditions, the novel addition-related primary phases have no change at all, indicating no dissolving of them into the Al matrix has happened during post-solidification heat treatment. Figure 33(a) and (b) shows that finer Cu particles disperse in the eutectic regions after first-stage treatment, instead of the bulk forms observed in an as-cast sample. This result indicates that Cu has started to move into the Al matrix. The difference between T_1 and T_2 lies on the nano-scale precipitation microstructure, which will be addressed in the following section by transmission electron microscopy (TEM). Third, the finer Cu particles in the eutectic regions have almost disappeared after a short-time solution treatment (Figure 33(c) and (d)). The microstructure observed after the second-stage treatment is very similar to that in the sample with the T7 solution treatment (Figure 33(e) and (f)). The qualitative EDXS composition measurements also demonstrate they have comparable Cu and Mg amount in the Al matrix. Combined with first-stage treatment, the short-time solution treatment is able to dissolve enough Cu and Mg into the Al matrix, which is going to provide precipitation strength through formation of semi-coherent θ' -AlCu phases and Q-AlSiMgCu after third-stage treatment. The quantitative EPMA is currently in progress to confirm this result.

Mechanical Properties of Heat 16 and Heat 17 with Different Heat Treatments

YS and UTS at both room and elevated temperature are one of the most important targets proposed by DOE. The tensile test results of Heat 16 and Heat 17 are shown in Figure 34. For room-temperature (RT) tensile properties, all tested alloys are above the DOE requirement, which is indicated by the blue line in Figure 34. For the 300°C tensile test, although all tested alloys without 100 hours pre-exposure at a testing temperature are much higher strength than the DOE target, the UTS of Heat 16 after 100 hours pre-exposure is lower than the DOE target. However, it is

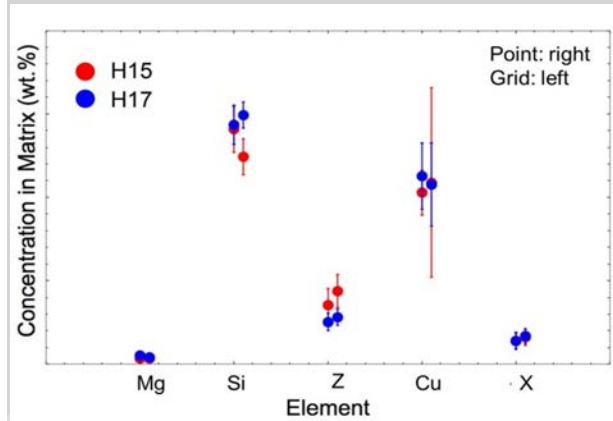


Figure 32. Quantitative composition measurement of Al matrix by EPMA of as-cast Heat 15 and Heat 17, showing different cooling rates that arise to similar amount of X-additions and different content of Z-additions.

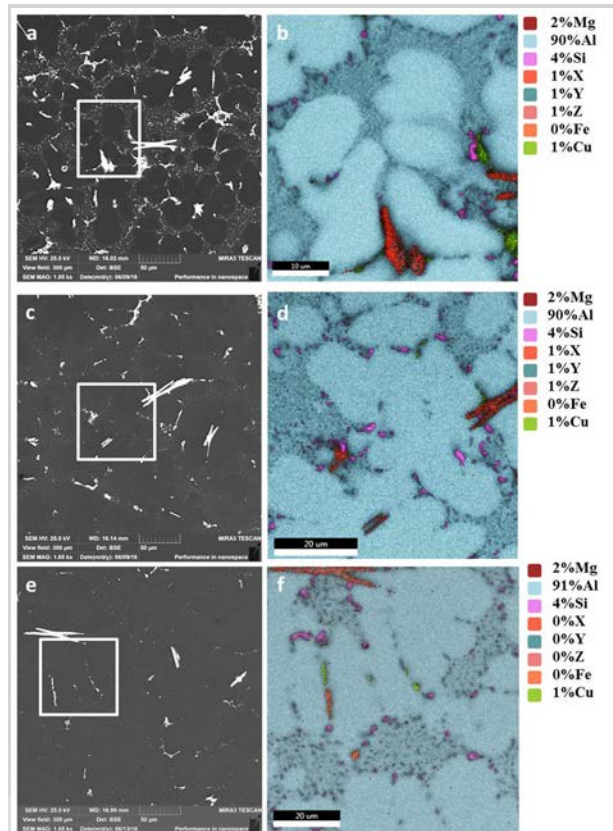


Figure 33. (a) and (b) Back-scatter imaging and EDXS mapping of Heat 17 after first-stage treatment showing Cu has started to move into the Al matrix; (c) and (d) back-scatter imaging and EDXS mapping of Heat 17 after second-stage treatment showing most Cu has been dissolved into the Al matrix; (e) and (f) back-scatter imaging and EDXS mapping of Heat 17 after T7 treatment showing most Cu has been dissolved into the Al matrix.

obvious that as-treated Heat 17, even with the T7 heat treatment conditions that cannot take the full vantage of novel additions, can meet the DOE requirement. Therefore, the proposed Heat 17 does benefit from novel addition at elevated temperatures.

According to tensile test results at both RT and 300°C, it seems that Heat 17 after complicated three-stage treatment has very similar results as that treated with the traditional T7 condition. However, the elevated temperature, high-cycle fatigue strength is improved by novel additions through the designed three-stage treatment rather than the T7 condition. A highest common factor (HCF) test at both RT and 120°C is performed under stress control on a servohydraulic testing machine. The criterion for HCF failure is complete fraction of the specimen. HCF data are summarized by a random fatigue limit model (Figure 35).

Heat 16-T7 and Heat 17-T7 have a little bit higher RT fatigue strength than Heat 17- T_1 and Heat- T_2 , which is consistent with RT tensile results. Once the testing temperature increases to 120°C, the fatigue strength of both Heat 16-T7 and Heat 17-T7 shows a different degree of decline, while the fatigue strength of Heat 17- T_1 can maintain its RT strength. This result accents that Heat 17 with three-stage treatment has superior elevated temperature fatigue strength than the baseline alloy and traditional heat treatment. Surprisingly, the 120°C fatigue strength of Heat- T_2 also shows a significant decrease from RT fatigue strength. The different 120°C fatigue performance among Heat 16 and Heat 17, with three different heat treatments, is discussed in next section.

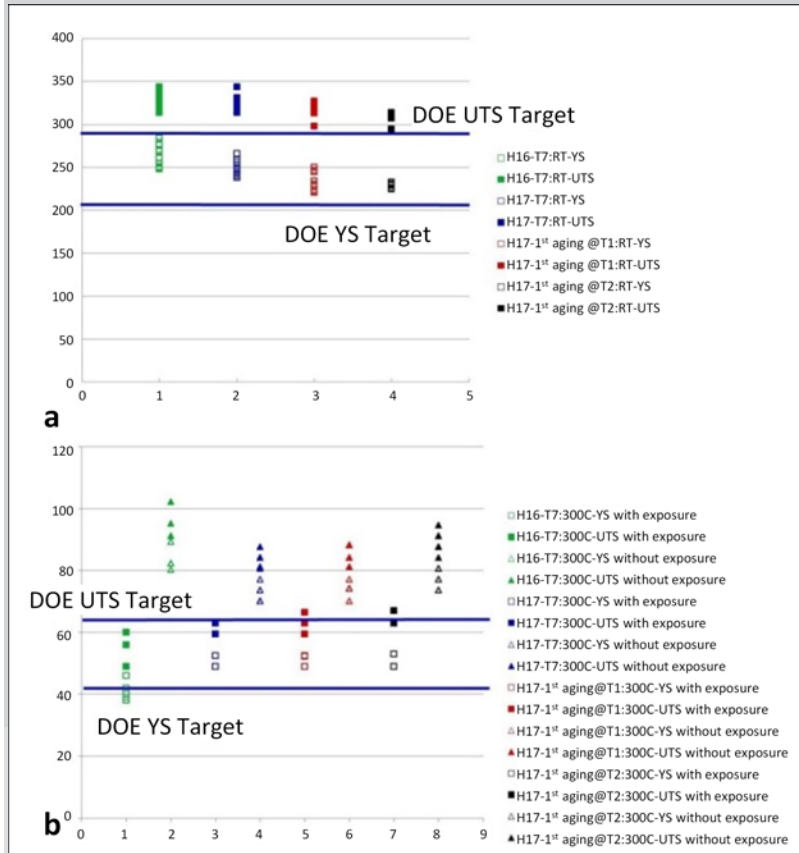


Figure 34. (a) Room temperature YS and UTS of Heat 16 and Heat 17 with different heat treatment, showing that all alloys can meet DOE requirements; (b) 300°C YS and UTS of Heat 16 and Heat 17 with a different heat treatment, showing only novel addition improved Heat 17 with an excess DOE target after 100 hours of pre-exposure.

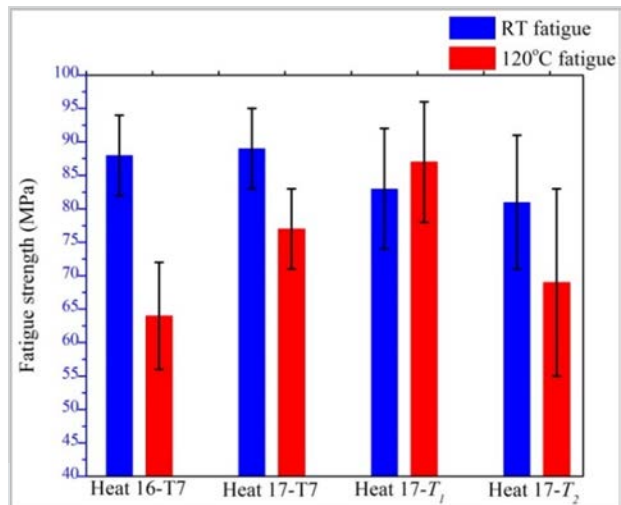


Figure 35. Room temperature and a 120°C endurance limit of Heat 16 and Heat 17 with different heat treatment, showing Heat 17- T_1 has excellent 120°C fatigue strength.

Microstructure Characterization of 120°C HCF Samples

Fatigue life is always correlated to a sample's porosity level. To figure out if the high 120°C fatigue strength of Heat 17- T_1 is due to its lower than others porosity level, the fracture surfaces of 120°C HCF test sample are characterized by scanning electron microscope. Most of the initiation sites for both Heat 16 and Heat 17 are shrinkage pores, as highlighted by black solid lines in representative images shown in Figure 36(a). Only a few gas pores are observed as initiation sites. The size of the initiation sites is illustrated by the average equivalent circle diameters, which just counts for shrinkage pores (Figure 36(b)). Results indicate that the initiation sites size of Heat 17 samples used for different heat treatment conditions are comparable with each other and they are higher than that of Heat 16. Thus, the novel alloying additions deteriorate rather than improve the samples' porosity. Based on the fact stated above, the excellent 120°C fatigue performance of Heat 17- T_1 , especially compared to Heat 17- T_2 , is due to nano-scale microstructure features. In addition, to eliminate the affects from different porosity levels, two trials of alloys based on Heat 16 and Heat 17 are going to be prepared without alloying with Sr and at the same casting temperature, because they are important factors in determining a sample's porosity level. This makes it possible to compare fatigue strength at the same porosity level.

The purpose of novel addition in this project is to provide solution strengthening or precipitation strength at elevated temperature. Therefore, two different first-stage temperatures are used: T_1 is a lower temperature to help dissolve Cu and Mg into the Al matrix and keep novel additions in it, while T_2 is used to form novel addition-contained precipitates. The dark-field TEM imaging of Heat 17 only heated with two different first-stage treatments (Figure 37(a) and (b)) confirms that no precipitate is observed for T_1 and sparse novel addition-contained precipitates are observed for T_2 . Based on 120°C HCF results, it is inferred that 120°C fatigue properties of Heat 17 should benefit from solution strengthening, rather than precipitation strength. This hypothesis is currently being verified in a simple system. This might be an innovative theory for enhancing elevated temperature fatigue life. In addition, TEM imaging of 120°C HCF Heat-T1 (Figure 37(c)) indicates that only plate-like theta'-AlCu and rod-like Q-AlSiMgCu are observed without novel addition-contained precipitates. TEM imaging of 120°C HCF Heat 17- T_2 is also in progress to confirm if novel addition-contained precipitates can be observed with plate-like theta'-AlCu and rod-like Q-AlSiMgCu after two-stage aging.

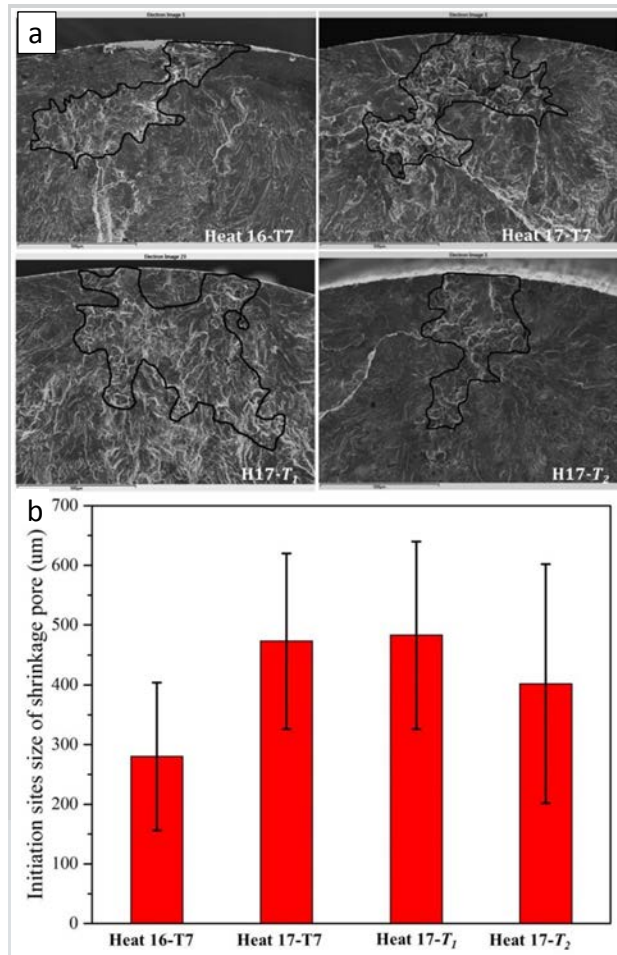
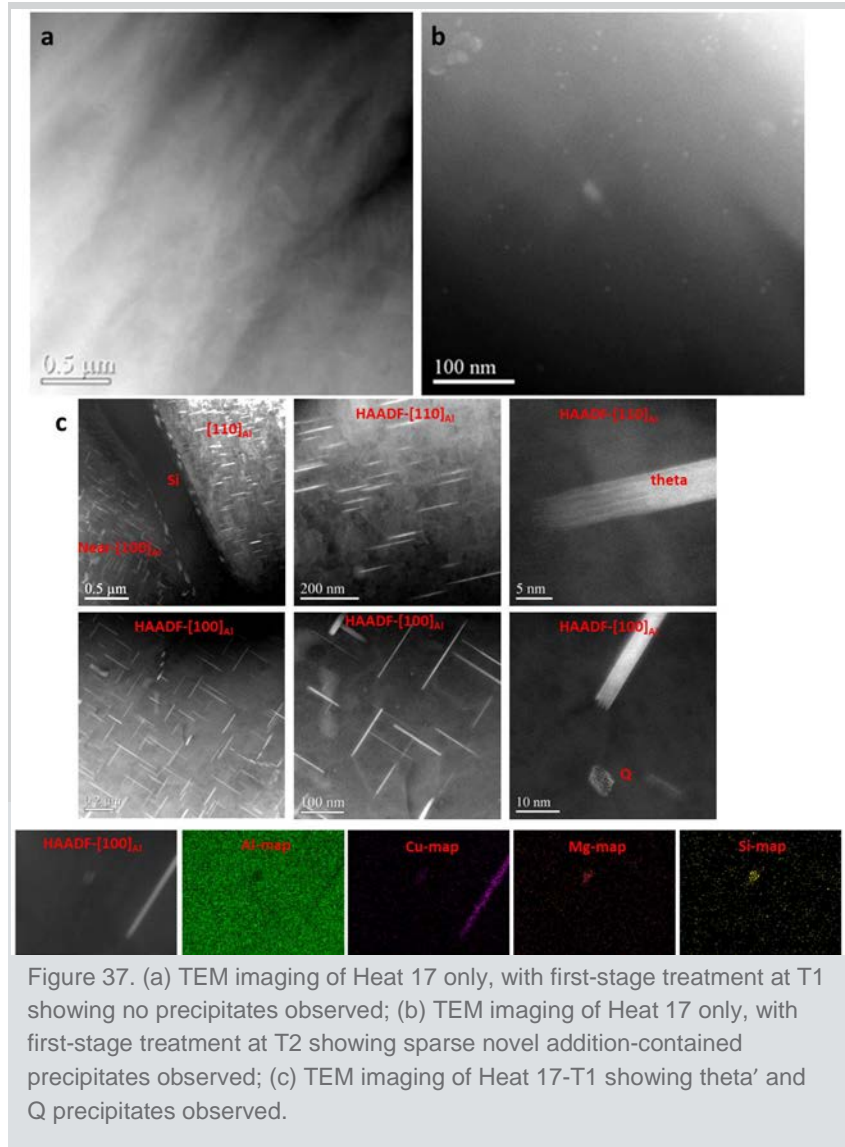


Figure 36. (a) Representative scanning electron microscope imaging of Heat 16 and Heat 17, showing the fraction surface of 120°C fatigue samples; (b) the average size of shrinkage pore for initiation sites, showing all Heat 17 samples have larger initiation shrinkage pore size than Heat 16.

Conclusions

A 319-based alloy with alloying of novel additions (i.e., Heat 17) is proposed and it aims to achieve improved high-temperature performance. Both traditional T7 and novel three-stage treatment are used to enhance the alloy's properties. Results indicated that Heat 17 with T7 or three-stage treatment has comparable YS and UTS with the baseline alloy (i.e., Heat 16) at room temperature. However, the 300°C tensile tests show that Heat 17 that is improved by alloying of novel additions can meet the DOE targets for YS and UTS, while Heat 16 is below this target.

Although there is almost no benefit observed between traditional T7 condition and complicated three-stage treatment for Heat 17 from the view of tensile strength, the elevated temperature HCF tests show that Heat- T_1 can maintain its fatigue strength at RT, while Heat- T_2 and Heat-T7 show a different degree of decline when compared with their RT fatigue strength. TEM imaging of Heat 17 only with first-stage treatment indicates that no precipitates observed for T_1 and sparse novel addition-contained precipitates are observed for T_2 . This microstructural difference is believed to lead to different elevated temperature fatigue strength between T_1 and T_2 .



Project-Cast Alloys for Engines

Funding Opportunity Announcement (FOA) 648-3a – Computational Design and Development of a New, Lightweight Cast Alloy for Advanced Cylinder Heads in High-Efficiency, Light-Duty Engines

Principle Investigator: Mike J. Walker
GM Research and Development Center
30500 Mound Road
Warren, Michigan 48090-9055
Phone: (586)651-3757
Email: mike.j.walker@gm.com

Principle Investigator: Qigui Wang
GM Global Powertrain Engineering
823 Joslyn Ave
Pontiac, Michigan 48340-2925
Email: qigui.wang@gm.com

DOE Technology Manager: Jerry L. Gibbs
Phone (202) 586-1182; fax: (202) 586-1600
E-mail: jerry.gibbs@ee.doe.gov

Contractor: General Motors LLC, Warren, Michigan
Prime Contract No.: DE-EE0006082

Abstract/Executive Summary

This collaborative project between GM, QuesTek Innovations LLC, Northwestern University, Massachusetts Institute of Technology, Camanoe Associates, AFS, and Dr. Fred Major uses ICME tools, expert knowledge, and experimental validation to accelerate development of an alloy that is capable of handling the higher temperatures and pressures utilized in the smaller, more efficient engines. During FY 2016, GM and its partners have characterized previous alloy designs created through the ICME process. By using analytic techniques such as local electrode atom probe (LEAP) and TEM imaging, the chemistry, shape, and growth characteristics of the precipitate phases have been identified. This has led to important corrections on the thermodynamic databases for Al alloys and has permitted the exploration of new alloy concepts. Through continued use of LEAP and TEM imaging on specimens conditioned at high temperatures, kinetic growth models for the precipitate phases have been improved. Alloy strength models based on the size and number distribution of precipitate phases have been calibrated accordingly. The final computational design of key alloy compositions has been completed. However, minor chemistry variations to improve castability, room temperature ductility, and high-temperature strength are being considered. A head casting trial has been carried out on three alloy variations to investigate alloy performance in a full-scale component. Mechanical property data are being generated and will be completed in 2017.

Accomplishments

- Validated alloy characterizations and designs (Milestone 9).
- Established a more accurate thermodynamic database that reflects phase boundaries in the Al-Cu-Mg-Si system. This database will apply to many wrought and cast alloy systems and will enable the design of new alloys.
- Completed final computational alloy design (Milestone 10).
- Completed head casting trial on three alloy variations, with 1,200 samples extracted and being used for measuring tensile properties, high-cycle fatigue properties, low-cycle fatigue properties, and castability.

Future Directions

- Complete testing of current cast alloys. Evaluate and compare properties between the baseline and newly developed alloys. Optimize chemistry of the new alloys for best overall mechanical properties and castability.
- Carry out a final head casting trial based on the final optimized alloy chemistry.
- Continue to produce laboratory-scale castings to improve high-temperature strength and room-temperature ductility.
- Conduct full recyclability analysis of the optimal alloy(s).
- Develop alloy and process cost models for full production implementation using the new high-temperature capable Al alloy.

Technology Assessment (Results are Now Based on Tensile Measurement from the Head Casting Trial)

- Target 1: 40 ksi (276 MPa) room-temperature tensile strength and 30 Ksi (207 MPa) room temperature yield strength.
- Gap: Our selected high-temperature alloy has achieved 47 ksi (328 MPa) room temperature tensile strength and 40 ksi (275 MPa) room temperature yield strength; therefore, we were able to meet these targets.
- Target 2: Maintain 3.5% elongation at room temperature.
- Gap: Our selected alloy that meets the highest high-temperature properties is achieving 2.5% plastic elongation in chilled areas. We are evaluating the microstructure of three alloys to identify which elements reduce ductility and will modify our future alloy to improve it.
- Target 3: Achieve 9.5 ksi (65.5MPa) tensile strength and 6.5 ksi (49 MPa) yield strength at 300°C
- Gap: Our selected alloy achieves 8.1 ksi (56 MPa) tensile strength and 6.9 ksi (48 MPa) yield strength at 300°C. Therefore, we have now achieved the high-temperature yield strength target. There is a 14% gap in achieving the high-temperature UTS target. However, it should be noted that this is a very significant improvement (i.e., about 25%) over Al alloy 356 and our measurements were made after 100-hour conditioning at temperature, which was not specified for the target. We have identified the role of certain minor elements in increasing the higher-temperature strength and are continuing research into this area.

Introduction

The DOE Energy Efficiency and Renewable Energy (EERE) Program is targeting a 25% lighter powertrain by the year 2025 and a 40% lighter powertrain by the year 2050. As a result, engine power density will be increased significantly. This will result in higher exhaust temperatures and a doubling of the cylinder peak pressures by the year 2050. To meet these requirements and achieve the stated goals, the properties of the state-of-the-art materials (e.g., cast Al alloys) must increase substantially. Historically, it has taken about 10 years to develop and implement a new alloy and it has taken about 100 years to improve the performance of a material (such as cast Al) by 50%. Thus, traditional methods of experimental trial and error are no longer sufficient. Fortunately, both computational and analytical methods have been vastly improved in the last few decades. ICME and advanced experimental analytical tools such as the focused ion beam microscope, high-resolution STEM, and LEAP are now available for accelerating the timeframe to develop new alloys. Combining ICME tools with expert knowledge from the field and judicious experiments for verification and validation is the quickest and the most effective way of achieving the goals of developing a new high-temperature capable Al alloy for cylinder head production.

Approach

State-of-the-art ICME tools (e.g., first principles calculations, computational thermodynamic and kinetic models, virtual casting modules, and commercially available casting process simulation and structural and durability analysis software) will be used to design a new, lightweight cast-alloy with ideal multi-scale microstructures and a minimum tendency for casting defects to achieve the desired high-temperature strength and fatigue performance requirements in complex castings. The *iCMD*TM platform is used in this project to develop concepts and to perform modeling, validating, and alloy refinement. QuesTek's proprietary *iCMD*TM platform is a core modeling software system that integrates proprietary and commercial mechanistic modeling tools to facilitate rapid design and development of new materials (see Figure 38).

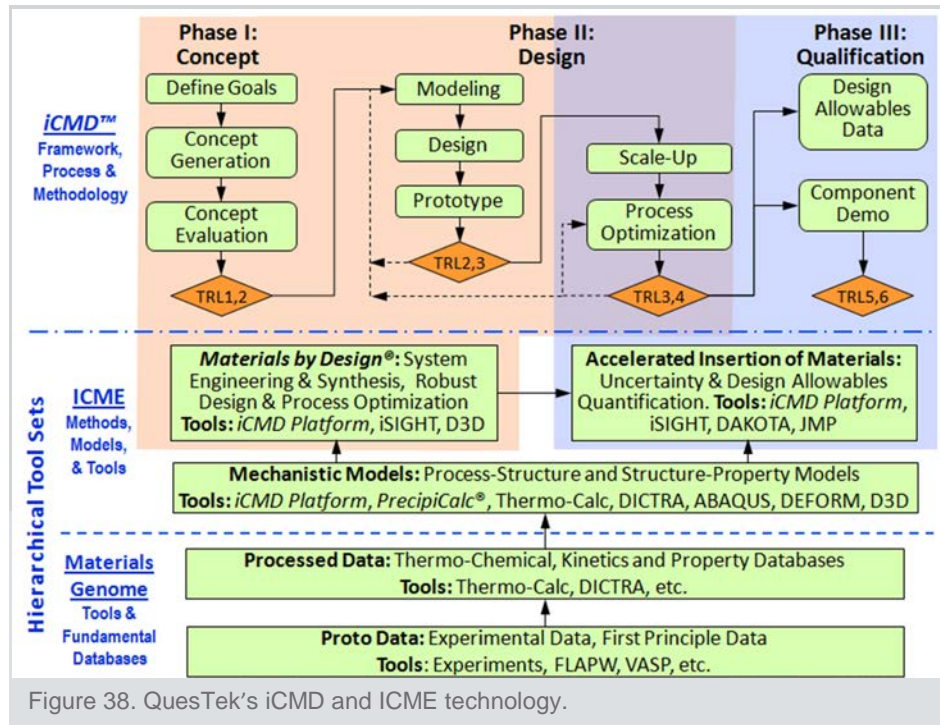
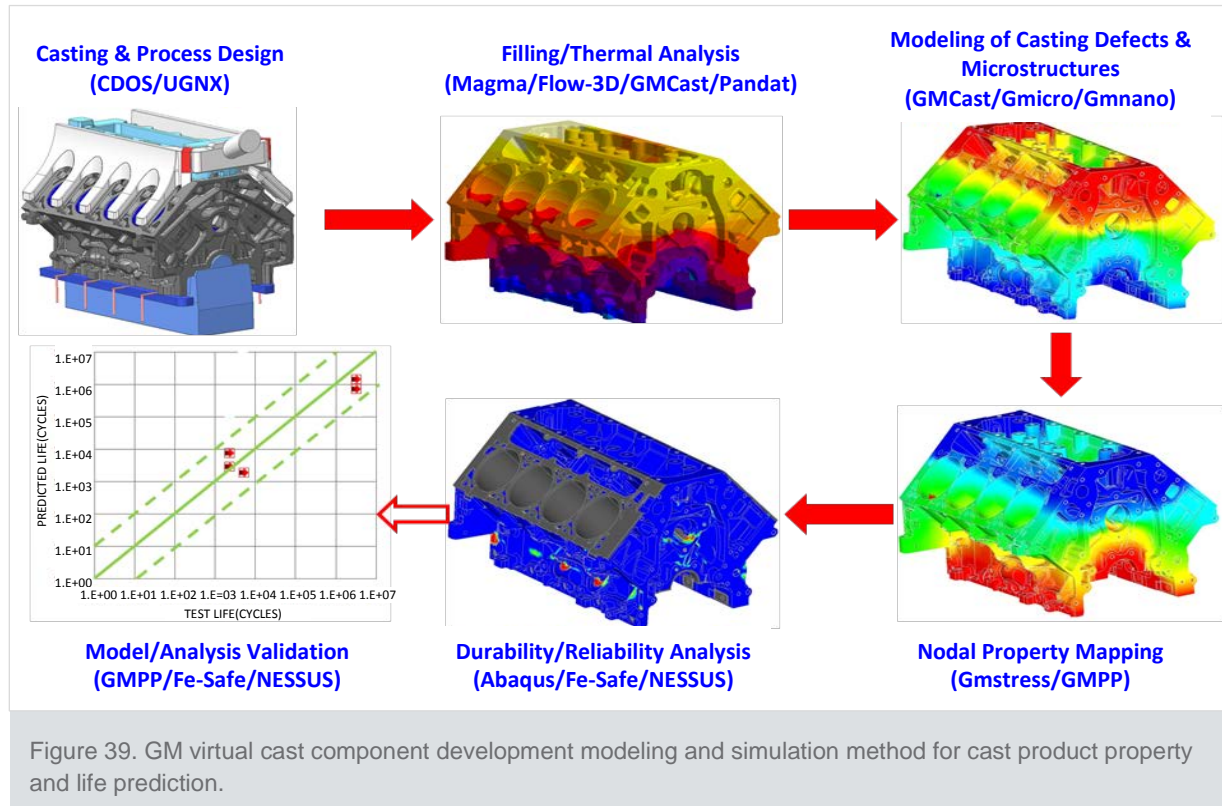


Figure 38. QuesTek's *iCMD* and ICME technology.

GM's Virtual Cast Component Development Program uses integrated state-of-the-art modeling and simulation methodologies for cast Al components, starting from computational alloy and casting design through casting and heat treatment process modeling, multi-scale defect and microstructure simulation and culminating in casting property and durability prediction (see Figure 39).



During the first stage of the project, a material requirement matrix was developed to guide alloy development. The first generation of the matrix was based on property requirements in the original DOE FOA and the best achievable properties of current cast Al alloys used in the heads. Improvements to the matrix were based on a design for six sigma optimization.

QuesTek's iCMD and ICME technology were used to develop the alloy concepts. Beginning with expert knowledge and past research as a guide, thermodynamic and kinetic databases were used to create the initial alloy concepts. Precipitation modeling was then used to design peak strengthening heat treatment cycles for targeted precipitate structures. Density functional theory (DFT) calculations were used to determine key input parameters beyond the reach of experimental methods. These inputs for thermodynamic and kinetic models include interfacial energies and accompanying changes with solute additions, high-throughput searches of new stable crystal structures, and solute partitioning energies to interfaces and precipitate phases. Once concepts were developed, buttons were cast and analyzed to find the precipitate phases through LEAP or TEM. Isothermal and isochronal hardness measurements were conducted to establish the long-term stability of precipitates for the various concepts. Isochronal hardness plots were used to identify optimal aging temperatures to achieve peak hardness and to confirm precipitation strengthening. Isothermal hardness plots were used to determine the time for peak aging and a first look at the strength and long-term stability of a concept.

Data collected from these experiments were also used as inputs in the strength models for future alloy

development. Continuing with QuesTek's iCMD and ICME approach, substitutional elements are selected that may reduce the coarsening of the precipitate phase or otherwise enhance the high-temperature mechanical properties of the alloy. Parametric models are created for alloys using the initial alloy concepts. These parametric models are then used to design prototype alloys that strive to meet the multi-faceted criteria of the material requirement matrix. Tensile strength, fatigue resistance, thermal conductivity, and good castability are all necessary for creating a viable alloy. At this stage, GM's Virtual Cast Component Development Process is used to predict casting defects such as macroporosity, microporosity, hot tears, and overall mechanical performance and product durability. In conjunction with the modeling approach, chilled plate castings are made for microstructure and mechanical property validation. After the parametric model and prototype stage, the alloy and process is scaled up to reflect a real application, which, in this case, is a production head. The alloy and process are optimized in terms of alloy composition tolerance, casting process variation, heat treatment temperatures and times, costs, and recyclability evaluation. In 2016, the goals were to characterize and validate parametric models (Milestone 9) to create the final embodiment of the cast alloy (Milestone 10), to produce laboratory-scale casting of the final alloy, and to prepare for the final head casting trial in 2017.

Results and Discussion

Milestone 9 Alloy Characterizations and Designs Validated

2016 began with characterization of alloys previously cast and validation of models. Quantification of the chemistry and growth morphology of the Q phase was the first focus. The Q-phase was identified using Mg-Si iso-surfaces in the LEAP microscope. TEM imaging was used to observe the growth kinetics. Figure 40 is for a comparison of the Q phase at 1 hour and 72 hours of conditioning at 200°C. The rod-shaped Q-phase mostly grows in length, whereas the diameter remains relatively constant. The Theta phase coarsens in two dimensions, producing large platelets (Figure 41). The difference in the growth morphology of the two phases results in a greater loss of properties in the theta phase at higher temperatures.

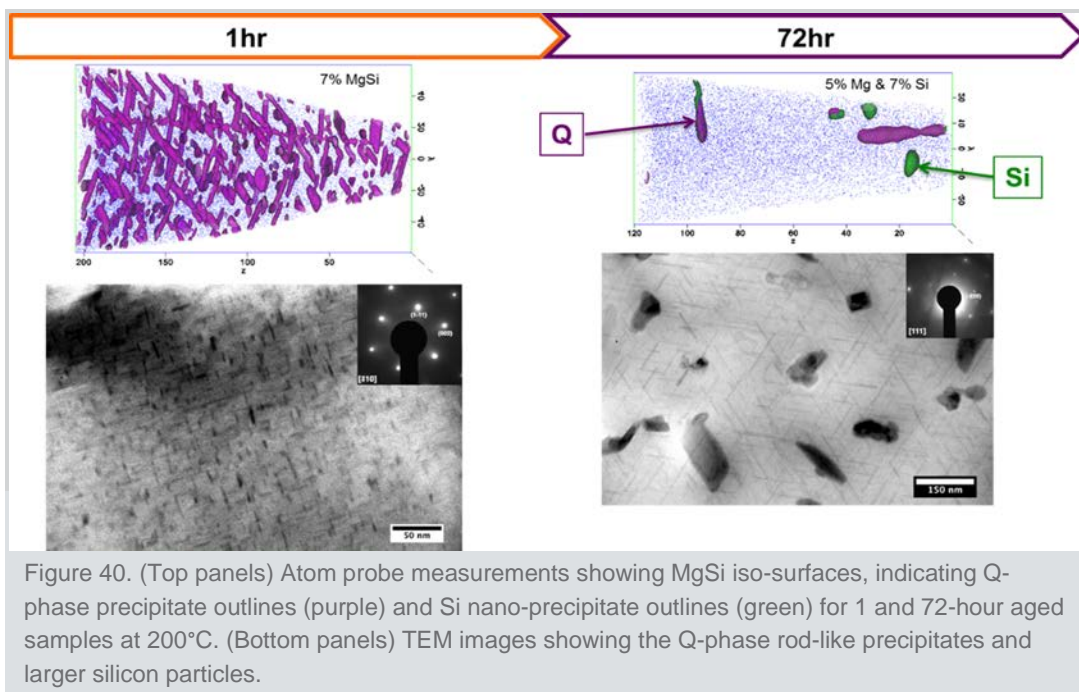
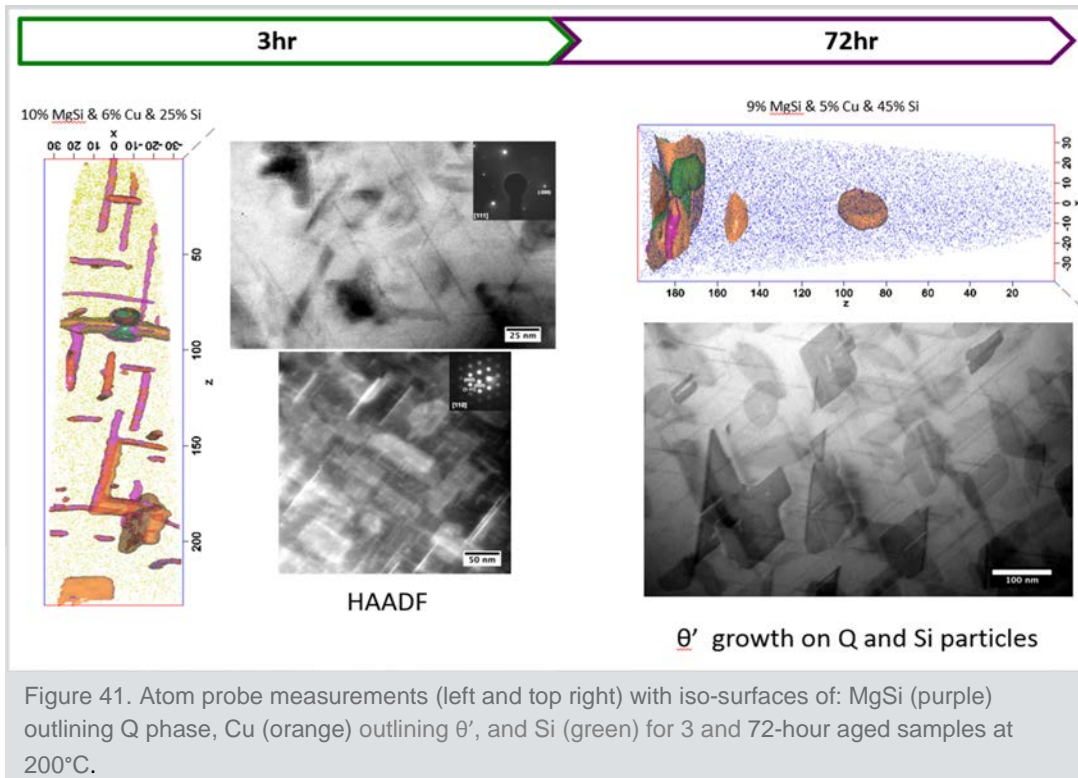
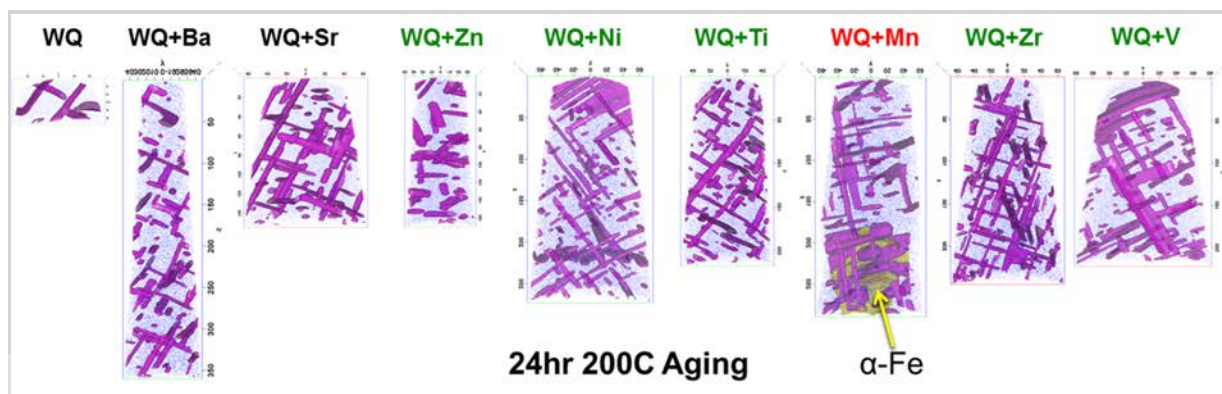


Figure 40. (Top panels) Atom probe measurements showing MgSi iso-surfaces, indicating Q-phase precipitate outlines (purple) and Si nano-precipitate outlines (green) for 1 and 72-hour aged samples at 200°C. (Bottom panels) TEM images showing the Q-phase rod-like precipitates and larger silicon particles.



Elemental additions to the Q-phase-based alloy were evaluated with QuesTek's thermodynamic databases, and button specimens were produced at GM. These elements were selected based on inputs from program advisors and DFT calculations showing the prevalence of certain elements to partition to the Q-phase. These additions may provide a strengthening effect either by reducing coarsening in the Q-phase (due to additional elements exhibiting slower diffusivities than Q-phase components) or by strengthening the interface between Q and Al. Atom probe experiments were performed on several of these samples (Figure 42). The Q-phase is present in all of these samples. The current analysis does not reveal clear differences in growth morphology, volume fraction, or sizes of the precipitates. However, segregation of certain elements was observed in these atom probe measurements (see Figure 42).



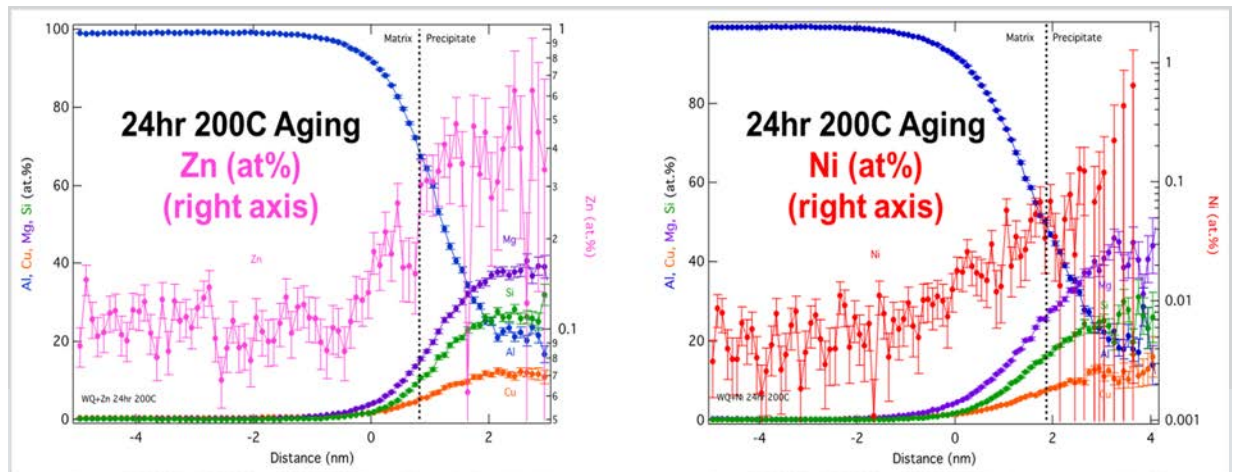


Figure 43. Proxigrams across Q-phase precipitate boundary in Zn and Ni-containing Q-alloy samples hours at 200°C. WQ+Mn also shows the existence of alpha-Fe particles.

As shown in the left side of Figure 43, Zn partitions to the Q-phase as expected from DFT calculations. The alloy contained 0.11 at% Zn shows that, at 200°C, the Q-phase consists of 0.42 at% Zn. This corresponds to a partitioning ratio (%Zn in precipitate/matrix) of 4.2. There also is a possible Ni partitioning to the Q-phase based on DFT calculations. The alloy contained 0.05 at% Ni; therefore, there is potential that partitioning is due to noise in the experiment. However, if partitioning was observed, the estimated partitioning ratio could be 8.55.

LEAP results also include findings for other elemental additions. Mn does not partition to the Q-phase; instead, it promotes α -Fe. Although not predicted by DFT calculations, zirconium (Zr), V, and Ti do partition to the Q-phase with partitioning ratios of 2.23, 2.74, and 4.52, respectively. However, uncertainty exists over what these elements would do to the alloy after it is further saturated with these additions. Continued studies will look at increased additions of these elements to determine the partition capability of these atoms in the Q-phase.

Unfortunately, strengthening effects due to elemental additions were found to be minimal based on current alloy compositions. A DOE study containing 16 varieties of alloying additions in Castalloy Q was performed to determine the effects of these elemental additions on precipitation strengthening and aging kinetics. Homogenization studies followed when isothermal heat treatments at 200°C were performed at a variety of aging times. While some samples showed an increase in hardness and modification to the over aging/softening and single and double hardness peak behavior over the baseline alloy (see Figure 44), it is difficult to draw conclusions about elemental addition effects. Correlations were found between the silicon (Si) phase fraction and Mg/Cu solid solution strengthening (via micro-hardness measurements) in alpha-Al.

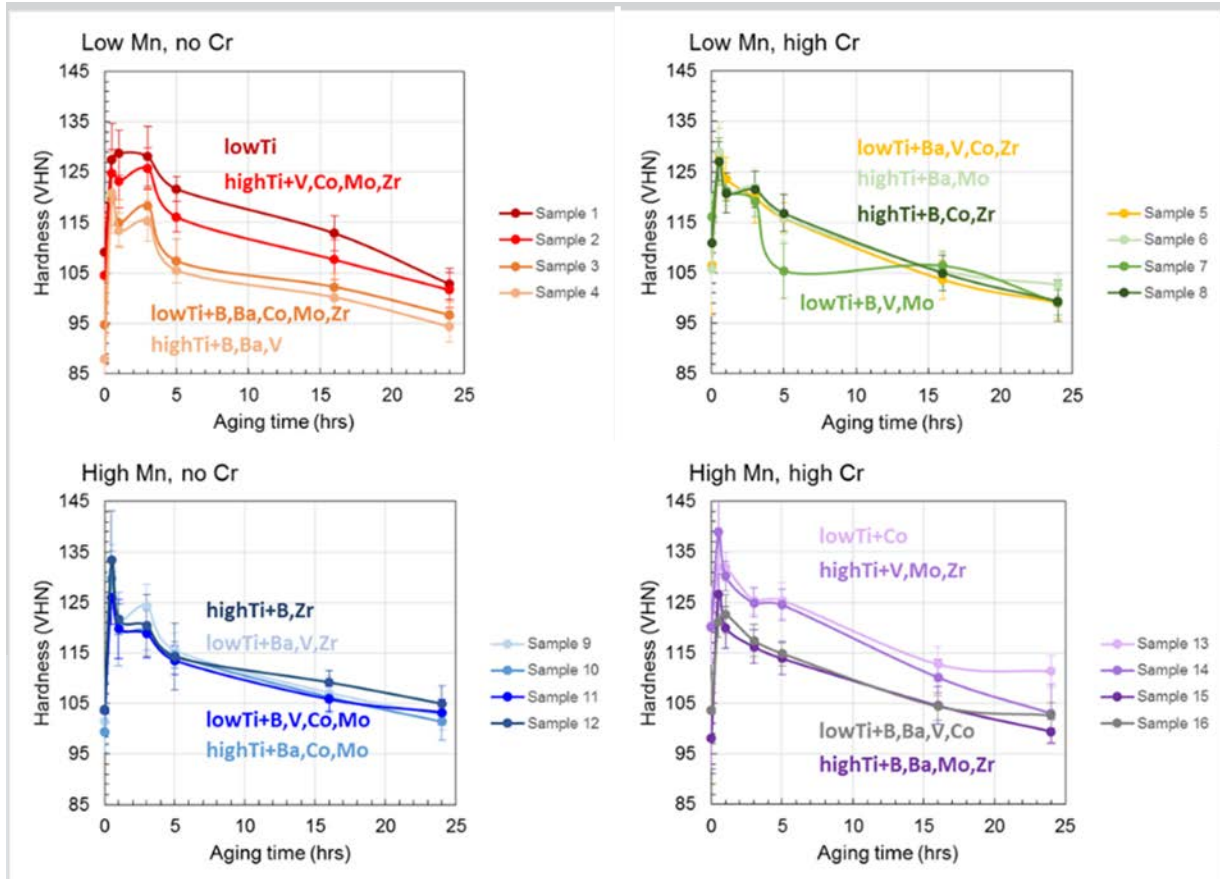


Figure 44. Isothermal hardness profiles of alloy additions.

Investigation of High-Q Phase Alloys

Modifications have been made to the database to account for a broadened Cu solubility in the Q phase. The extended solubility of Cu in Q was validated by choosing both “high-Cu” and “low-Cu” designs at either end of the fcc+Q phase field. The LEAP experiment measured the Cu content of the Q phase. The fcc+Q phase region and the maximum possible Q phase fraction at 200°C changes as a function of Si content. The Si level also affects the stability of the θ , β , and Si phases; for example, for a given Mg and Cu composition, only a small range of Si compositions will result in a two-phase fcc+Q alloy at 200°C. Two Si levels were selected, corresponding to a mid-Q phase fraction and a high-Q phase fraction. For each Q level, a high-Cu and low-Cu design was selected to lie on the phase boundaries between Q/diamond-Si and Q/ θ , respectively. LEAP was performed on these designs in order to measure the Cu content of the Q phase and to validate the predicted Cu solubilities. As shown in Figure 45, both LEAP and TEM analyses validated that these alloys remain in the Q-phase region because no θ phase was found.

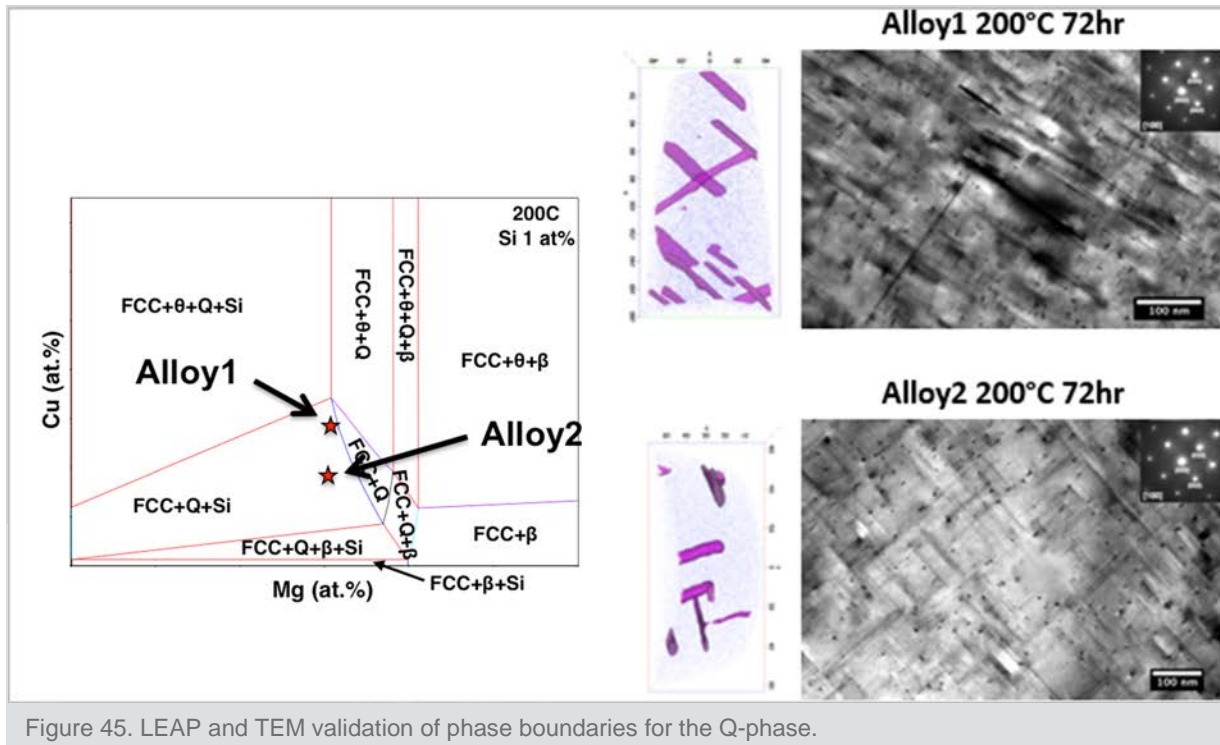


Figure 45. LEAP and TEM validation of phase boundaries for the Q-phase.

Strength Model Development

QuesTek precipitation simulation software, PrecipiCalc®, was used to generate particle-size, phase fraction, and matrix composition evolution during aging treatment at 200 and 250°C. Because the software cannot yet simulate rod-shaped growth and coarsening mechanisms, spheric particle data were used in the strength model to get predicted yield strength as a function of aging time. Figures 46 and 47 show the results of this exercise for HQLCu, HQHCu, Qalloy2, and WroughtQ aged at 200 and 250°C, respectively. Experimental data for each of the alloys are also shown in the figures. These values are micro-hardness converted yield strength values.

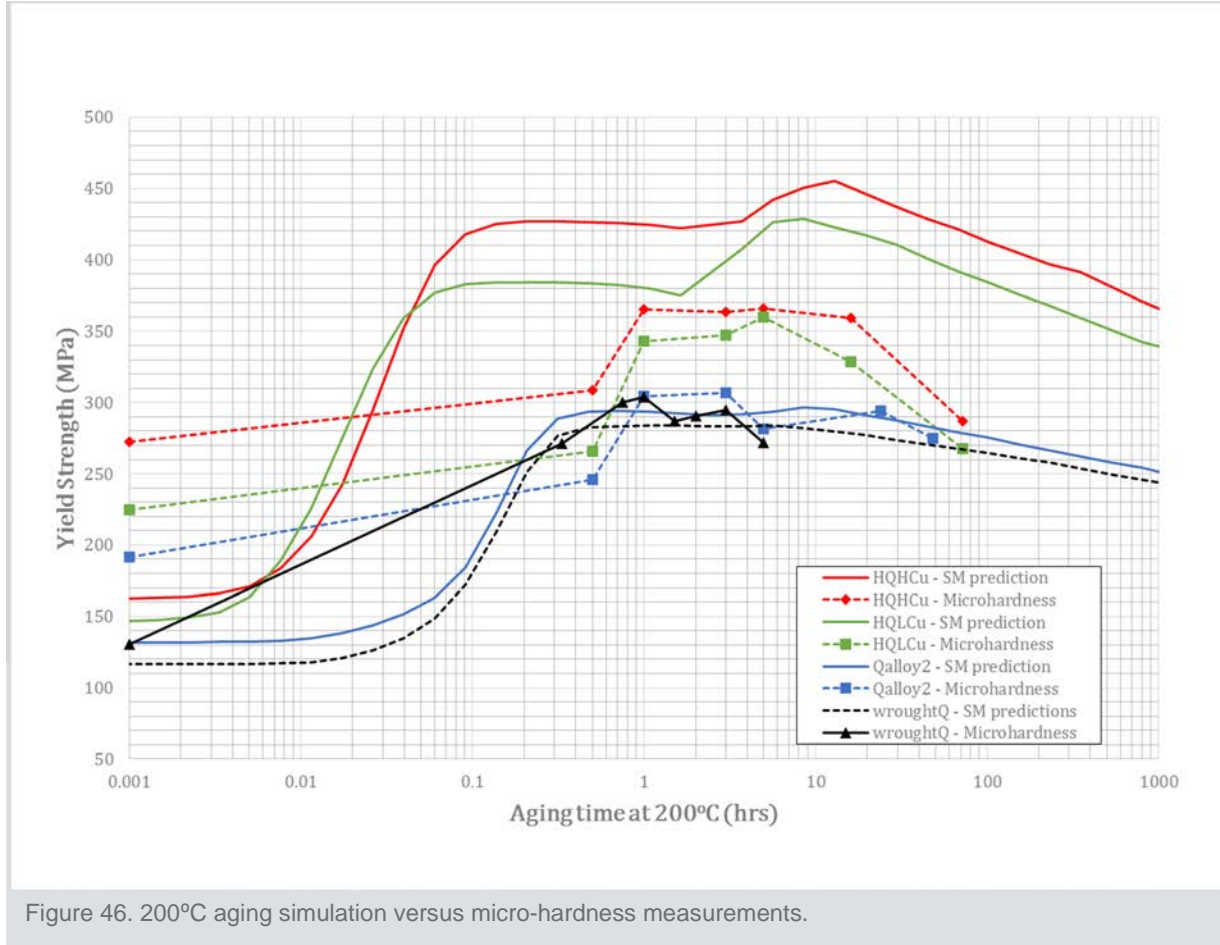
Interfacial energy was again fitted to the new thermodynamic database. The new database reduced the value of the interfacial energy calculated at each data point, which we believe reduces the sensitivity of precipitation to the interfacial energy. The interfacial energy in PrecipiCalc is modeled by the following function:

$$\gamma = C4[1 + D1 \tanh(D2(r + D3))]$$

where r , is the radius of the precipitate.

It can be observed in Figure 46 that the strength model predictions for Qalloy2 have good agreement with experimental data; however, the model is overpredicting the strength of the HighQ alloys. This discrepancy may be due to the fact that the predictions for the strengthening contributions due to the Q-Phase are being overestimated. However, as shown in Table 2, the measured volume fraction Q-phase is significantly lower than predicted. It is possible that some magnesium oxidized and never entered solution. It should be noted though that the model predicts the correct trend in the strength increment observed for the four alloys tested. However, differences remain between the magnitude of the measured and predicted strength levels for different compositions. This could be due to many factors, including rod-shaped precipitate structures. Future work will

focus on uncovering the origin of this modeling and/or experimental error.



A similar conclusion can be drawn from Figure 47, which shows the isothermal aging study at 250°C. For Qalloy2, it seems that the model predicts a good peak-aged strength; however, the drop in strength is not explained by the model, implying an incorrect coarsening behavior predicted by PrecipiCalc. Apart from the fact that the model overestimates the strength, it also predicts a lower strength of HighQ-HighCu alloy at longer aging times. It can be concluded that the model predicts a higher coarsening rate in HQHCu when compared to the HQLCu alloy, which is not true according to the experimental results. We believe this discrepancy is because we have to change the interfacial energy to get PrecipiCalc to run for each of the different alloys, and this change in interfacial energy is not calibrated by experimental observations. We have identified correction factors in the PrecipiCalc framework to incorporate rod-shaped precipitate evolution for reducing the uncertainty in the model and mitigating inconsistencies.

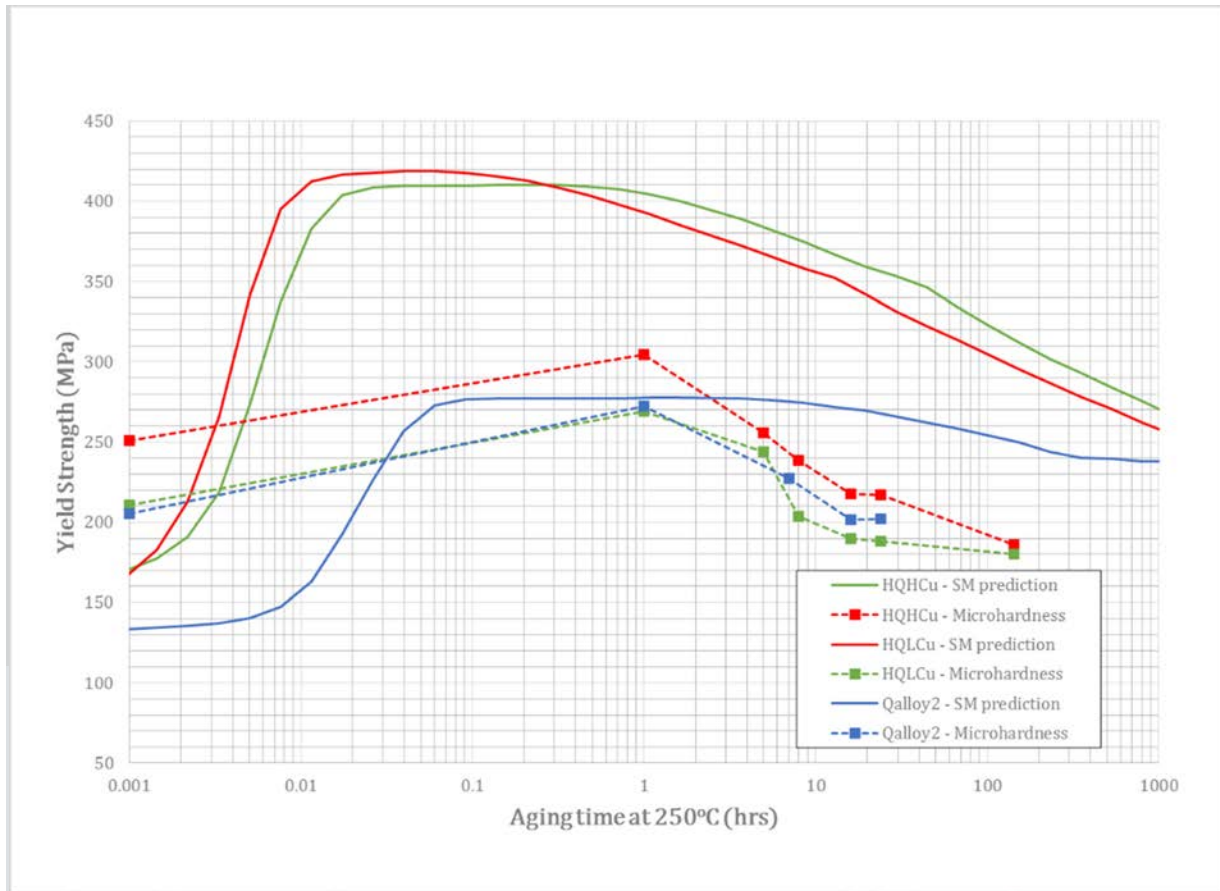


Figure 47. 250°C aging simulations versus micro-hardness measurements.

Table 2. Prediction and measured Q-phase fraction at 200°C.

| Alloy | Q-phase Volume Fraction at 200°C. | |
|--------------|-----------------------------------|------------------|
| | Prediction | LEAP measurement |
| Castalloy Q | 1.26 | 0.96 |
| HighQ-HighCu | 3.1 | 1.97 |
| HighQ-LowCu | 3.1 | 1.06 |

Milestone 10 Final Computational Design Completed

The Q-phase-based alloy provided the best combination of properties to meet most of the DOE program strength targets. CastalloyTQ and the eutectic versions of TQ and Q could not meet room-temperature ductility targets. Although TQ alloys provide higher room temperature strength, high-temperature properties were no better than the Q-phase-based alloy. The current Q-phase alloy has not yet met the high-temperature targets of the DOE program, and we are still investigating the role of small alloying additions. A comparison of measured values to DOE targets for the Q-phase alloy is shown in Table 3. These results are based on cast plates made in sand molds on a copper chill. Fine microstructure would represent properties likely seen in the combustion chamber area, where the highest properties are required. Medium microstructure would likely represent properties seen in head bolt bosses. Coarse microstructure could represent areas near the risers, where the

slowest cooling conditions take place. To evaluate the castability of the Q-phase-based alloy and the mechanical properties, including fatigue properties at room and high temperature, a head casting trial has now been carried out. Results are being measured now.

Table 3. A comparison of mechanical properties between DOE targets and Q-phase alloy. All high-temperature measurements made after 200 hours of conditioning at test temperature.

| Property | DOE Target | Q-Phase Alloy Fine Microstructure | Q-Phase Alloy Medium Microstructure | Q-Phase Alloy Coarse Microstructure |
|-------------------|------------|-----------------------------------|-------------------------------------|-------------------------------------|
| UTS (MPa) | 276 | 350 | 335 | 323 |
| YS RT (MPa) | 207 | 286 | 283 | 279 |
| Elongation RT (%) | 3.5 | 6 | 3.8 | 2.3 |
| UTS 250°C (MPa) | --- | 110 | 107 | 103 |
| YS 250°C (MPa) | --- | 89 | 83 | 80 |
| UTS 300°C (MPa) | 65 | 51 | 53 | 54 |
| YS 300°C (MPa) | 45 | 39 | 43 | 42 |

The Q-phase alloy is able to meet most DOE targets except for 300°C UTS and yield strength (Table 3). Because these samples were conditioned at temperature for 200 hours, where significant coarsening takes place, we are certain to meet these targets in unconditioned samples. However, our aim is to continue to improve the upper temperature targets.

It is recognized that adding elements will not increase ductility. An Mg/Si beta-phase strengthening alloy (e.g., A356) has the best ductility. However, the beta phase coarsens rapidly above 150°C. Theta-Q based alloys (e.g., 319 alloy) have low ductility although they have excellent room temperature strength. The Theta-Q-based alloys also coarsen rapidly and do not maintain their strength at 300°C. The combination of ICME tools, such as thermodynamic CALPHAD models, kinetic growth models, and strength models (all backed up by microstructural analysis of phases and measurement of mechanical properties) has directed our final selection of a Q-phase-based alloy as our final computational design. The Q-phase alloy has not only good ductility but also good high-temperature strength.

First Head Casting Trial

A total of 80 three-cylinder heads have now been cast and heat treated. A baseline alloy and two alloy variants of the final alloy composition were produced. From these heads, over 1,100 tensile, low-cycle fatigue, high-cycle fatigue, and microstructure specimens are being extracted and prepared for testing. The testing will be carried out over the next two quarters. Results from the two alloy variants will be compared to the baseline production alloy (i.e., A356) and the DOE targets. Tensile results are now coming in. Preliminary results do indicate improved high-temperature strength to the baseline alloy, with some loss of room temperature ductility (Table 4). However, it should be noted that improvements of tensile strengths at 300°C are very significant and we have now achieved our 300°C yield target.

Table 4. A comparison of tensile properties measured in head castings compared to DOE targets and a 356 alloy cast into chill plates. Head properties made after 100 hours of conditioning.

| Property | DOE Target | 356 Alloy | Baseline Alloy | Q-Phase Alloy |
|-------------------|------------|-----------|----------------|---------------|
| UTS (MPa) | 276 | 324 | 312 | 328 |
| YS RT (MPa) | 207 | 261 | 247 | 275 |
| Elongation RT (%) | 3.5 | 8.8 | 5.8 | 2.6 |
| UTS 250°C (MPa) | --- | 59 | 93 | 95 |
| YS 250°C (MPa) | --- | 55 | 84 | 86 |
| UTS 300°C (MPa) | 65 | 44 | 41 | 55 |
| YS 300°C (MPa) | 45 | 41 | 37 | 48 |

Along with material property measurements, the microstructural analysis will evaluate the true castability of the alloy in the head. A direct comparison will be made to the production intent alloy. Porosity measurements and full analysis of fracture surfaces will be used to identify the cause of fracture in tensile and fatigue samples.

Technology Transfer Path

During the last year of the project, when the final alloy and process is established, a second casting trial will be carried out on production heads. The purpose of this trial is to measure tensile and fatigue properties, particularly, to evaluate castability of the alloy in a head. This will also be the second step in evaluating the alloy for production.

Secondly, an evaluation of the recyclability will be carried out. It is essential that any alloy put into production will not adversely affect the Al recycling stream.

Thirdly, as required by the FOA and implemented into the second phase of the project, comprehensive cost models will be developed to include materials production, component casting, heat treatment, and machining costs for annual production runs up to 500,000 units of cylinder heads using the new alloy. A technology transfer and commercialization plan will be developed for the new alloy using the material properties and results of the cost model.

Once these steps have been established and the DOE project has concluded, GM will evaluate and select what future head will be the best first candidate for this new alloy. The head design will take into account the improved higher-temperature properties offered by this alloy. As is always carried out for a new head program, prototype tooling would be made and additional casting trials would be carried out. These casting trials would again collect material property data; however, heads would also undergo various benchmark tests and, finally, engine build and dyno-tests. GM would either select a supplier to conduct the trials or plan for production at one of our captured foundries. After patent protection has been established, Tier one suppliers will be given full access to knowledge of how to produce the alloy and process it for production purposes.

Summary

In 2016, GM and its partners completed validation of the alloy concepts and Milestone 9. Phase boundaries, based on improved thermodynamic databases, were validated by creating alloys near the upper phase boundary of the Q-phase region and analyzing the microstructure using TEM and LEAP imaging. Strength models were validated through hardness measurements and weaknesses were noted. A final alloy composition has been selected, thus completing Milestone 10. Minor variations are still being considered to improve room temperature ductility, high-temperature strength, and castability. Our first head casting trial has been completed. Tensile properties of head castings at room and high temperature have now also been completed; we are waiting on fatigue results. Microstructural analysis is being carried out. In 2017, further development of the alloy will be conducted, as well as a final head casting trial. A recyclability analysis and a full-cost analysis on the alloy and process will be performed.

Publications and Presentations

Bobel, Andrew C., Weiwei Zhang, Nick Hatcher, Qigui Wang, Mike Walker, and Greg Olson, 2016, "Thermodynamic and Compositional Assessment of Q-phase in Al-Si-Mg-Cu Alloys Using 3DAPT and in-situ TEM," presented at *The International Conference on Physical and Numerical Simulation of Materials Processing*, Seattle, Washington, October 14, 2016.

Project-Cast Alloys for Engines

FOA 648-3a – High-Performance Cast Aluminum Alloys for Next Generation Passenger Vehicle Engines

Amit Shyam, Dongwon Shin, Lawrence Allard Jr, Yukinori Yamamoto, Adrian Sabau, Thomas Watkins, Phil Maziasz and Wallace Porter

ORNL

1 Bethel Valley Road

Oak Ridge, Tennessee 37831

Phone (865) 241-4841; fax: (865) 574-6098

E-mail: shyama@ornl.gov

Christopher Glaspie, Seyed Mirmiran, and Lin Zhang

FCA US LLC

Jose Talamantes, Andres Rodriguez, and Alejandro Gonzalez

Nemak, S.A.

DOE Technology Manager: Jerry L. Gibbs

Phone: (202) 586-1182; fax: (202) 586-1600

E-mail: jerry.gibbs@ee.doe.gov

ORNL Technical Advisor: J. Allen Haynes

Phone: (865) 576-2894; fax: (865) 574-4913

E-mail: haynesa@ornl.gov

Contractor: ORNL, Oak Ridge, Tennessee

Prime Contract No.: DE-AC05-00OR22725

Objectives

The overall project has the following two objectives:

- To develop high-performance cast Al alloys with improved castability, high-temperature strength, and fatigue performance compared to industry standard 319 and 356 baseline alloys. Engine cylinder heads cast with the new alloys will have a minimum of 25% strength improvement compared to those cast from the baseline alloys. The cost of engine cylinder heads manufactured by the new alloys will be less than 110% of heads manufactured by 319 or 356. The developed alloys will enable an increase in maximum component operating temperature by about 50°C.
- To evaluate the adequacy of existing ICME models and codes for prediction of properties and development of cast Al alloys, a gap analysis report for existing ICME codes for cast Al alloy development will be generated.

Approach

- Develop microstructure property maps for baseline compositions
- Predictive modeling and ICME approach for alloy development and material/component property prediction

- Casting and mechanical property measurements for select compositions
- Components cast for materials that meet cost and property requirements
- Engine testing for components
- Cost analysis for production of a large number (i.e., hundreds of thousands) of components
- Commercialization plan.

Accomplishments

- Developed a family of affordable Al-Cu alloys with excellent elevated temperature mechanical properties and excellent hot tear resistance; filed a patent application and another invention disclosure.
- Completed preliminary casting trials on these alloys to manufacture engine cylinder heads.

Future Directions

- Continue engine cylinder head casting trials.
- Select an alloy for full-scale engine testing following cylinder head casting trials and thermomechanical fatigue evaluations.
- Develop a cost analysis and commercialization plan.

Introduction

Cast Al alloys that are standard across the automotive industry (e.g., 319 and 356 Al) have now been available for several decades. Design and implementation of higher-efficiency passenger automotive engines is currently limited by the absence of economical lightweight materials with improved castability, high-temperature strength, and fatigue performance. The next generation of lightweight alloys must allow a significant reduction in the total weight of automobiles, while still maintaining vehicle performance and safety.

Development of new cast Al alloys that allow improved performance will be dictated, to a large extent, by the ability to manipulate and enhance the desirable features of microstructural constituents. However, precipitation-hardened alloy systems are too complex to undertake this development process through trial and error. The trial and error alloy development approach is inefficient and expensive in the long run. In this regard, predictive modeling and ICME provide powerful tools for accelerating development and deployment of new cast Al alloys. In the present project, we plan ICME-based iterative design and development of new cast Al alloys with improved performance characteristics compared to industry standard 319/356 alloys. The new cast Al alloys will represent a significant opportunity for the automotive industry to increase engine efficiency.

Results

FY 2016 was the third year of this alloy development effort and culminated with filing a joint patent from the CRADA team (i.e., ORNL, FCA, and Nemak) for a family of cast, precipitation-hardened Al alloys with exceptional elevated temperature mechanical properties. The key alloy design concept was based on the knowledgebase developed during FY 2014 and FY 2015, defining the propensity of certain elements to segregate to high-energy interfaces of key strengthening precipitates to stabilize these interfaces (and metastable precipitates) to higher homologous temperatures than was previously considered possible for cast Al alloys. For example, one of the alloys in our new family of alloys had a room temperature yield and UTS of 200 and 356 MPa, respectively. These compare well to the target yield and UTS properties at room temperature of 205 and 275 MPa, respectively. At 300°C, this same alloy had yield strength and UTS of 105 and 137 MPa, respectively. These mechanical properties are greater than two times the DOE FOA target yield and UTS properties at 300°C of 45 and 65 MPa, respectively. In addition, the new families of alloys possess outstanding creep resistance at higher temperatures.

FY 2016 focused heavily on hot tearing analysis and initiation of casting trials of full-sized cylinder heads. Cast and heat-treated Al alloy materials were received from CRADA partner Nemak. The following seven alloys were cast and machined in the form of blocks (about 1 × 1 × 7-in.) from an area in a wedge casting with secondary dendrite arm spacing/grain size of about 30 μm:

- 319 – T7
- 356 – T6
- A356 – T6
- A356 + 0.5 Cu – T6
- 206 – T6
- Al-5Cu-Ni – T6
- Al-7Cu-T6.

Hot tearing resistance of the alloys must be adequate for a complex casting such as a cylinder head. In that regard, a multi-institution alloy development plan for improving the hot tear resistance of alloys with an elevated temperature stable microstructure was launched during this fiscal year. An image of a multi-leg hot tear evaluation casting from Nemak is shown in Figure 48.

For a quantitative comparison of the hot tearing susceptibility, several castings were performed in the shape shown in Figure 48. Each casting was examined and given a hot cracking rating number. This numerical rating value was obtained by examining



Figure 48. An image of the casting for evaluation of susceptibility to hot tearing.

each arm and assigning a value between 0 and 1 according to the following scheme:

- 1 point for a fully broken arm
- 0.75 points for a severe crack (arm fully cracked but still strongly attached to the central section)
- 0.5 points for a visible crack (arm not fully cracked)
- 0.25 points for a crack detectable only under magnifying glass
- 0 points when no cracks were present.

The average hot tear resistance was measured for the baseline and newly developed alloys. We also performed some quantitative hot tear tests at Worcester Polytechnic Institute (WPI) using an instrumented system. Models for hot tear resistance of cast Al alloys were implemented and compared to experimental casting results for the same compositions that were performed at WPI. The WPI casting experimental results, along with model predictions for baseline and high-temperature alloys, are shown in Figure 49. Images of hot tear experimental castings

of high-temperature alloys showing superior hot tear resistance are shown in Figure 50. The CRADA team submitted a patent application summarizing the improved mechanical and casting properties of the new alloys.



Figure 50. Images of hot tear castings that were performed at WPI.

Much of the effort during the current fiscal year included selection of an optimal alloy composition that allowed good mechanical properties (i.e., microstructural stability), hot tearing resistance, and low cost. The effect of grain refinement level on select alloys with good hot cracking resistance is shown in Figure 51.

A highlight of our project this fiscal year was successful casting of automotive cylinder heads with select compositions developed during the current effort (Figure 52). There were no chemistry-related

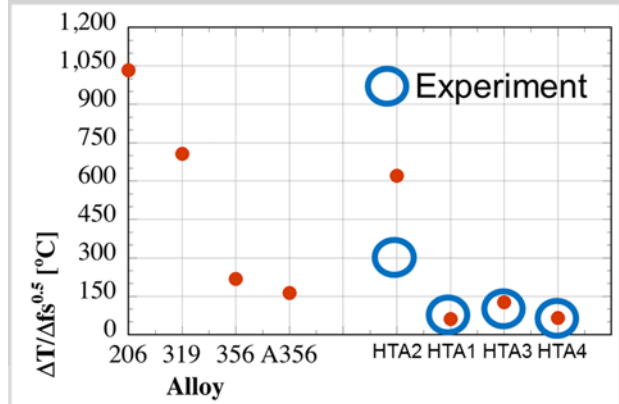


Figure 49. Model predictions and experimental hot tear resistance results for cast commercial baseline and new prototype high-temperature alloys.

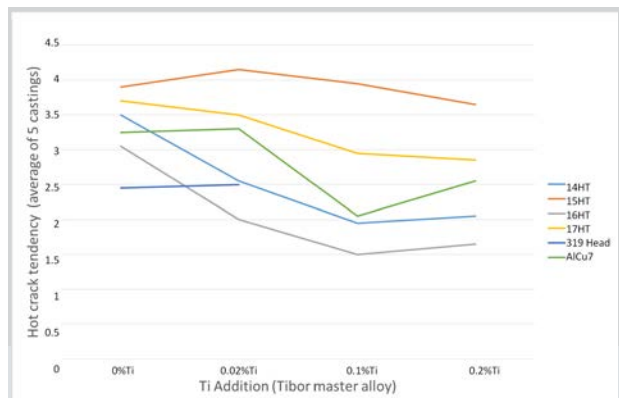


Figure 51. Hot cracking tendency for selected high-temperature cast Al alloy compositions.

defects in the cylinder heads during the initial quality inspections performed by Nemak. Another activity that was initiated in FY 2016 was use of high-performance computing to determine the favorable combination of alloying elements that could stabilize the strengthening precipitate in Al-Cu alloys.

Future Directions

Further work on characterizing cylinder heads, developing appropriate heat treatments, and characterization of residual stress, machinability, and corrosion resistance will continue in FY 2017, which is the final year of this project. Additional activities will include engine testing of cylinder heads from one or more new alloys and development of cost analysis and commercialization plans. A gap analysis report on the current state-of-the-art in modeling of cast Al alloys will also be composed in FY 2017.

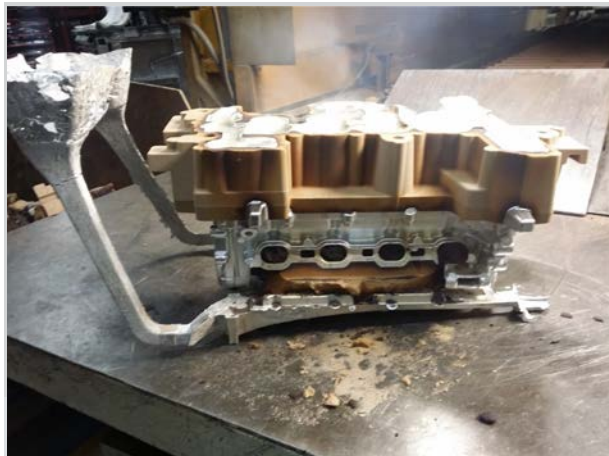


Figure 52. A full-scale cylinder head casting from a new alloy composition that was developed during the present CRADA project.

Conclusions

A new family of cast Al alloys was developed that substantially exceeded the DOE FOA tensile strength targets at 300°C. Further, casting strategies for these alloys resulted in very good laboratory-scale hot tearing behavior at two independent laboratories. Initial casting trials of the new alloys as full-scale cylinder heads showed no indications of chemistry-related casting defects. The project is on pace for full-scale engine testing of cylinder heads cast from the new alloys in the third quarter of FY 2017.

Publications and Patent

Roy, S., L. F. Allard, A. Rodriguez, T. R. Watkins, and A. Shyam, “Comparative evaluation of cast Aluminum alloys for automotive cylinder heads: Part I - Microstructure evolution,” in revision, *Metallurgical and Materials Transactions A*.

Roy, S., L. F. Allard, A. Rodriguez, W. D. Porter, and A. Shyam, “Comparative evaluation of cast Aluminum alloys for automotive cylinder heads: Part II: Mechanical and thermal properties,” in revision, *Metallurgical and Materials Transactions A*.

Sabau, A. S., S. Mirmiran, C. Glaspie, S. Li, D. Apelian, A. Shyam, J. A. Haynes, and A. F. Rodriguez, 2017, “Hot-tearing of multicomponent Al-Cu alloys based casting load measurements in a constrained permanent mold,” submitted to *TMS Annual Meeting 2017* proceedings.

Sabau, A. S. “Modeling of Casting Defects in an Integrated Computational Materials Engineering Approach,” in *Advances in the Science and Engineering of Casting Solidification: An MPMD Symposium Honoring Doru Michael Stefanescu* (eds: L. Nastac, B. Liu, H. Fredriksson, J. Lacaze, C.-P. Hong, A. V. Catalina, A. Buhrig-Polaczek, C. Monroe, A. S. Sabau, R. E. L. Ruxanda, A. Luo, S. Sen, and A. Diószegi), John Wiley & Sons, Inc., Hoboken, New Jersey, USA, doi: 10.1002/9781119093367.ch28.

Sabau, A. S., 2016, “Modeling of Interdendritic Porosity Defects in an Integrated Computational Materials Engineering Approach for Metalcasting,” accepted for publication in the *International Journal of Cast Metals Research*, February 2016.

Sabau, A.S., W. D. Porter, S. Roy, and A. Shyam, 2014, "Process Simulation Role in the Development of New Alloys Based on an Integrated Computational Materials Engineering Approach," (invited) paper IMECE2014-37982, *Proceedings of the ASME 2014 Int. Mech. Eng. Congress & Exposition IMECE2014, Volume 14: Emerging Technologies; Engineering Management, Safety, Ethics, Society, and Education; Materials: Genetics to Structures*, Montreal, Quebec, Canada, November 14 through 20, 2014.

U.S. Patent Application, filed May 2016, "Cast aluminum alloys with improved microstructural stability and strength at 350°C," with inventors Amit Shyam, Yukinori Yamamoto, Dongwon Shin, Shibayan Roy, J. Allen Haynes, Philip Maziasz, Adrian Sabau, Andres Rodriguez, J. Alejandro Gonzalez, Jose Talamantes, Lin Zhang, Seyed Mirmiran, and Christopher Glaspie.

Presentations

Cooper, R. C., S. Roy, A. Sabau, C. S. Hawkins, and A. Shyam, 2015, "Defect modeling and endurance limit prediction for cast aluminum alloys," (invited) *2015 TMS Annual Meeting*, Orlando, Florida, March 16, 2015.

Roy, S., L. F. Allard, and A. Shyam, 2015, "Nano-scale strength modeling of cast aluminum alloys," *2015 TMS Annual Meeting*, Orlando, Florida, March 16, 2015.

Roy, S., C. S. Hawkins, D. McClurg, G. Muralidharan, and A. Shyam, 2014, "Microstructure-mechanical property correlation in several cast aluminum alloys," *Materials Science and Technology (MS&T) 2014*, Pittsburgh, Pennsylvania.

Roy, S., C. S. Hawkins, D. McClurg, G. Muralidharan, L. F. Allard, A. Rodriguez, and A. Shyam, 2014, "Microstructure-mechanical property correlation in several cast aluminum alloys," *MS&T 2014 – Materials Science & Technology Conference*, Pittsburgh, Pennsylvania, October 12 through 16, 2014.

Sabau, A.S., 2015, "Modeling of Casting Defects in an Integrated Computational Materials Engineering Approach," *2015 TMS Annual Meeting & Exhibition, Proceedings: Advances in the Science and Engineering of Casting Solidification: An MPMD Symposium Honoring Doru Michael Stefanescu*, Orlando, Florida.

Shin, 2015, "Solute Cluster and Vacancy Interaction in Multi-Component Al Alloys," *2015 TMS Annual Meeting*, Orlando, Florida, March 16, 2015.

Shin, D., 2014, "High Performance Cast Aluminum Alloys for Next Generation Passenger Vehicle Engines," (invited) *Materials Genome Initiative: Materials Data Workshop*, Dayton, Ohio, July 15 and 16, 2014.

Shyam, A., 2016, "High Performance Cast Aluminum Alloys for Next Generation Passenger Vehicle Engines," *U.S. DOE Vehicle Technologies Office 2016 Annual Merit Review and Peer Evaluation Meeting*, Washington D.C., June 9, 2016.

Project-Materials for High Efficiency Engines

Agreement 13329 (Task 26190) – High-Temperature Materials for High-Efficiency Engines

G. Muralidharan, D. T. Pierce, and B. Pint
ORNL Materials Science and Technology Division
1 Bethel Valley Road
Oak Ridge, Tennessee 37831
Phone (865) 574-4281; fax: (865) 574-4357
E-mail: muralidhargn@ornl.gov

DOE Technology Manager: Jerry L. Gibbs
Phone: (202) 586-1182; fax: (202) 586-1600
E-mail: jerry.gibbs@ee.doe.gov

ORNL Technical Advisor: J. Allen Haynes
Phone: (865) 576-2894; fax: (865) 574-4913
E-mail: haynesa@ornl.gov

Contractor: ORNL, Oak Ridge, Tennessee
Prime Contract No.: DE-AC05-00OR22725

Objectives

- Identify and catalog the materials property requirements for exhaust valves in the next generation of high-efficiency engines.
- Evaluate mechanical properties and oxidation resistance of leading, existing, Ni-based alloys candidates and alternate materials with the capability to operate at 950°C.
- Adopt ICME-based techniques to develop alternate, lower-cost, Ni-based alloys for exhaust valve applications at temperatures up to 950°C.

Approach

- Mechanical property requirements for operation at 950°C will be defined and the microstructure required to achieve target properties will be identified.
- Oxidation tests will be performed to understand composition effects on oxidation behavior and establish limits of critical elements.
- A synergistic computational modeling and experimental evaluation approach followed during design of new alloys for exhaust valve applications up to 870°C in a previous project will be refined and used to identify promising compositions for service at 950°C.
- Trial heats of new compositions will be prepared, properties measured, and compositions refined in an iterative manner.

Accomplishments

- Demonstrated new alloys with better high-temperature strength than Alloy 751 and Alloy 520 at 950°C.
- Identified avenues for improving oxidation resistance.
- Identified appropriate processing temperature for industrial processing.

Future Directions

- Evaluate alloying element additions and strategies to improve high-temperature oxidation resistance.

Introduction

Improving engine efficiencies of passenger and commercial vehicles is a major goal of the Vehicle Technologies Program. Propulsion materials play a significant role in achieving this objective. An important strategy in achieving the goals of improving engine thermal efficiency is advancing technologies that increase engine combustion efficiency such as lean-burn operation (i.e., high efficiency clean combustion), high levels of exhaust gas recirculation, turbocharging, variable valve actuation, and/or variable compression ratios. A significant barrier to achieving increased efficiency is the need to simultaneously reduce pollutant formation and be achievable through high-efficiency combustion technologies. One potential method for achieving improved engine efficiency while reducing emissions is through retaining more heat in the exhaust gas.

Strategies for retaining more heat in the exhaust naturally result in increased exhaust gas temperatures, thus increasing the operational temperature requirements of components in the exhaust gas path, particularly exhaust valves. It has been projected that exhaust gas temperatures would increase from a current value of 760°C to values of at least 870°C and very likely reaching as high as 1000°C in the long-term (DOE 2013a, DOE 2013b). Availability of materials with adequate high-temperature mechanical properties and oxidation resistance to enable the projected engine operating parameters without exceeding automotive cost constraints is a barrier to adoption of new high-efficiency technologies. The objective of the current project is to address the needs of cost-effective materials for exhaust valves for operation up to 950°C.

A recently concluded project successfully addressed development of new lower-cost alloys for use in exhaust valves at temperatures up to 870°C through a “materials-by-design” approach (Muralidharan 2014a,

Muralidharan 2014b). “Materials-by-design” is a concept that encompasses a collection of materials-related techniques, including modeling, correlation, and materials modification. The premise behind materials-by-design is that mechanical properties are correlated to microstructure and phase composition. Desirable phase compositions and microstructures can be achieved through

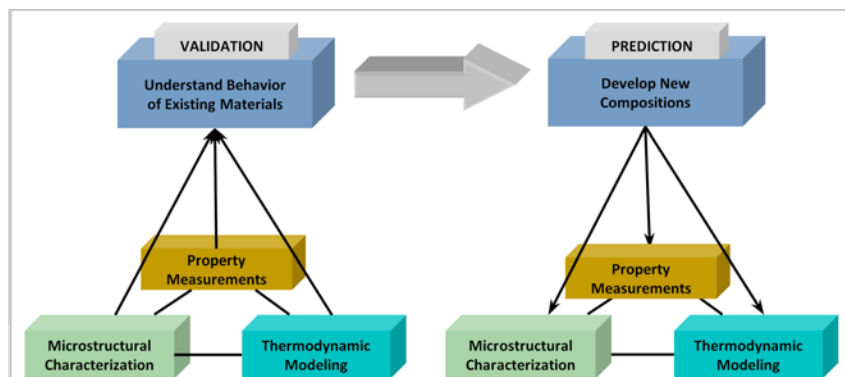


Figure 53. Materials-by-design approach used for design of new valves alloys.

thermodynamic equilibrium or through non-equilibrium techniques such as quenching, rapid casting solidification, and mechanical working. These characteristics can be correlated to the desired mechanical properties through computational equilibrium thermodynamics or through a variety of correlation techniques. The correlations allow untested compositions or treatments to be computationally modeled; therefore, the desired trends can be rapidly established. Small heats of targeted materials can then be processed to confirm the modeled properties and to broaden the correlation database. Figure 53 captures the concepts in this approach.

High-performance exhaust valves currently used at temperatures up to about 760°C are fabricated using Ni-based alloys such as commercial Alloy 751. Other higher-performance, Ni-based alloys primarily developed for aerospace applications have the potential to operate at temperatures of 950°C with desired strength and oxidation resistance, but may be expensive for automotive applications and may also be very difficult to fabricate into desirable shapes. Therefore, new alloys with appropriate strength, oxidation resistance, and formability may have to be specifically developed for the operating characteristics and lifetime expectations for automotive valves.

In an earlier study on automotive valves for performance at 870°C, a “materials-by-design” approach consisting of synergistic computational and experimental aspects was used to develop cost-effective Ni-based alloys for use at this temperature (Muralidharan 2014a, Muralidharan 2014b, Muralidharan 2016). High-temperature tensile strength and high-cycle fatigue strength were identified as critical properties required for the performance of these alloys in valve applications. An understanding of the strengthening mechanisms in existing commercial alloys was required to use the computational modeling approach for developing materials with improved properties and lower cost. A range of Ni-based alloys, with potentially varying weight fractions (or volume fractions) of γ' , were identified in efforts to correlate fatigue properties with the microstructure of alloys. Selection of nine commercial, Ni-based alloys included Alloy 751, Waspaloy, Udimet 520, and Udimet 720. The Ni+Co contents ranged from 66 to 76 wt%. To obtain initial information about the microstructures of these alloys at equilibrium, thermodynamic calculations were carried out. Comparison of the calculation results showed that all alloys have a matrix of γ with the major strengthening phase as γ' . One or more carbide phases (e.g., $M_{23}C_6$, MC, and M_7C_3) may also be present in different alloys. The primary difference between the microstructures of the various alloys was the weight percent of the γ' phase at a given temperature and the highest temperature at which the γ' phase is stable in the different alloys. Because the size of the strengthening precipitates is also critical, it was anticipated that the coarsening kinetics of this phase would also be influential in the long-term performance of the alloys in this application.

Using the microstructures of these alloys as a guide, computational thermodynamics were used to design new alloys with a microstructure similar to the commercial alloys in an

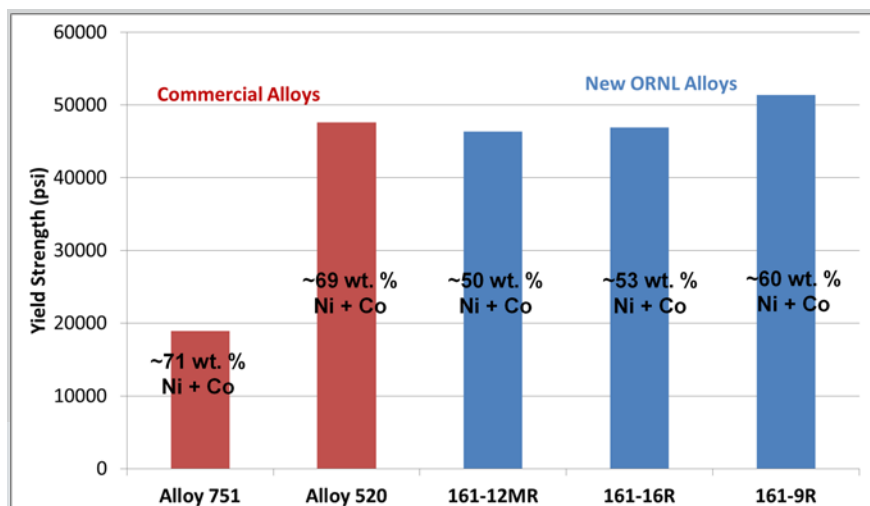


Figure 54. Yield strength of some of the new ORNL alloys at 950°C exceed that of Alloy 520.

effort to obtain materials with desirable properties. In contrast to the commercially available alloys with Ni+Co contents greater than 66 wt%, the Ni+Co content in these newly identified candidate alloys was lower than 50 wt% (Ni being replaced with other elements such as Fe) with the potential to achieve comparable properties. The lower Ni content implies that the alloys would be of lower cost, but with the potential to achieve targeted improvements in fatigue life versus Alloy 751.

Based on results from this computational alloy design process, small batches of the new, lower-Ni candidate alloys were cast. The alloys were then homogenized and rolled at high temperatures. Small tensile specimens were machined from these alloys and tensile tests were conducted in-situ at 870°C. Based on results from tensile tests, several candidate alloys from the newly developed suite of promising compositions with Ni+Co contents lower than 50 wt% were down selected for preparation of larger-sized heats. These were cast under inert gas cover and mechanically processed into plates for further machining. High-temperature fatigue tests were performed on the down selected alloys. New alloys with fatigue lives of 100 million cycles at stresses of 25 to 30 ksi at 870°C were identified.

The purpose of this project is to extend this successful approach to identification/ development of materials for exhaust valves that could operate at temperatures up to 950°C. In addition to high-temperature mechanical properties (i.e., tensile strength and fatigue), oxidation resistance is expected to play a role in determining the lifetime of exhaust valves at higher temperatures and will be considered in identification/development of new materials for exhaust valves. Required materials properties will be identified, baseline material properties will be evaluated, and development of new materials will be targeted to pursue required properties at a lower materials cost.

Results

In an effort to understand the effect of alloy composition on mechanical properties and oxidation resistance of candidate Ni-based alloys, several new alloys were cast and fabricated in FY 2016 and high-temperature tensile testing and oxidation testing were performed on newly developed Ni-based alloys. In FY 2015, the yield strengths of new ORNL alloys were found to be much better than Alloy 751 and were observed to be almost comparable to that of Alloy 520 at 950°C. In FY 2016, the yield strength target was to exceed that of Alloy 520 at 950°C, while keeping the cost of alloying element additions as low as possible. Figure 54 shows the yield strengths of several new alloys that were fabricated during FY 2016, along with their Ni levels. Note that one alloy (i.e., 161-9R) shows yield strength greater than Alloy 520 at 950°C, but it contains a lower Ni+Co-level (60 wt% Ni+Co vs 69 wt% Ni+Co in Alloy 520). Thus, a path to developing new alloys with lower Ni+Co levels and strength comparable to or greater than 520 have been identified in this work.

The second major goal of this project was to obtain the best combination of high-temperature strength and oxidation resistance at 950°C in alloys with lower Ni-levels. To attain this goal, effort was expended in FY 2016 to devise design schemes that would improve the oxidation resistance of a family of new alloy compositions developed at ORNL. In FY 2015, several alloys with improved oxidation at 900°C were identified. In FY 2016, these and other alloy compositions were evaluated for their oxidation behavior at 950°C. Figure 55 shows the effect of increasing the testing temperature from 900 to 950°C. Figure 55(a) shows weight change as a function of the number of 1-hour cycles in air + 10% water vapor environment at 900°C obtained during FY 2015. It should be noted that adding water vapor to simulate the actual exhaust environment creates a more aggressive oxidation test than using oxygen, dry air or lab air, particularly for alloys that form protective chromia (Cr₂O₃)

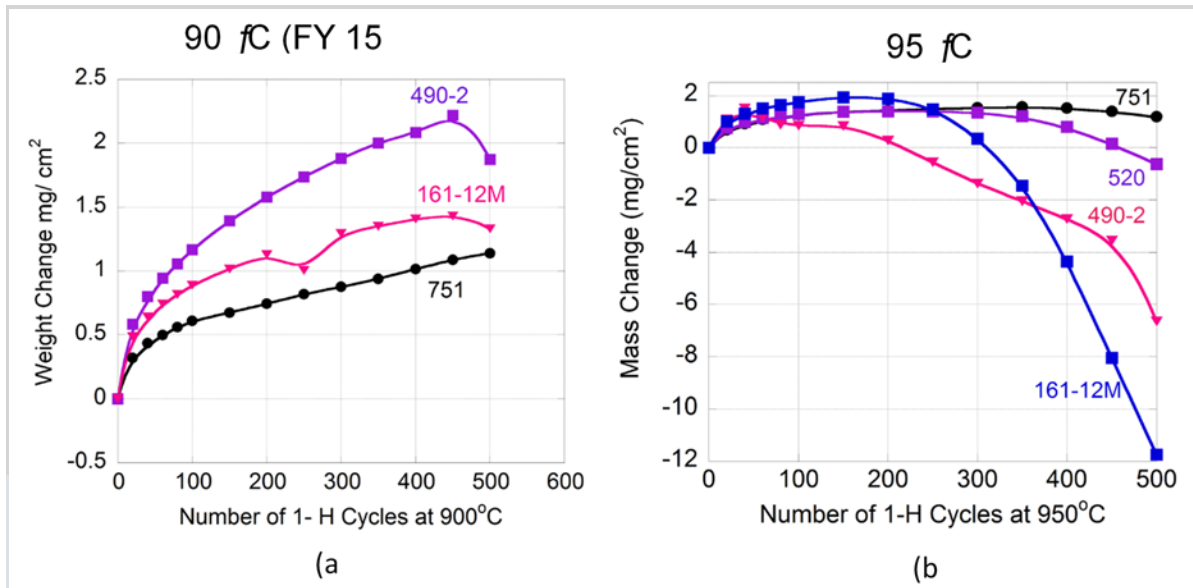


Figure 55. Effect of temperature on the weight change measured in 1-hour cycles in air + 10% water vapor environment: (a) 900°C and (b) 950°C.

scales. This study utilized ORNL's unique laboratory facilities for cyclic oxidation testing in controlled atmospheres. Figure 55(b) shows the weight change for same alloys in the same environment, except for at 950°C. Note that ORNL prototype alloys such as 490-2 and 161-12M that show gradual positive weight change (the desired performance) at 900°C show evidence of oxide-scale spalling (i.e., mass loss) at 950°C. Alloy composition modifications were undertaken that included additions of trace amounts (less than 0.1 wt%) of reactive elements such as Hf, La, and Y.

Improvement in weight change as a function of the number of thermal cycles at 950°C in air + 10% water vapor environment is shown in Figure 56. Alloy 161-12M+ shows a gradual increase in specific mass as a function of thermal cycles in contrast to 161-12M, which shows a substantial decrease in specific mass under the same conditions. Figure 57 shows a cross-section of specimens from two alloys (i.e., Alloy 751 and 161-12M) exposed to 500 cycles at 950°C. Note the 161-12M alloy shows comparable internal oxidation to Alloy 751. Therefore, the newly developed ORNL alloys have the potential to provide improved strength while maintaining oxidation resistance similar to that of existing chromia-forming valve alloys.

Processing Optimization

One of the difficulties encountered during this work has been processing of this class of alloys on a commercial scale at Carpenter Technologies. One commercial-scale heat each of two different ORNL alloys was previously prepared at Carpenter, but the processing conditions were far from optimized in those first heats, as reported previously. To understand the optimum processing

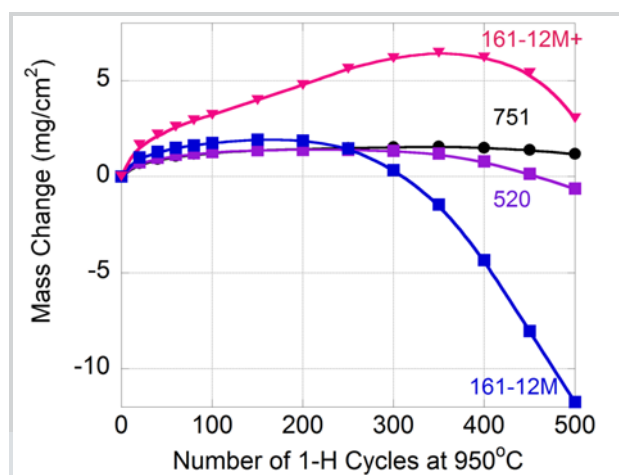


Figure 56. Effect of reactive elements additions on oxidation behavior of an ORNL alloy in 1-hour cycles at 950°C in air+ 10% water vapor.

temperatures, Gleeble experiments were performed at ORNL in FY 2016 to understand the effect of temperature on alloy ductility at high strain rates. Results showed that processing temperatures need to be lowered for improved high-temperature ductility in ORNL alloys when compared to those used for earlier industrial-scale processing trials. This information will be used for processing of the next industrial-scale alloy heats at Carpenter.

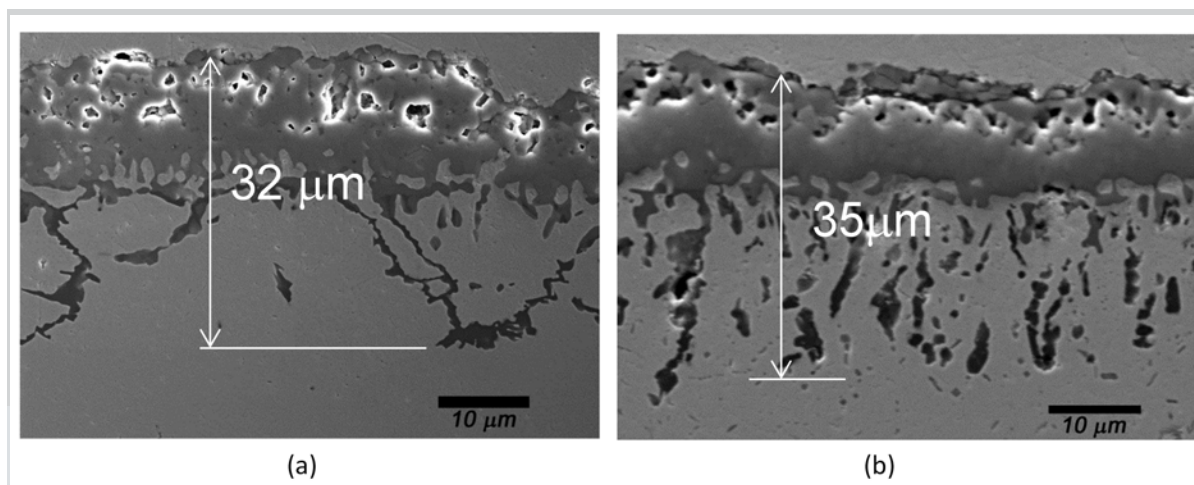


Figure 57. Effect of alloy composition on the oxide scale after 500-hour exposure to air + 10% water vapor environment at 950°C: (a) Alloy 751 and (b) Alloy 161-12M.

Conclusions

Development of exhaust valve materials for use at temperatures up to 950°C requires balancing oxidation resistance with high-temperature mechanical properties. New NiCrFe-based alloys with yield strengths greater than that of Alloy 520 at 950°C have been successfully designed. A new generation of alloys with improved oxidation resistance at 950°C has been designed and fabricated at laboratory scale. Results show that this family of alloys with lower Ni+Co levels than existing commercial Ni-based alloys (e.g., Alloy 751 or Alloy 520) and equivalent or higher strength can also achieve comparable oxidation resistance at 950°C. Processing routes for industrial-scale processing of these new alloys has been identified.

References

- DOE, 2013a, “Light-Duty Vehicles Technical Requirements and Gaps for Lightweight and Propulsion Materials,” DOE Vehicle Technologies Workshop report, February 2013.
- DOE, 2013b, “Trucks and Heavy-Duty Vehicles Technical Requirements and Gaps for Lightweight and Propulsion Materials,” DOE Vehicle Technologies Workshop report, February 2013.
- Muralidharan, G., 2014a, “Low-Cost Fe-Ni-Cr Alloys for High Temperature Valve Applications,” U.S. Patent Application 14/307,733, filed June 18, 2014.
- Muralidharan, G., 2014b, “Low-Cost, High-Strength Fe-Ni-Cr Alloys for High Temperature Exhaust Valve Applications,” U.S. Patent Application 14/497,550, filed September 26, 2014.
- Muralidharan, G., 2016, “Effect of Composition on the High-Temperature Strength of Several Model Ni-Based Alloys,” poster presentation, *TMS Meeting 2016*.

Presentations

Muralidharan, G., 2016, “High Temperature Materials for High Efficiency Engines,” *U.S. DOE Vehicle Technologies Office 2016 Annual Merit Review and Peer Evaluation Meeting*, Washington D.C., June 9, 2016.

Project-Materials for Control of Exhaust Gases and Energy Recovery Systems

PNNL – Innovative SCR Materials and Systems for Low-Temperature After-treatment (FCA US LLC CRADA)

Yong Wang
PNNL
902 Battelle Boulevard
Richland, Washington 99354
Phone (509) 371-6273; fax: (509) 371-6498
E-mail: yong.wang@PNNL.gov

DOE Technology Manager: Jerry L. Gibbs
Phone: (202) 586-1182; fax: (202) 586-1600
E-mail: jerry.gibbs@ee.doe.gov

ORNL Technical Advisor: J. Allen Haynes
Phone: (865) 576-2894; fax: (865) 574-4913
E-mail: haynesa@ornl.gov

*Contractor: PNNL, Richland, Washington
Prime Contract No.: DE-AC05-00OR22725*

Objectives

- Enabling an SCR catalyst system that will function at a very high efficiency to attain the most demanding emissions regulations and thereby facilitate market introduction of advanced powertrains that will support domestic energy independence and security.
- Further develop newly invented materials for SCR of NO_x by NH₃ that show promise for significantly reducing ‘light-off’ temperatures compared to current commercial catalysts. Specifically, the goal of the proposed work is to achieve ‘light-off’ of NH₃ SCR at 150°C in order to realize conversion efficiencies of 90% at these low temperatures.

Approach

In this CRADA, there are primary and sub-objectives for both SCR catalyst development and the SCR catalyst system. With respect to the SCR catalyst development project, the main goal and associated sub-goals are as follows:

- Adapt a newly developed SCR material to provide 90% conversion efficiency of NO_x at 150°C under conditions consistent with low-temperature portions of the FTP cycle.
 - Demonstrate selectivity toward N₂ formation of 90%
 - Demonstrate the SCR catalyst, aged under realistic conditions, will continue to provide 90% conversion efficiency at 150°C and N₂ selectivity

- Evaluate the SCR catalyst activity using a matrix of both passive and active NH₃ sources.

With respect to the SCR catalyst system, the primary objective and sub-objectives are as follows:

- Demonstrate that an SCR catalyst system will attain Tier III and SULEV30 NO_x emissions using an engine or simulated engine FTP cycle.
 - Characterize fresh and aged NO_x reduction efficiency and selectivity toward N₂ formation of the SCR system using both active and passive NH₃ generation strategies
 - Determine the fuel penalty associated with each NO_x reduction strategy
 - Estimate the control/onboard diagnostics complexity and cost
 - Estimate the component and system cost.

These goals and objectives are aligned with the work plan for this project. In general, PNNL will focus on development of the low-temperature SCR catalyst. FCA US LLC activities (in collaboration with the University of Houston) will center on upstream reductant generation strategies that provide necessary NH₃ NO_x reduction over the new SCR catalyst. Both PNNL and FCA US LLC will work on testing and integrating the system on a bench (PNNL) and dyno (FCA US LLC) level. The high-level layout of activities is shown in Figure 58.

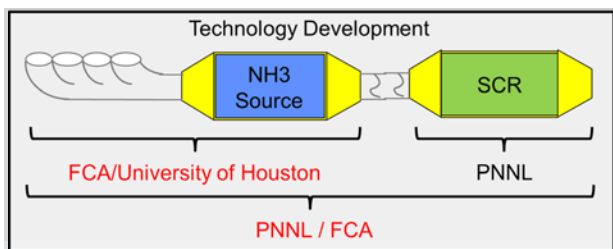


Figure 58. Work plan focus areas for PNNL and FCA US LLC.

Accomplishments

- Demonstrated greater than 90% NO_x conversion efficiency at 175°C with a first generation catalyst, which is much improved when compared to the current commercial catalysts.
- Identified research direction for the development of the second generation catalysts.
- Synthesized a large batch of first generation Cu/SSZ-13 catalyst (greater than 500 g) with excellent reproducibility. This will be used to identify key issues that may exist in preparation of washcoat and to conduct hydrothermal aging studies of core samples.
- Down selected on a possible alternative (to urea) NH₃ generation strategy and identified the operation characteristics of NH₃ generation catalyst.

Future Directions

- Develop a second generation SCR catalysts to meet the conversion efficiency target.
- Verify sufficient hydrothermal stability of second generation SCR catalysts.
- Design NH₃ generation.
- Conduct system component aging.

Introduction

Future powertrains that will be significantly more efficient than currently available technologies will be needed by automotive manufacturers to meet rapidly increasing Corporate Average Fuel Economy and greenhouse gas standards. However, these powertrains cannot enter into the U.S. light-duty vehicle market unless they are coupled with an after-treatment system that will sufficiently remediate tailpipe emissions to meet Environmental Protection Agency Tier III and California super ultra-low emission vehicle emissions standards. The low-temperature exhaust associated with these powertrains is especially challenging for any current after-treatment technology for meeting these standards.

In 2010, Cu²⁺-exchanged molecular sieves with Chabazite (CHA) zeolite structures (e.g., Cu/SSZ-13 and Cu/SAPO-34) were commercialized as NO_x after-treatment catalysts in diesel-powered engines for transportation due to their much improved activity, selectivity, and durability (Gao et al. 2013). The ability of these catalyst materials to reduce NO_x with NH₃ in the presence of excess of oxygen provides the foundation for this remarkable new vehicle emission control technology. However, currently commercialized catalyst formulations are not sufficiently active at temperatures below 200°C (performance is required in order to enable introduction of new and more fuel-efficient lean combustion powertrains). PNNL's recent studies of Cu/CHA-based catalysts for NH₃ SCR recently discovered that incorporation of alkali and alkaline earth atoms (such as Na, Li, K, Cs, Mg, and Ca) can significantly affect the temperature at which these catalysts perform (Gao et al. 2015).

The focus of this program is to further develop alkali and alkaline-promoted Cu/SSZ-13 materials for SCR of NO_x by NH₃ that show promise for significantly reducing 'light-off' temperatures compared to current commercial catalysts. Specifically, the goal of the proposed work is to achieve 'light-off' of NH₃ SCR at 150°C in order to realize conversion efficiencies of 90% at these low temperatures. This will enable deployment of lean combustion powertrains with significantly increased fuel efficiencies but lower exhaust temperatures. To accomplish these overall goals, it will be essential to also identify an appropriate NH₃ supply strategy for the SCR after-treatment device that can controllably deliver NH₃ at these low temperatures.

Results

Co-Cation Effects

To study the co-cation effect on standard SCR performance, SSZ-13 support with a Si/Al ratio of six was used to prepare Cu/SSZ-13 with a Cu loading of 1 wt%. Co-cation (Na) was added to this sample (denoted as PNNL catalyst). This catalyst was compared with an industrial standard catalyst (i.e., Cu/SSZ-13) under the standard SCR conditions and the results are shown in Figure 59 (left). Addition of Na improved the low-temperature NO_x conversion as evidenced by reducing the temperature required to reach 90% conversion from 200 to 175°C. Separate ²⁷Al-MAS-NMR studies also demonstrated that addition of Na to Cu/SSZ-13 improves the catalyst hydrothermal stability. Increasing Cu loading from 1 to 3% can further improve low-temperature NO_x conversion (Figure 59 right), as evidenced by reaching 70% NO_x conversion as opposed to 50% NO_x conversion at 150°C for Na-promoted 1%Cu/SSZ-13. However, there is a negligible effect of Na on both low and high-temperature NO_x conversion at 3% Cu loading (Figure 59 right). This is likely due to competition of Na for the optimized Cu dispersion and location within SSZ-13 at high Cu loadings. Additional studies suggest that improved crystallinity of SSZ-13 and the presence of NO₂ could be future directions to further improve the

low-temperature NO_x conversion. Synthesis procedures can be optimized in order to achieve better crystallinity of SSZ-13. These results lay out the foundation for development of a second generation catalyst.

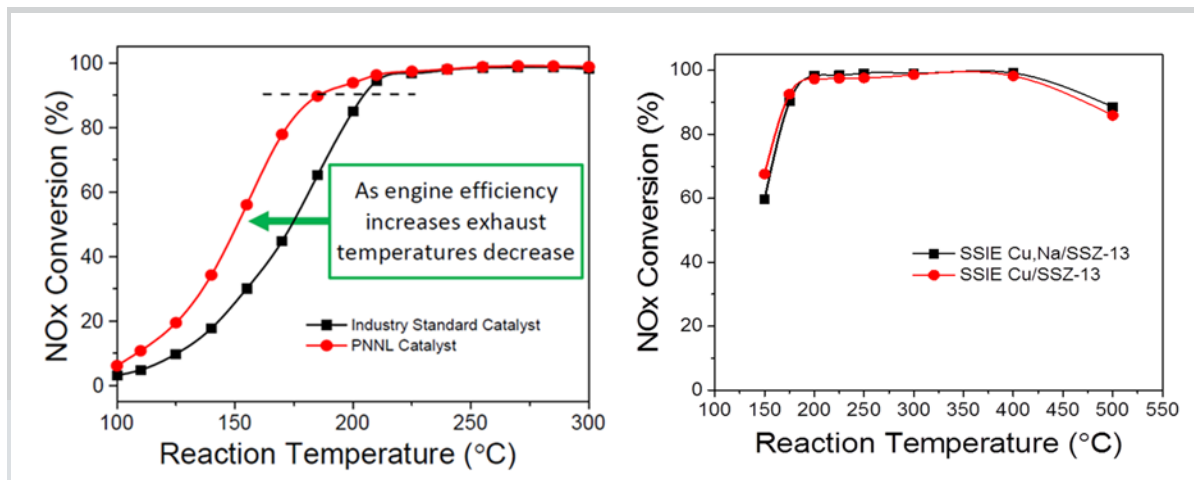


Figure 59. Standard NH₃-SCR light-off curves for the fresh Cu/SSZ-13 samples: addition of Na to 1%Cu/SSZ-13 (left), and addition of Na to 3%Cu/SSZ-13 (right).

Synthesis of Large Batch Cu/SSZ-13

Efforts have been made during Year 1 on development of synthesis protocol in order to reproducibly synthesize Cu/SSZ-13. Both physical and chemical characterizations (e.g., XRD, N₂ physisorption, helium ion microscopy, and ²⁷Al-MAS-NMR) were used to provide detailed information on SSZ-13 prepared in various batches. We have developed a producible synthesis protocol that not only provides similar crystallinity, morphology, phase purity, and structure of the SSZ-13 prepared in various batches, but also shows very reproducible NO_x conversion behaviors (Figure 60). The reproducible synthesis protocol developed in this program allows us to synthesize a large batch, first generation Cu/SSZ-13 catalyst (500g). Ongoing effort is being conducted to use this large batch catalyst to prepare the core sample and identify the key issues involved in preparation and hydrothermal aging of core samples.

NH₃ Generation

An appropriate NH₃ supply strategy is essential for the SCR after-treatment device. Various NH₃ generation strategies have been evaluated and an approach based on TW+NSC has been down selected. Detailed studies based on TW+NSC provides operational characteristics. For example, it was found that NH₃ is generated in the 250 to 400°C window; NH₃/NO_x (ammonia NO_x ratio) reaches maximum at 250°C; and low L/R cycles favors NH₃ and N₂ yields. These results help guide future direction in development of NH₃ generation strategies.

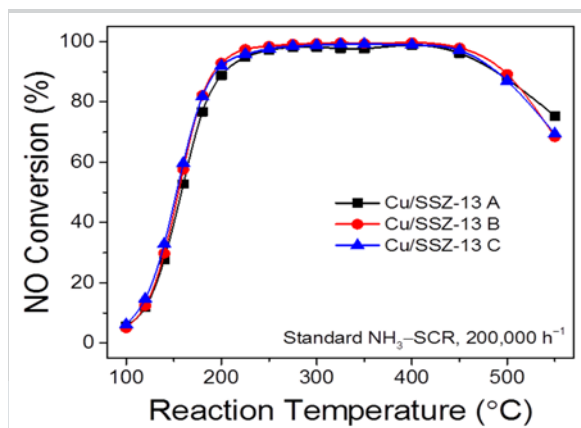


Figure 60. Standard NH₃-SCR light-off curves for the Cu/SSZ-13 samples prepared in various batches.

Milestones

The following milestones for the Year 1 effort have been met:

- Complete synthesis of small batches of various catalysts and a large batch of the best catalyst (September 2015)
- Complete initial performance tests (December 2015)
- Determine optimized composition of the first generation of the low-temperature SCR catalyst (March 2016)
- Deliver a large batch of first generation SCR catalyst (April 2016)
- Initiate synthesis of the second generation SCR catalyst (September 2016)
- Operational status of NH₃ generation – incorporated baseline NH₃ generation catalyst into engine dyno exhaust after-treatment (June 2016).

Conclusions

We have met all key milestones developed for Year 1 on this joint CRADA project with FCA. Detailed studies about the first generation SCR helped identify research direction for development of second generation SCR catalysts that will potentially meet the target conversion efficiency. We also have developed a synthesis protocol that allows reproducible synthesis of a large batch Cu/SSZ-13 catalyst (greater than 500 g), which will be used to identify key issues that may exist in preparation of washcoat and to conduct high-temperature alloys studies of core samples. A joint effort between FCA and the University of Houston led to down selection of a possible NH₃ generation strategy. Consequently, detailed performance characteristics of the NH₃ generation catalyst have been generated and areas for further improvement of modeling accuracy have been identified.

References

- Gao, F., J. H. Kwak, J. Szanyi, and C. H. F. Peden, 2013, “Current Understanding of Cu-Exchanged Chabazite Molecular Sieves for Use as Commercial Diesel Engine DeNO_x Catalysts,” *Topics in Catalysis* 56: 1441-1459.
- Gao, F., Y. Wang, N. M. Washton, M. Kollar, J. Szanyi, and C. H. F. Peden, 2015, “Effects of Alkali and Alkaline Earth Cocations on the Activity and Hydrothermal Stability of Cu/SSZ-13 NH₃-SCR Catalysts,” *ACS Catalysis* 5: 6780-6791.

Publications and Presentations

- Gao, F., Y. Wang, N. M. Washton, M. Kollar, J. Szanyi, and C. H. F. Peden, 2015, “Effects of Alkali and Alkaline Earth Cocations on the Activity and Hydrothermal Stability of Cu/SSZ-13 NH₃-SCR Catalysts,” *ACS Catalysis* 5: 6780-6791.
- Prodinger, S., M. A. Derewinski, Y. Wang, N. M. Washton, E. D. Walter, J. Szanyi, F. Gao, Y. Wang, and C. H. F. Peden, 2017, “Sub-micro Cu/SSZ-13: Synthesis and application as selective catalytic reduction (SCR) catalysts.” *Applied Catalysis B: Environmental* 201: 461-469.

Project-Materials for Control of Exhaust Gases and Energy Recovery Systems

Ford – Next Generation Three-Way Catalysts for Future, Highly Efficient Gasoline Engines

Dr. Christine K. Lambert
Ford Motor Company
2101 Village Road
Dearborn, Michigan 48121
Phone (313) 323-1038; fax: (313) 594-2963
E-mail: clamber9@ford.com

Dr. Todd J. Toops
Oak Ridge National Laboratory
2360 Cherahala Boulevard
Knoxville, Tennessee 37932
Phone (865) 946-1207; fax: (865) 946-1354
E-mail: toopstj@ornl.gov

Dr. Johannes Schwank
University of Michigan
2300 Hayward
Ann Arbor, Michigan 48109
Phone (734) 764-3374; fax: (734) 763-0459
E-mail: schwank@umich.edu

DOE Technology Manager: Jerry L. Gibbs
Phone: (202) 586-1182; fax: (202) 586-1600
E-mail: jerry.gibbs@ee.doe.gov

DOE NETL Program Manager: Aaron Yocum
Phone: (304) 285-4852; fax: (304) 285-4403
E-mail: aaron.yocum@netl.doe.gov

Contractor: Ford Motor Company, Dearborn, Michigan
Prime Contract No.: DE-EE0006845

Objectives

- Develop new three-way catalyst materials that show progress toward durable 90% conversion of carbon monoxide, HCs, and nitrogen oxides at 150°C (T90).

Approach

- Establish common test protocols between the project partners.
- Identify and characterize known, proven exhaust catalyst materials in new ways.

- Develop new catalyst formulations that improve PGM dispersion and promote activity after aging.
- Predict vehicle performance and finished catalyst cost.
- Leverage cross-laboratory analytical capabilities.

Accomplishments

- Confirmed layered and core shell catalyst configurations via electron microscopy.
- Found lowest durable T90s with a 0.5% rhodium (Rh) on titania on a stabilized alumina support, 55 to 100°C lower than a commercial three-way catalyst.
- Found that other promising materials included palladium (Pd) deposited on Ce-Zr nanoparticles and precious metal on silica cores in zirconia shells.
- Created two invention disclosures and prepared patent applications.

Future Directions

- Transfer most promising technologies to a major catalyst coater during the third year of the project.
- Continue synthesis on most promising directions with increased emphasis on Rh.
- Use realistic catalyst aging at high temperatures to represent high mileage.

Introduction

Ford Motor Company has successfully used catalysts on cars and trucks to control emissions for over 40 years. Changes in gasoline engine technology have allowed the use of “high tech” three-way catalysts to simultaneously control HC, CO, and NO_x at nearly 100% efficiency. Waste heat is used upon engine start to bring the catalyst up to its full operating temperature of greater than 350°C, lowering fuel economy and creating particulate matter. The goal of this project is to develop and test new catalysts for lower-operating temperatures that may occur with future, more efficient, gasoline-powered vehicles. The work includes laboratory preparation, aging, and poisoning of catalyst materials, activity tests, and chemical analyses. The objective is to make progress toward the USDRIVE goal of achieving a durable 90% activity for HC, CO, and oxides of NO_x at 150°C.

Results

Catalyst Structure

The project partners focused on several supported metal catalyst structures to promote lower light-off temperatures, enhance metal support interaction, and improve durability. The raw materials (i.e., oxides of Al, cerium, Si, titanium, and Zr) were not new, but

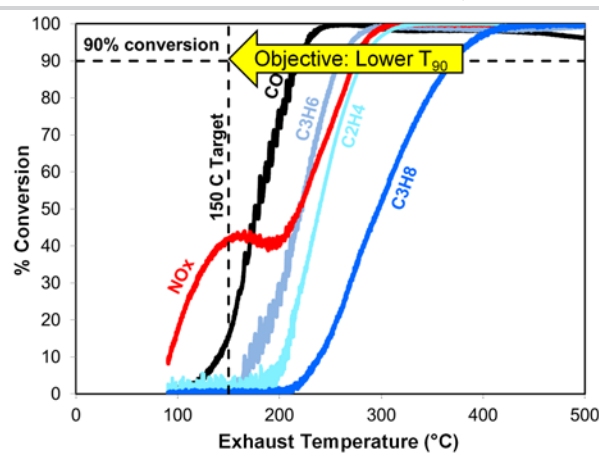


Figure 61. Light-off curves for CO, three HCs, and NO_x using a commercial three-way catalyst for gasoline vehicles.

were used in novel ways. Pd or Rh were supported on layered metal oxide supports, on nanoparticles, or used in various core@shell configurations. ORNL also made a ternary base metal oxide that converted CO below 200°C. Ford had the most success with Rh on a layer of titania (TiO₂) on a stabilized alumina (Al₂O₃) support. Microscopy was conducted on this material using the FEI Talos F200X STEM (provided by the DOE Office of Nuclear Energy Fuel Cycle Research and Development Program and the Nuclear Science User Facilities) at ORNL to confirm its structure. Similar structural confirmation was completed on ORNL's deposition of Pd on Ce-Zr nanoparticles onto an alumina support using a strong electrostatic adsorption method. Images were also obtained of a hollow zirconia sphere that could be used to support precious metals. The University of Michigan team succeeded in developing a one-pot synthesis method for Pd@SiO₂ silica core@shell catalysts, as well as Pd@CeO₂.

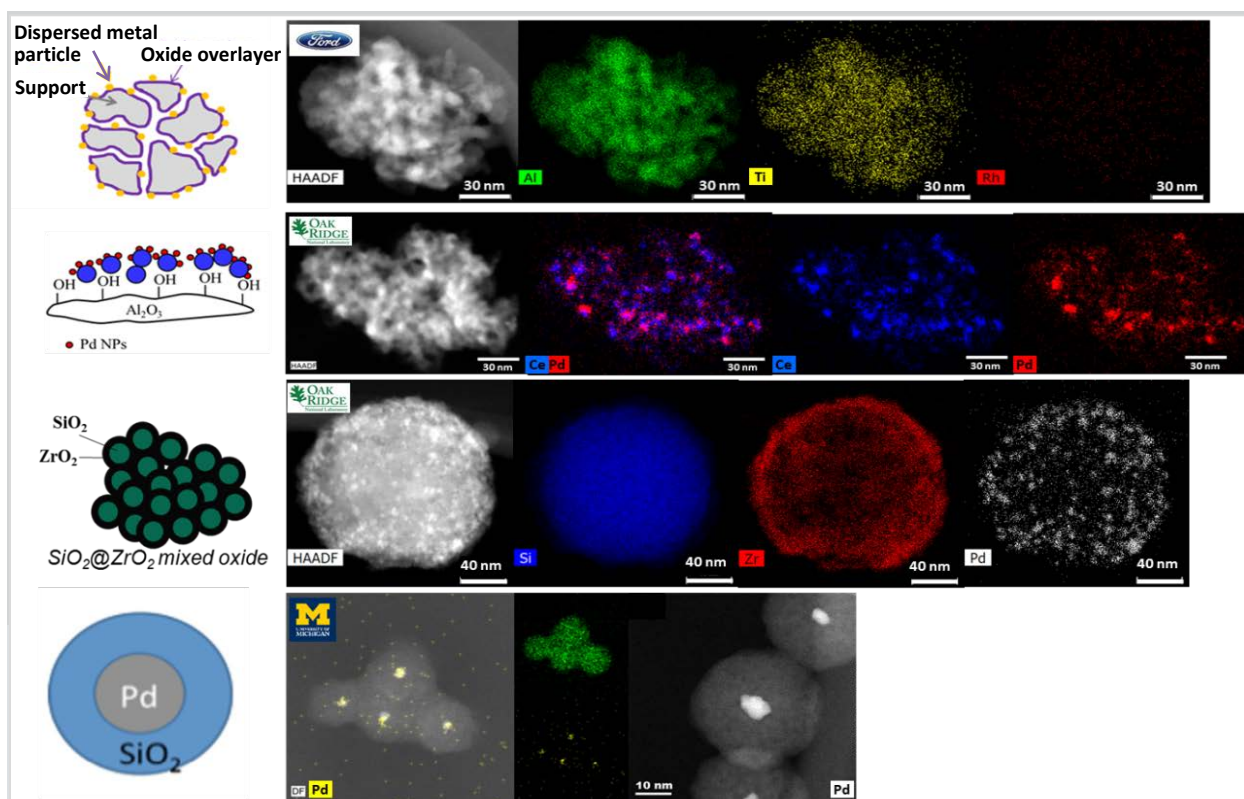


Figure 62. Confirmation of catalyst structures using the Talos electron microscope at ORNL.

Low-Temperature Performance

Several confirmed materials showed promise for lower light-off of CO, HC, and NO after aging to represent high mileage. Table 5 compares T90s for new catalysts versus a commercial sample. The commercial three-way catalyst contained 1.7% Pd and was aged on a four mode (i.e., lean, stoichiometric, rich, and exothermic) cycle with peak temperatures of about 960°C. Most notably, the 0.5% Rh/TiO₂/Al₂O₃ sample aged in the same manner displayed 90% CO conversion below 200°C, and the total HC and NO T90s were 253 and 222°C, respectively. This was 55 to 108°C lower T90s than the commercial catalyst while using a reduced precious metal loading. Smaller improvements in CO and HC T90s were seen with a low (1%) Pd content on ceria nanoparticles (6 to 17°C), while a second sample of higher (2%) Pd on Ce-Zr nanoparticles reduced the HC and

NO T90s by 32 to 40°C. While none of these samples achieved 150°C aged T90s, results show meaningful progress toward this goal.

Table 5. Temperatures for 90% conversion of carbon monoxide, HCs, and nitrogen oxide.

| | 1.7% Pd Commercial Three-Way Catalysts (960°C Four Mode Aged) | 0.5% Rh/TiO ₂ /Al ₂ O ₃ (960°C Four Mode Aged) | 1% Pd/Ce/Al ₂ O ₃ (900°C stoich. aged) | 2% Pd/Ce-Zr/Al ₂ O ₃ (900°C stoich. aged) |
|----------|---------------------------------------------------------------|---------------------------------------------------------------------------------|--------------------------------------------------------------|-----------------------------------------------------------------|
| T90 (CO) | 245°C | 190°C (-55°C) | 228°C (-17°C) | 245°C (0°C) |
| T90 (HC) | 345°C | 253°C (-92°C) | 339°C (-6°C) | 305°C (-40°C) |
| T90 (NO) | 330°C | 222°C (-108°C) | 334°C (+4°C) | 298°C (-32°C) |

Milestones

The following project milestones were met during the second year: cross-laboratory reactors were confirmed to be reasonably compatible using a commercial three-way catalyst. All partners compared their catalyst samples to the commercial benchmark. Test protocols were revised to include an oxygen sweep, resulting in slightly rich and slightly lean air/fuel ratios for identification of optimum catalyst activity. The partners met with a major catalyst manufacturer to kick off a technology transfer and scale-up plan.

Conclusions

The decision was made to continue with Rh/TiO₂/Al₂O₃ and a few other selected materials during the third project year. Invention disclosures were filed by Ford and ORNL.

Publications

Binder, Andrew J., Todd J. Toops, James E. Parks II, and Sheng Dai, 2015, “Low Temperature CO Oxidation over Ternary Oxide with High Resistance to Hydrocarbon Inhibition,” *Angewandte Chemie International Edition* 54: 13263-13267.

Binder, Andrew J., Todd J. Toops, Raymond R. Unocic, James E. Parks II, and Sheng Dai, 2015, “Inhibition-Resistant Ternary Oxide Catalyst for Low Temperature CO Oxidation in Automotive Exhaust,” *14th Annual Fall Symposium of the Southeastern Catalysis Society*, Clemson, South Carolina, September 28, 2015.

Lambert, Christine, 2016, *DOE Annual Merit Review*, June 2016.

Seo, C. Y., X. Chen, G. B. Fisher, M. Nahata, and J. Schwank, 2016, “Preparation of thermally stable Pd core@shell catalysts for CO oxidation,” *Michigan Catalysis Society 37th Annual Spring Symposium*, Midland, Michigan, May 4, 2016.

Toops, Todd J., James E. Parks, Eleni Kyriakidou, Andrew Binder, Jae-Soon Choi, and Michael Lance, 2015, “Approaches to the Challenges of Treating Emissions at Low Temperatures,” *PACIFICHEM*, Honolulu, Hawaii, December 15, 2015.

Project-Materials for Control of Exhaust Gasses and Energy Recovery Systems

Cummins – Sustained Low-Temperature NO_x Reduction

Yuhui Zha
Cummins Inc.
1900 Mckinley Avenue
Columbus, Indiana 47201
Phone (812) 377-7043; fax: (812) 377-7050
E-mail: Yuhui.zha@cummins.com

DOE Technology Manager: Jerry L. Gibbs
Phone: (202) 586-1182; fax: (202) 586-1600
E-mail: jerry.gibbs@ee.doe.gov

Contractor: Cummins Inc.
Prime Contract No.: DE-EE0006795

Objectives

- Develop the catalyst and system technology needed to enable a commercially viable system to sustain at least 90% conversion of the NO_x emissions entering the SCR catalyst at 150°C.

Approach

- Development of a zeolite catalyst and catalyst architectures with enhanced catalytic activity at 150°C, targeting 90% conversion at an inlet nitrogen dioxide (NO₂)/NO_x ratio of 0.50.
- Development of an integrated catalyst system capable of providing inlet SCR catalyst NO₂/NO_x ratios in the range of 0.40 to 0.50 at turbine outlet temperatures of 150°C.
- Determination and development of an appropriate means to robustly deliver reductant under sustained operation at low-temperature SCR catalyst inlet conditions.
- Development of SCR and oxidation catalyst models under conditions relevant to the sustained low-temperature NO_x reduction (SLTNR) system.
- Divided into three budget periods: (1) SLTNR System Analysis and Model Development; (2) SLTNR System Technology Development; and (3) SLTNR System Demonstration.

Accomplishments

- Developed a manufacturing process to scale up the first generation SCR formulation from laboratory preparation to an industrial preparation method; core size sample was tested on a reactor with performance meeting the SLTNR target (greater than 90% deNO_x at 150°C at 0.5 NO₂ fraction) and full-size parts are in the process of engine test.

- Developed second generation SCR formulation with improved thermal stability and low-temperature performance; core sample was tested on reactor with improved low-temperature performance (98% NO_x conversion at 0.5 NO₂ fraction and greater than 90% at 0.4 NO₂ fraction); the manufacturing process is undergoing optimization; and full size parts are in the process of engine test.
- Completed DOC prototype parts manufacturing and architecture design; engine test is ongoing.
- Completed diesel exhaust fluid (DEF) ultrasonic vaporizer device design and developed integration and control strategy; bench test is ongoing.
- Started engine test on first generation SLTNR prototype system.
- Developed preliminary commercial assessment against pre-defined evaluation criteria based on best engineering judgement on current architecture/technology selection and development.

Future Directions

- Complete engine test on first prototype system
- Develop improvement strategy with second prototype system
- Complete DEF vaporizer bench test, control strategy development, and engine test
- Complete exhaust manifold re-design for pre-turbo catalyst
- Complete final commercial assessment.

Introduction

The objective of this project is to develop the catalyst and system technology needed to enable a commercially viable system to sustain at least 90% conversion of the NO_x emissions entering the SCR catalyst at 150°C.

The project will develop the enabling catalyst technology needed to sustain at least 90% conversion of NO_x emissions entering the SCR catalyst at 150°C; demonstrate SLTNR, using a prototype system and relevant emulated exhaust gas composition and temperatures; and develop a cost model for assessing the commercial viability of the proposed SLTNR system.

Results

The objectives for the project management portion of the work are to provide project planning, coordination, and reporting as required to successfully achieve the overall objectives of the project.

NOTE: Continuation – In accordance with the award terms and conditions, specifically the provision named “CONTINUATION APPLICATION AND FUNDING,” and the Go/No Go technical criteria outlined above, the recipient is **NOT** authorized to proceed beyond Budget Period 1 or Budget Period 2 without the DOE Contracting Officer’s approval of acceptable technical progress associated with the Go/No Go technical criteria outlined above and the submission of a continuation application submitted no later than 90 days prior to the end of the current budget period. If selected to continue into a subsequent budget period, the recipient will continue to perform the overall tasks listed in this statement of project objectives, or, adjusted tasks as deemed necessary

and negotiated during the negotiation of subsequent continuation application(s). If the recipient unilaterally decides to continue into the subsequent budget period prior to the DOE Contracting Officer's approval, all costs are incurred at the Recipient's risk and no DOE funds may be utilized for such costs prior to the DOE Contracting Officer's approval of the technical Go/No Go criteria and continuation application.

- **Budget Period 1: SLTNR Systems Analysis and Model Development**

- Task 1.0 – Develop a Zeolite Catalyst Development with Enhanced Intrinsic Catalytic Activity
This task includes SCR mechanistic studies, chemical and physical properties of various SCR formulations, and performance model development.
- Task 1.1 – SCR Mechanistic Studies
The limiting mechanisms that result in light-off temperatures of 200⁰C for commercially available SCR materials will be determined. A range of catalyst compositions that vary the metal (i.e., Cu and/or Fe) content, the zeolite composition (e.g., Si/Al ratios), and varied acidity will be selected to address ammonia storage (i.e., NO₂/NO_x ratios and N₂/N₂O selectivity). The differences in ammonium nitrate formation and varying selectivity to NO₂ during standard and fast SCR on Cu and Fe will be determined. Low-temperature light-off on metal (Cu and/or Fe) reducibility will also be determined with variations in the metal (Cu and/or Fe) content and zeolite Si/Al ratios.
- Task 2.0 – Integrated Catalyst System Development
This task will specify and design integrated catalyst systems through analysis and reactor testing that are expected to meet the SLTNR NO₂/NO_x ratio requirements.
- Task 2.1 – Develop Models for Oxidation Catalysts
Reaction engineering and kinetic modeling will be applied to develop oxidation catalyst models under conditions representative of a pre-turbine location. Laboratory tests to confirm oxidation catalyst performance will be performed.
- Task 2.2 – NO₂/NO_x Ratios Assessment for Pre-Turbine Oxidation Catalysts
Oxidation catalyst models and reaction engineering principles will be applied to perform trade-offs regarding oxidation catalyst functions and size required to meet the SLTNR NO₂/NO_x ratios. Both pre-turbine and close-coupled oxidation catalysts will be considered.
- Task 2.3 – Pre-Turbo Catalyst Performance Testing
Laboratory tests will be performed to characterize oxidation catalyst performance under conditions representative of the pre-turbine location. The oxidation catalyst models will be updated as needed based on test results.
- Task 2.4 – Catalyst System Integrated Oxidation Options
Engine cycle simulation tools, in combination with developed catalyst models and practical design considerations, will be used to estimate the potential benefits and trade-offs of the pre-turbo and close-coupled oxidation catalyst locations. Based on simulation results, integrated catalyst systems for testing will be recommended.
- Task 3.0 – SLTNR System Designs
Specify and design low-temperature reductant delivery systems that are expected to meet SLTNR requirements. Designs for configurations recommended for testing will be developed and preparatory work for procurement of the systems will be completed.
- Task 3.1 – Assess Options Available to Deliver Reductant for Continuous Operation
Available reductant options for low-temperature operation will be assessed. The advantages and disadvantages of the low temperature reductant delivery options will be developed. A literature survey and a concept generation process will be completed to create a list of options to assess against the requirements. The available options will be rated and recommendations made about the reductant delivery system(s) to integrate as part of the SLTNR systems to assess through engine testing.

- Task 3.2 – Design and Prepare to Procure the Recommended Reductant Delivery System(s)
The most promising low-temperature reductant configurations will be designed and integrated into the engine system. Practical design and standard analysis work for assessing the robustness of the required changes will be carried out. Drawings to procure the new components will be created. Suppliers for manufacturing the prototype hardware will be identified and estimates for procurement lead times will be obtained.
- Task 4.0 – Commercial Potential and Capability of the SLTNR Configurations
The commercial potential and capability of the proposed SLTNR configurations will be assessed. The SLTNR configuration against both medium-duty vehicle and heavy-duty engine system requirements will be evaluated.
- Task 4.1 – SLTNR Options Assessment
The key requirements and baseline configurations against which to assess the integrated SLTNR options will be defined. A cost model will be developed to assess the commercial potential of the integrated SLTNR configurations. The relevant cycles for both medium-duty vehicle and heavy-duty engine systems will be used to assess the commercial potential of the SLTNR configurations.

Table 6. Milestones for Budget Period 1

| Milestone | Type | Description |
|-----------------------------------------------|-----------|--------------------------------------------------------------------------------------------------------------------------------------------------------------|
| SLTNR Requirements | Technical | Document key requirements against which to assess commercial viability of the SLTNR concepts |
| Catalyst Formulation and Reaction Unit Design | Technical | Analysis complete for catalyst formulation and reaction unit design |
| Oxidation Catalyst | Technical | Oxidation catalyst received for laboratory testing |
| LT SCR Formulations | Technical | Critical functions of LT SCR formulations established |
| Technology Development Assessment | Go/No Go | Analysis indicates 90% conversion of NO _x emissions entering the SCR catalyst is achievable at 150°C with NO ₂ /NO _x at 0.5 |

● **Budget Period 2: SLTNR System Technology Development**

- Task 1.0 – Develop a Zeolite Catalyst Development with Enhanced Intrinsic Catalytic Activity (Continued)
- Task 1.1 – SCR Mechanistic Studies (Continued)
- Task 1.2 – Chemical and Physical Properties of the LT SCR Formulations
Experiments will be performed to establish the chemical and physical properties of the alpha SCR catalyst. The requirements for a beta version of the LT SCR will be defined.
- Task 1.3 – Alpha LT SCR Performance Model
Reactor tests will be used to characterize the alpha LT SCR catalyst functionality. Experimental data will be used to calibrate and/or develop an SCR catalyst model. The model will be refined as required to characterize the beta LT SCR formulations.
- Task 1.4 – LT SCR Formulations Thermal Stability and Sensitivity to Poisoning
Laboratory-scale testing will be conducted to verify LT SCR catalysts possess sufficient hydrothermal stability and resistance to poisoning from fuel and engine oil impurities (e.g., sulfur).
- Task 2.0 – Integrated Catalyst System Development (Continued)
- Task 2.3 – Pre-Turbo Catalyst Performance Testing (Continued)

- Task 2.4 – Catalyst System Integrated Oxidation Options (Continued)
- Task 2.5 – Exhaust Manifold with Integrated Pre-Turbo Oxidation Catalysts Design
Exhaust manifold designs integrating oxidation catalysts for the most promising configurations will be prepared. The robustness of the required exhaust manifold changes to accommodate oxidation catalysts configurations will be established. Drawings for procuring new engine system components will be prepared. Suppliers for manufacturing the prototype hardware will be identified and estimates for procurement lead times will be obtained.
- Task 3.0: SLTNR System Designs (Continued)
- Task 3.2 – Design and Prepare to Procure the Recommended Reductant Delivery System(s) (Continued)
- Task 4.0 – Commercial Potential and Capability of the SLTNR Configurations (Continued)
- Task 4.2 – Commercial Potential of SLTNR Configurations
The SLTNR system configurations will be assessed against the key requirements relative to baseline systems. The commercial viability of the systems will be assessed based on initial and operating costs.
- Task 5.0 – SLTNR Prototype Systems
This task includes design, procurement, and testing of SLTNR prototype systems.
- Task 5.1 – SLT NR Systems Final Design and Procurement
The design of the SLTNR subsystems (i.e., oxidation catalyst, exhaust manifold changes, SCR catalyst configuration, and low-temperature reductant dosing) will be finalized. Parts will be procured and assembled. Control modifications and other preparations for testing in the test cell will be completed. The base engine system configuration for testing will also be procured. Detailed test plans for assessing subsystem performance will also be developed.
- Task 5.2 – SLTNR Subsystems Performance Characterization
The base engine will be installed and commissioned in a test cell. Baseline configuration performance will be validated. It is anticipated that the subsystems will be characterized independent of one another. A specific test plan for characterizing the capability of the different integrated oxidation catalyst systems to generate target NO₂/NO_x and the impact on engine performance will be measured without the presence of low-temperature reductant dosing or SCR catalysts. Similarly, performance of the low-temperature reductant delivery systems will be assessed independently of the other subsystems, and the low-temperature SCR catalyst performance will be tested with and without the integrated oxidation catalysts and low-temperature dosing system. The tests will be designed to collect data in support of system model validation.
Performance of the subsystems will be assessed against expectations. Based on test results, SLTNR subsystems will be selected for additional testing.
- Task 5.4 – Risk and Programmatic Impact Assessment
A cross-functional team will be assembled to assess the risks associated with the proposed SLTNR configurations. The high-risk areas associated with proposed changes to the system architecture will be identified and action items developed to mitigate the highest risk factors.

Table 7. Milestones for Budget Period 2

| Milestone | Type | Description |
|--------------------------------------|-----------|---------------------------------------------------------------------------------------------|
| LT SCR Models | Technical | Alpha LT SCR model completed |
| Integrated Catalyst System | Technical | Bench-scale testing confirms catalyst system meets NO ₂ /NO _x targets |
| Cost Benefit Analysis | Technical | Initial cost benefit analysis complete and SLTNR systems selected for testing |
| Prototype SLTNR Systems | Technical | SLTNR subsystems complete and ready for engine testing |
| SLTNR System Procurement and Testing | Go/No Go | Reaffirm decision to proceed with procurement of hardware and testing of SLTNR systems |

• **Budget Period 3:**

- Task 1.0 – Develop a Zeolite Catalyst Development with Enhanced Intrinsic Catalytic Activity (Continued)
- Task 1.2 – Chemical and Physical Properties of the LT SCR Formulations (Continued)
- Task 1.4 – LT SCR Formulations Thermal Stability and Sensitivity to Poisoning (Continued)
- Task 5.0 – SLTNR Prototype Systems (Continued)
- Task 5.2 – SLTNR Subsystems Performance Characterization (Continued)
- Task 5.3 – Prototype SLTNR System Demonstration
A limited number of SLTNR configurations will be tested as full systems. The SLTNR system test plan will be developed. SLTNR system performance will be characterized at a number of key operating points.
- Task 5.4 – Risk and Programmatic Impact Assessment (Continued)
- Task 5.5 – SLTNR System Performance and Robustness Testing
 - A single SLTNR system will be selected for performance characterization and preliminary robustness testing. A test plan will be developed and engine testing performed.

Table 8. Milestones for Budget Period 3

| Milestone | Type | Description |
|----------------------------------------------|-----------|-----------------------------------------------------------------------------------|
| LT SCR Beta Formulation | Technical | Deliver SCR beta formulation |
| SCR Thermal Stability and Sulfur Sensitivity | Technical | Quantify thermal stability and sulfur sensitivity of LT SCR catalyst formulations |
| Prototype SLTNR Systems Testing | Technical | Select SLTNR system for engine demonstration |
| SLTNR Demonstration System | Technical | Complete SLTNR system engine performance and robustness testing |

The main areas where work was performed include (1) low-temperature SCR formulation development, (2) integrated high NO₂ system development, (3) DEF vaporizer development, (4) engine test, and (5) commercial. The milestones status from these work areas during 2016 is shown in Table 6.

Table 9. Milestone status in 2016.

| Budget Period | Milestone | Description | Target Completion Date | Actual Completion Date | Progress % |
|---------------|-----------|-----------------------------------------------------------------------------------------------------------------------------------------------------------------------|------------------------|------------------------|------------|
| 2 | 3.2 | Completion of Design of reductant delivery system | 19-Mar-16 | 19-Apr-16 | 100% |
| 2 | 1.2 | JMI delivers alpha formulation | 24-Mar-16 | 20-Mar-16 | 100% |
| 2 | 2.3 | Model development Bench scale testing complete to confirms catalyst system meets NO2/NOx targets | 13-May-16 | 10-May-16 | 100% |
| 2 | 1.3 | Model developed by CMI for alpha LT SCR formulation to aid in sizing of prototype system | 17-Jun-16 | 17-Jun-16 | 100% |
| 2 | 4.2 | Initial cost-benefit analysis completed and recommendation made for prototype SLTNR system to test (take input for a sample, exhaust manifold, DOC, Reductant system) | 19-Jun-16 | 19-Jun-16 | 100% |
| 2 | 6.4 | Decision point on Path forward of design, hardware procurement and testing | 30-Jun-16 | 9-Jun-16 | 100% |
| 2 | 1.4 | PNNL complete the study of alpha formulation and recommends catalyst formulation changes (beta) | 21-Nov-16 | 30-Jul-16 | 100% |
| 2 | 2.4 | Oxidation catalyst prototype parts provided for prototype testing | 10-Dec-16 | 1-Jul-16 | 100% |
| 2 | 5.1 | Sub system complete and ready for engine testing | 18-Dec-16 | | 70% |
| 2 | 6.3 | Go/no Go Review: Reaffirm decision to proceed with procurement of hardware and testing of SLTNR systems | 6-Dec-16 | | 80% |

Conclusions

The SLTNR team made significant progress during 2016 and had all milestones delivered on time. We developed a manufacturing process to scale up the first generation SCR formulation from laboratory preparation to industrial preparation method. The core from full-size parts were tested in the laboratory with a satisfactory performance. Based on the fundamental study of alpha formulation, the team developed a second-generation SCR formulation with improved low-temperature performance; the manufacture process is in currently being optimized. The core from full-size parts was tested in the laboratory with superior performance at the SLTNR condition; however, it still requires improvement of the manufacturing process and system integration to meet the SLTNR requirement for engines. The team also completed DOC prototype parts manufacturing and architecture design and is evaluated via engine test. The DEF ultrasonic vaporizer device design was also completed and is in the process of developing an integration and control strategy. The bench test is ongoing. The first generation of a prototype component is in the process of engine test. At the same time, the team developed a preliminary commercial assessment against the pre-defined evaluation criterial based on best engineering judgement of current architecture/technology selection and development. We are well planned for 2017 against

milestones and deliverables and expect to meet the program's ultimate target and timeline by the end of 2017.

References

- Capek, L., V. Kreibich, J. Dedecek, T. Grygar, B. Wichterlova, Z. Sobalik, J. A. Martens, R. Brosius, and V. Tokarova, 2005, *Microporous and Mesoporous Materials* 80: 279.
- Hadjiivanov, K., 2000, *Catalysis Review Science and Engineering* 42: 71.
- Jia, C., P. Massiani, and D. Barthomeuf, 1993, *Journal of Chemical Society Faraday Transactions* 89: 3659.
- Mihaylova, A., K. Hadjiivanov, S. Dzwigaj, and M. Che, 2006, *Journal of Physical Chemistry B* 110: 19530.
- Panov, G. I., A. S. Kharitonov, and V. I. Sobolev, 1993, *Applied Catalysis A* 98: 1.
- Vimont, A., F. Thibault-Starzyk, and J. C. Lavalley, 2000, *Journal of Physical Chemistry B* 104: 286.
- Zecchina, A. and A. C. Otero, 1996, *Chemical Society Reviews* 25: 187.

U.S. DEPARTMENT OF
ENERGY

Energy Efficiency &
Renewable Energy

For more information, visit: energy.gov/eere/vehicles

EE-1563 • May 2017